Numerical Research of Flow Structures Behind Bluff Bodies in Tandem Arrangement

Farshid Azizi

Submitted to the
Institute of Graduate Studies and Research
In partial fulfillment of the requirements for the degree of

Master of Science
in
Mechanical Engineering

Eastern Mediterranean University
September 2016
Gazimağusa, North Cyprus

Approval of the Institute of Graduate Studies and Research

Prof. Dr.Mustafa Tümer
Acting Director

I certify that this thesis satisfies the requirements as a thesis for the degree of Master of Science in Mechanical Engineering.

Assoc. Prof. Dr.Hasan Hacışevki
Chair, Department of Mechanical Engineering

We certify that we have read this thesis and that in our opinion it is fully adequate in scope and quality as a thesis for the degree of Master of Science in Mechanical Engineering.

Assoc. Prof. Dr.Hasan Hacışevki
Supervisor

Examining Committee

1. Prof. Dr. Fuat Egelioğlu

2. Assoc. Prof. Dr.Hasan Hacışevki

3. Asst. Prof. Dr. Murat Özdenefe

ABSTRACT

In this research flow structures that are in downstream regions of two flat plates which are inclined in tandem positions have been examined. Different gap ratio of $0.5<g/D<2.0$ that are between plates have also been examined for their impacts on the wake structures and the frequency for shedding vortex. Also, various angles of attack between the ranges of 45-90 degrees have been investigated to depict their impacts on the wake region in terms of shedding frequency and Strouhal number variation. The width of the flat plate which was investigated had a Reynolds number based on 33000. Computational Fluid Dynamics (CFD) codes ANSYS/FLUENT 13.0® was used to simulate the flow around the flat plates. The equations of shear stress transport $k-\omega$ model and Reynolds Stress Model (RSM) were considered as solution techniques. But since, the validity of any theoretical prediction can only be assessed in practice, the comparison was done between numerical data and achieved data from the experiments, for both cases based on literature.

Keywords: CFD, Vortex Shedding, Incoherent Products, Bluff bodies in tandem

ÖZ

Bu çalışmada arka arkaya belirli bir açı ile yerleştirilmiş iki adet düz plakanın arkasındaki akış özelliklerinin araştırılması yapılmıştır. Plakalar arasında değişik aralık oranlarının 0.5 < g/D < 2.0.Aralığında dalga yapıları ve sarmal frekansları üzerindeki etkilerida araştırılmıştır. Ayrıca 45 – 90 dereceler arasında atak açısının dalga bölgesinde sarmal frekensı ve Strouhal sayısının değişimine olan etkileri araştırılmıştır. Plaka genişliğine bağlı olan Reynolds sayısı 33000 olarak seçilmiştir.Bilgisayar destekli Akışkanlar Dinamiği (CFD) kodları ANSYS/FLUENT 13.0 programı kullanılarak plakalar etrafındaki akış simüle edilmiştir. Çözüm tekniği olarak kesme gerilimi denklemleri, k – w ve Reynolds stress modellemeleri kullanılmıştır. Sonuçların geçerliliği ve sağlanması literatüre bağlı olan nümerik ve deneysel sonuçlar ile mukayese edilmiştir.

Anahtar kelimeler: CFD, Sarmal olusum, incoherent ürünler, ardışık gövdeler,

ACKNOWLEDGMENT

I would first like to thank my thesis supervisor Assoc. Prof. Dr. Hasan Hacışevki of the mechanical engineering at Eastern Mediterranean University. The door to Prof. Hasan Hacışevki office was always open whenever I ran into a trouble spot or had a question about my research or writing. He consistently allowed this paper to be my own work, but steered me in the right the direction whenever he thought I needed it. I must express my very profound gratitude to my parents for providing me with unfailing support and continuous encouragement throughout my years of study and through the process of researching and writing this thesis. This accomplishment would not have been possible without them. Thank you.

TABLE OF CONTENTS

LIST OF FIGURES

NOMENCLATURE

μ	The first dynamic viscosity $[kg/m.s]$
λ	The second coefficient of viscosity $[kg/m.s]$
β	Coefficient of thermal expansion [k]
ϕ	Dissipation function
ρ	Density $[kg/m^3]$
ε	Dissipation rate $[m^2/s^3]$
ω	Specific dissipation rate [1/s]
u''^2	Normal Reynolds Stress in x-direction $[m^2/s^2]$
v''^2	Normal Reynolds Stress in y-direction $[m^2/s^2]$
C_D	Drag coefficient
C_P	Specific heat at constant pressure $[J/kg.k]$
CFD	Computational Fluid Dynamics
d	Width of the plate [mm]
EFD	Experimental Fluid Dynamics

EWT	Enhanced Wall Treatment
g/d	Gap ratio
k	Kinetic energy $[m^2/s^2]$
LIF	Laser-Induced Fluorescence
PISO	Pressure-Implicit with Splitting of Operators
Re	Reynolds number
RSM	Reynolds Stress Model
rms	Root Mean Square
SST $k-\omega$	Shear Stress Transport Turbulence Model
St	Strouhal number
Smx	Total force on the element due to body forces in x directions $[N/m^2]$
Smy	Total force on the element due to body forces in y directions $[N/m^2]$
Smz	Total force on the element due to body forces in z directions $[N/m^2]$
T	Temperature [k]

Chapter 1

INTRODUCTION

1.1 Computational Fluid Dynamics

Fluid behavior in interaction with solids or other fluids has been studied and analyzed vastly by scientists and engineers for centuries now. There are two major approach in fluid dynamics, one being experimental and the other theoretical or numerical.

Experiments and wind tunnels are used to study the fluid behavior. The wind tunnel testing is a powerful simulation tool and very helpful during design stages but the cost of running wind tunnel testing is very high, the equipment are expensive and it is very time consuming. Furthermore, there is a scaling issue for large bodies like aerial vehicles, ships and submarines. These factors and mathematical progress together with the advent of computers enabled the engineers to come to a cheaper solution called computational fluid dynamic or in short CFD. In other words, analysis of fluid flow, heat transfer and associated phenomena through Computer simulation. The mathematical statement of governing equations of moving fluid is the conservation law of physics which are conservation of mass, momentum (Newton's second law) and energy (Thermodynamics first law).

In every point of the domain all three for mentioned laws must be satisfied. Numerical solution to these expressions is the sole purpose of CFD.

1.2 Problem Statement

The aim of this thesis is to numerically analyze the unsteady change in the structure and flow parameters behind two normal and inclined flat plates which have the same dimension and width and are arranged in a row at different gap or spacing ratio at varying angles. Flat plates are often utilized in the design of skyscrapers, air planes, marine turbine etc. While inclined plates are also used in airplane turbine. The effect of flat plates wake on shedding from normal and inclined flat plate was investigated with regard to gap ratio, geometry and angle. The Reynolds number set to the magnitude of 33,000 so the unsteady turbulent wake occurs. The model was created using ANSYS/CFX 13.0® software. The boundary conditions, input, output and wall are set to be exactly like the wind tunnel conditions. The ANSYS CFD Post was implemented for post processing the output data.

1.3 Practical Importance of Vortex Shedding in Engineering

Vortex shedding from different bluff geometries is one of the most attractive and significantly important areas in fluid mechanics. Recent years with global warming issues, raising fuel prices and safety measures, the vortex shedding has become more important. Energy conservation examples include but not limited to automobiles, skyscrapers (convection heat loss) and heat exchangers. Furthermore, it is important in structural design to limit the oscillation amplitude of the structure as well as preventing resonance phenomena. This occurs when the shedding frequency is close or higher than the natural frequency of the structure. The famous failure of Tacoma Narrows Bridge in 1940 is a subject of a chapter of nearly every Physics book.

1.4 Processing the Problem Using CFD

Numerical investigation performed to determine the flow characteristics behind two bluff bodies by CFD. The program ANSYS/FLUENT 13.0 ® was used to simulate the flow. The flow considered as incompressible, unsteady flow. The shear stress transport model (SST) $k-\varepsilon$ together with Reynolds stress model (RSM) were considered as viscous models.

In general, all problems in follow these steps:

- Geometry- geometry is selected and geometry parameters are defined
- Grid generation- consist of both structured and unstructured grids
- Physics- flow properties, viscous model, compressible or incompressible conditions are determined
- Initial conditions and boundary conditions are applied
- Solve- spatial discretization scheme and numerical schemes considered together with required accuracy for the problem
- Processing- the program is running
- Results- the CFD results can be visualized at this part.

1.5 Discussion of the Chapters

The background information on the investigations done on the comparison between the CFD and experimental fluid dynamics are presented in literature survey in chapter 2.

The methods applied to collect the data and the reasons of how these methods were taken are introduced in the chapter 3 with the methodology title.

In chapter four the interpretation on findings and comparison between the experimental and numerical result are illustrated by the aid of contours and graphs. And finally the conclusion of this study together with the recommendation for the future work is presented in chapter 5.

Chapter 2

LITERATURE REVIEW

2.1 Introduction

Analyzing the fluid flow behavior can be done by the aid of experimental and empirical studies. Many efforts have been done in order to study and investigate the characteristics of the fluid flows. These attempts result in new field of science which is called the „Fluid Mechanics". In other word, fluid mechanics is the consequence of the experimental studies and observations. The outcome of different tests, the widely usage of differential equations and mathematical relations caused obtaining the theoretical-applicable and up to date equations. As a result, there are two general methods to examine the fluid manner: 1) experimental method and 2) Theoretical or numerical method.

The analytical solutions that were obtained from the experimental observations were difficult to compute; therefore experiments remained the only suitable way to compute the flow properties in the past. As the time passes, the experimental equipment improved to give the more accurate and better results. Despite of all efforts in the developments of experimental apparatus, some experimental restrictions remained the same.

Scale effects, environmental effects and high cost experiments made engineers to think about the cheaper methods that are capable to solve the scale effect problems. Development and progress of computer science and programming brought about the genesis of Computational Fluid Dynamics (CFD) with the purpose of solving the numerical equations in the recent century. According to Professor Dean Chapman at

Stanford University providing an important new technology capability and economics are two major motivations behind CFD and they will not change in the coming decades [3]. The large number of investigations on the validation and verification of CFD, as a practical analysis and design tool, are the proofs for the strong need for CFD.

Aerospace is one of the areas of CFD applications in the last 30 years. Some problems in this field still remain unknown, even with simple geometries and after many simulations. One of the fluid flow difficulties is the case of vortex shedding from bluff bodies that has attracted markedly attention for over four decades. The vortex shedding phenomenon is a consequence of flow movement over long cylinders and spheres as the Reynolds is greater than 90 [4]. The significance of these periodic unsteady flows past from bluff bodies comes from the wide range of their applications in engineering, such as offshore platforms and high tower buildings in civil engineering and tube and heat exchangers in mechanical engineering branch. In the layouts of these constructions multiple bluff bodies are available which make the flow complex [5]. Vortices are capable to produce the vibrations near the body which may result in the resonation of body to dangerous level if the frequencies of the vortices get close to the natural frequency of the body [4].

2.2 Experimental Investigations

This section emphasizes chiefly on past investigations into the fluids flow from bluff bodies in various phases. The presence of the various regimes of flow and differences with the variables of flow is argue as the shape of the body and its distance are altered. The produced investigations in these part are carried by from various researches.

Investigations on a two-dimensional bluff in a closed return wind- tunnel were carried out by P.W. Bearman at varying Reynolds number which were from 1.4×10^5 to 2.56×10^5 [6].

P. W.Bearman and D. M.Trueman [7] did some experimental investigations on two-dimensional rectangular plate, located perpendicular to the wind direction, in two closed-return wind tunnel with low turbulence level, but with different cross section areas. Despite of the well-known fact that, the drag coefficient of both thin flat plate and thicker body normal to wind direction in about 2.0 , they could get the coefficient as high as 2.94. For this purpose, they started increasing the thickness of the two dimensional rectangular plate from 0.2 to 1.2. The critical block dimension, where the maximum value of drag coefficient achieved, was when the thickness was just over the half of the width (thickness/width = 0.62).

According to P. W.Bearman and D. M. Trueman, high drag is a result of regular vortex shedding. Hot wire and a wave analyzer were used to detect and measure vortex shedding and frequency of shedding, respectively. Water tunnel was also applied for the flow visualization purposes. Bearman [8] has shown that the higher base pressure is a result of the formation of vortices away from the body. The distance to vortex formation and the strength of fully formed vortices are related to the amount of vorticity that is being shed from the body, which is determined by base pressure.

The results of these experiments were in a good agreement with the findings in Japan. Chi_Hung Liu and Jerry M.Chen [9] carried out different experiments, on two square cylinders in tandem arrangement, to investigate the effects of 1) ratio of the spacing

between the square cylinders to the width of the cylinder, and 2) the manner of varying this spacing ratio, on the flow properties. The experiments were done in a low speed, open circuit wind tunnel. Spacing between the cylinders was changed in the way of progressive increase and progressive decrease, between the ranges from 1.5 to 9.0 widths. Reynolds numbers were also varied in the ranges of $2.0 \times 10^3 - 1.6 \times 10^4$ The hysteresis regime on drag observed for all Reynolds number, as drag forces that were obtained by integrating the mean pressure distributions for both upstream and downstream cylinders, as the spacing between the cylinders varied in a progressively increasing and decreasing manner. Two different flow patterns referred to mode I and mode II where associated with two discontinues jumps that occurred in hysteresis regime, were observed. For both upstream and downstream cylinder, two branches of drag coefficient (C_D) were observed in the hysteresis regime. The progressive increase in the spacing is associated with the flow pattern called mode I and is referred to the lower branch. And the flow pattern of mode II is associated with the upper branch which is a result of progressive decrease in the spacing. They pointed out that there is only one stable mode occurs in the hysteresis regime despite of the, presence of the intermittent change between Mode I and Mode II for higher Reynolds numbers as mentioned by previous authors. They also showed that the flow characteristics depend strongly on the manner of the varying the spacing between the cylinders in addition to the well-known fact of their dependency to the spacing ratio. The presence of discontinuous jump in each flow pattern is associated with hysteresis.

For the low Reynolds number, the values of upper and lower spacing limits of the hysteresis regime are large. As the Reynolds number increased to 300 and beyond, the spacing limits leveled off rapidly. Further increase in the Reynolds number result in

having the spacing limits at a nearly constant value of 10D independent from Reynolds number. Both drag coefficient and fluctuating pressure of two cylinders for Mode I are in lower level than the computed values for Mode II. Chain_Hung Liu and Jerry M.Chen demonstrated the changes in Strouhal Number in the progressive increase and decrease in the spacing ratio. In addition to drag coefficient, the hysteresis is present for Strouhal number as well. There is only one significant jump for the hysteresis in Strouhal number and this jump is lower spacing limit of regime. As the spacing ratio goes beyond the upper limit of hysteresis regime, the amount of Strouhal number increases for the higher Reynolds number. Increasing the Reynolds number to 8000 and 16000 in the Mode II flow pattern result in the weaker vortex shedding from the first cylinder, and decrease in the fluctuating pressure coefficient on the side and rear face of the first cylinder and on the front and side face of the second cylinder. As the base pressure increases the drag coefficient differences decreases between Mode I and Mode II.

S. C. Yen et al. [10] did experimental investigations on two square cylinders in tandem arrangement in a vertical water tunnel at low Reynolds numbers. They categorize the flow into three categories by the aid of the particle image velocimetry (PIV) scheme as the spacing ratio between the cylinders and Reynolds number changed. The first flow pattern was the vortex sheet of single mode as it resembles the single cylinder model. The reattachment of the vortices as the cross-section of the downstream cylinder is associated with the vortex sheet of reattach mode which is the second flow pattern. And the last observed pattern was the vortex sheet of binary mode which is associated with co-shedding. As they concluded, at very low Reynolds number the Strouhal number decreases as the Reynolds number increases. But for the higher range

of Reynolds number, Strouhal number increases as the Reynolds increases, and the Strouhal number will reaches the relatively constant value as the Reynolds get even higher.

Dependency of Strouhal number on the spacing ratio of two inline circular cylinders and Reynolds number was examined by G. Xu and Y. Zhou [11]. They carried out their investigation in a closed-circuit wind tunnel, at $800 - 4.2 \times 10^4$ Reynolds. The vortex shedding frequencies were measured by the aid of two hot wires located behind each circular cylinder. Laser-induced fluorescence (LIF) technique was used in the water tunnel to visualize the flow. They found the Strouhal number in the strong dependence with the spacing ratio and Reynolds number. The relationship between the Reynolds number and Strouhal number were divided into four different groups as the spacing ratio changes. There is a spacing ratio, called critical spacing ratio, which there exist no vortex shedding behind the upstream cylinder as the spacing ratio is less than the critical value, and there are vortex shedding from both cylinders simultaneously when the spacing ratio is greater than the critical value. When the gap ratio is between1 - 2, the shear layers were separated at the first cylinder and the vortices were formed behind the second cylinder. As the gap ratio increases and examined in the range of 2 and 3, there exist transition from the formation of vortices behind the second cylinder to the reattachment of the separated shear layers on the second cylinder. The presence of another transition regime from the reattachment to co-shedding was observed, as the spacing ratio was in the range of $3 - 5$.

The final regime is associated with the shedding of vortices from both cylinders at the same time for the spacing ratios greater than 5. According to the authors

observations, when the Reynolds is greater than 2×10^4 the Strouhal number appears to be relatively constant for a given gap ratio. They also found out the critical Reynolds number decreases for the transition regimes as the spacing ratio increases. Another experimental study was carried out by Chin_Yi Wei and aJeng_RenChang [12] on the flow properties of wake and base bleed flow downstream of two bluff bodies arranged side by side. Two dimensional flat plates, square cylinders and circular cylinders were the adopted bluff bodies. Their investigations were divided into two different parts. For the first part, the biasing behavior and flow characteristics of two body arrangements with the same cross sectional dimensions but with different vortex shedding frequencies but with different cross sectional dimensions. Their tests were executed in a close return type low speed wind tunnel and the flow visualization was performed by the aid of water table. The Reynolds number for these investigations ranges from 4000 to 6000. Authors pointed out that, for the case of same cross sectional dimensions, the vortex shedding frequency downstream from two side by side bodies is about the half of the average of the shedding frequency for each single body when the gap distance is small. As the gap ratio increases to the distance which called large related to the geometry of bluff body adopted, the vortex shedding frequency reaches asymptotically to the value of single body condition.

Analysis of biasing behavior of the flow revealed that the gap flow leans to deflect toward the narrow wake side downstream of two bluff bodies in side by side arrangement. They also observed the relatively unstable biasing characteristic of gap flow when the widths of the wake downstream of each bluff body were almost same.

Coherent and incoherent flow structures in wake of bluff bodies were another area of flow characteristics that attracted attention for over four decades. Cetin Mazharoglu and Hasan Hacisevki [13] did some experimental investigations in the open type low speed wind tunnel to analyze the periodic unsteady flows behind a single plate, as well as the double plate in tandem arrangement [14]. The free stream velocity was adjusted at 16.4 ± 0.02 $(\frac{m}{s})$ and kept constant. The tests were done at Reynolds 33000. Phase averaging methods were used to analyze the data together with triple decomposition technique. Dimensions of the single flat plate were selected in the way that could be compatible with the previous works. So, the ratio of thickness to width was 0.02 or 20%. Their obtained values were consistent to within $\pm$5%, with the work of Kiya and Matsumara [15]. According to authors as the distance from the rear face of the flat plate increases the wake behind it widens and the stream wise velocities decrease to maintain the continuity. The computed values of the case of single plate were compared with the case of two in line plates, with different gap ratios. The stream wise velocity contours, coherent velocity contours and incoherent velocity contours, were depicted at the same distance from the rear face of single plate and the rear face of the downstream plate for the case of double plates. The ratio of gap between the plates to the width of the flat plates for tandem plates, were taken at 0.5 and 1.0.

The graphs of the velocity contours showed the similar patterns, but the peak value of single plate was as high as 15% in compare with the double plates. Contours of coherent velocity were almost same for all cases, but the magnitude of the peak values were reduced 12% from single plate to double plate with the gap ratio of 0.5 and arise 12% from single plate to the case of 1.0 gap ratio. Finally, the peak values of the incoherent flow structures of the single plate was achieved 70% and 40% higher than the values of tandem plates with 0.5 and 1.0 gap ratio, respectively.

F. Auteri et al. [16] performed an experimental investigation on two normal flat plates in tandem arrangement to check the dependency of the flow on the separation between the plates. As they stated there are two different flow regimes as the distance between the plates change. There is also a small interval of separation that both flow regimes are available and change periodically. To get such conclusion the test was executed in an open loop wind tunnel, with turbulence level as low as 0.3%, and 10% solid blockage. The study was done by means of a constant temperature hot wire anemometer and oil smoke visualization at Re=8340. The narrow interval of separation where both flow regimes can be observed is called „critical separation". In this region the wake behavior changes abruptly and the presence of a maximum Strouhal number is almost same as the Strouhal number for the single plate. As the separation increases from the critical separation, the Strouhal number decreases dramatically to reach its minimum.

As the separation distance passes this point it starts increasing slowly to gain the near single plate value as expected. F. Auteriet et al. concluded that the first flow regime exists when the plated are closed to each other ad at this point the flow properties slightly are related to the Reynolds number. They also mentioned that as

the Reynolds number increases the critical separation value increases as well. For the small separation, since there is no enough space for the vortex formation the separated shear layers transit the dead flow region and start shedding behind the downstream plate. This situation is called “one body mode”. For the case of large separation the vortex shedding phenomena is visible behind both upstream and downstream plates. “Dual body mode” is denominated for this case. As a result the shedding frequency depends on the gap vortex dimension as uttered by authors. Also, the changes in Strouhal number depend strongly on the plate separation as it was showed by authors and mentioned in literature.

2.3 Validity of Numerical Analysis in Comparisons with Experiments

Numerical study and the comparison between the results from the numerical and experimental researches are presented in this section. These comparisons have been done to check the eligibility of different numerical methods to apply in different research areas. These efforts made to improve the existed methods or to create new methods.

Gerhard Bosch and Wolfgang Rodi [17] simulated the flow past on square cylinder, which was located at different distance from adjacent wall, at Re= 2.2×10^4 to check the validity and accuracy of numerical method. Equations of two-dimensional unsteady flows were solved together with two versions of $k-\varepsilon$ turbulence model, since the presence of superimposed turbulent fluctuation on the flow in sensible. The standard $k-\varepsilon$ model provide the extensive turbulent kinetic energy in the stagnation region, so as authors stated when the cylinder is relatively close to the wall this model showed steady solution which is in disagreement with the available experiments in the literature. The simulation was performed with modified $k-\varepsilon$

model, (Kato and Launder) which eliminates the unusual production of turbulent kinetic energy. As demonstrated by Gerhard Bosch and Wolfgang Rodi, the vortex shedding production of this modification is in agreement with experiments.

As the square cylinder was adjusted closer to the wall, both turbulence models got the steady state solution which was compatible with the experimental findings. Increasing the gap resulted in the formation of the vortex shedding from both versions of $k-\varepsilon$ models. The shedding for the case of standard $k-\varepsilon$ model was much more damped. They expressed their main conclusion in the way that "the modification of Kato- Launder improves significantly the predictions of vortex shedding flow past a square cylinder also in the presence of an adjacent wall."
Unclear points on the applicability of numerical methods caused KatsuyaEdamoto and Mutsuto Kawahara [18] to do two- (2-D) and three-dimensional (3-D) numerical analysis on the flow around two in-line square cylinders. Finite element analysis was performed for the some range of spacing ratio between the cylinders and for the various Reynolds numbers. The numerical results were compared with wind tunnel results. They interpreted their data by the aid of the time-averaged pressure coefficient graphs at various Reynolds number. According to their findings, the computed time-averaged pressure coefficient was not in the good agreement with the experimental data as the shedding of strong vortices behind the cylinders was observed independent from widely changed Reynolds.

The authors stated that the 2-D analysis is congruous with the experimental data as the spacing ratio between the cylinders was wide or narrow enough. 3-D

computation was found to be consistent with experimental results at Reynolds 10,000. 3-D analysis determined as an effective way to interpret the data in this area.

Jiunn.Chi Wu and Young.Chun Hu [5] did the numerical study on the wake of two circular cylinders with same cross sectional area in both inline and tandem arrangement. The investigation was done for different spacing ratios between cylinders varying from 1.5 to 4.0. Finite difference method was selected as a solution for unsteady Navier-Stokes equations in terms of stream function and vorticity formulation. The flow was simulated at Re=200. The results of their simulation were expresses for different spacing ratios. When the ratio of the longitudinal spacing between cylinders center (L) to the cylinder diameter (D) is equal to 1.5 (L/D=1.5) cylinders are relatively close to each other. At this step for inline cylinders they act more like a single body. Shear layers separated from the front cylinders and reattached to the rear cylinder. Two cylinders act as an elongated body which results in enclosure of cylinders by shear layers. A regular vortex shedding can be seen behind the second cylinder. They also, mention that "flow motions inside the interspace of two cylinders are not stagnant." As L/D increases to 3.0, periodic vortices start forming from two separated shear layers from the upstream cylinder, and reattach alternately at the rear cylinder. Jiunn_Chi Wu and Yung-Chun Hu yield the regular vortex shedding from each cylinder as the spacing ratio exceed 3.8.

Despite of simultaneous vortex shedding from both front and rear cylinders the characteristics of surface pressure, vortex shedding and aerodynamics forces of two cylinders are markedly different. The relationship between the drag coefficient and spacing ratio was also of their concern. As the gap ratio increases, the amount of drag coefficient decreases for the front cylinder, while the drag coefficient of rear cylinder increases. The numerical results of their study was compatible with the pervious experimental works (Ishigai, et al., [19]; Zdravkovish ,[20] and Bearman and Wadcock [21]) for the gap ratio smaller than the critical value. (Critical spacing was taken at L/D= 3.4 ~ 3.8 as reported in experiments. The computed drag coefficient of the upstream cylinder was greater than the other experimental and numerical data. Large eddy simulation (LES) model applied by Chen. L. et al., [22] to analyze the formation and the convection of vortices behind two cylinders arranged side-by-side. Finite element method employed on an unstructured mesh that consisted of hexahedral elements to come through the solution to the three-dimensional Navier-Stokes governing equations. Prediction of the wake dynamics elucidated at Reynolds 750 for two different spacing ratios, the large ratio and the intermediate one. For the case of large spacing ratio, the formation of two symmetrical wake streets observed which is in the agreement with experimental results. As the ratio decreases to some intermediate value, the tendency of gap flow to “flip” observed. Gap squeezing effect and merging the generated vortices behind the cylinders can explain the gap flow behavior. The gap flow deflection that obtained from the numerical simulation was compatible with the experimental observations.

N. N. Mansour et al. [23] simulated the flow fields from a turbulent channel to determine the turbulent kinetic energy (k) and dissipation rate (ε) profiles. Two equation $k-\varepsilon$ model was used to imitate the flow to interpret the dependency of the eddy viscosity damping function on the both Reynolds number and distance from the wall. The authors stated that the existing transport models must be improved in the near wall region. Long time-scale simulations, of vortex shedding in unsteady flow past a thin plate placed orthogonal to the flow direction, were performed by H.R. Tamaddon et al. [24] to check the validity of Taylor-Galerkin/pressure-correction finite element algorithm for solving the transient Navier-Stokes equations and complex unsteady problems. The flow characteristics were studied at Reynolds 1.2625×10^5 and 500. The investigations were done in two different cases, unperturbed flow and perturbed flow. According to observations flows started from steady state and after some time the vortex shedding phenomenon occurred. This phenomenon happened for both unperturbed and perturbed flows. The flow perturbations were done, firstly by positioning the plate vertical to the flow direction and moving it upward by half of a plate size and then moving it down and downer, again by the half of the plate length. Changing the inlet boundary conditions in a way to set the velocity of half the inlet nodes equal to zero and the rest of nodes equal to twice the free stream velocity is the second way to apply perturbations on the flow. As H.R. Tamaddon Jahromi et al concluded the vortices started shedding in the first approach of perturbed flown 200 seconds sooner than the case of unperturbed. And this matter happened some300 seconds sooner in the second approach of perturbation in compare with the first approach.

They also mentioned that these disturbances have no effects on the shedding frequency, and the Strouhal number computed from the periodic shedding was same with the case of unperturbed flow as expected. The results of this study are compatible with the previous results of the experimental investigation, numerical results and pictorial results. So, they found their method, obviously capable of solving problems engaged with long time scales of operation, and determined it as a powerful tool to analyze such unsteady problems.

Unsteady flow behind a flat plate located perpendicular to the flow direction was simulated by D.S. Joshi et al., [25]. This numerical investigation carried out by integrating the three-dimensional unsteady Navier-Stokes equations. Second order accuracy in time and space were considered in a finite-volume numerical scheme. The three-dimensional results were compared with the comparable two-dimensional at Reynolds 1000.

Obvious differences between the two-dimensional and three-dimensional results were observed. The computed value for the drag coefficient in 2-D analysis oscillates at twice the vortex shedding frequency with the higher mean value than the obtained value from experiment. But in three-dimensional analysis this value is relatively close to the experimental value. The mean velocities are compatible with the experimental results, but the root mean square (rms) quantities are slightly higher than the experimental values. According to researchers the three-dimensional simulation seems more suitable for the interpretation of flow in this area.

Robert N. Merney et al. [26] executed experimental and numerical simulations on the flow and dispersion of gasses, released by the sources in the vicinity of the different building shapes. These studies were done in various wind tunnels for the experimental part of the research and the numerical analysis were fulfilled by FLUENT and FLUENT/UNS utilizing $k-\varepsilon$ standard, RNG $k-\varepsilon$, and Reynolds stress model (RSM) approximations. The results from the both sections were compared to check the eligibility of turbulence model for this case. According to the researchers, the RSM turbulence model gave the more realistic results in comparison with the standard and RNG $k-\varepsilon$ models.

H. M. Skye et al. [27] provided the study on the vortex tube by the aid of both computational fluid dynamics and experimental measurements which taken by applying a commercially available vortex tube. Two-dimensional, steady axisymmetric model simulated by two turbulence model, the standard and renormalized (RNG) $k-\varepsilon$ models, specially, to measure the inlet and outlet temperature of the tube. Experimental and computational results were compared, and the successful use of CDF in this regard confirmed. As a result, CFD can be used as a powerful tool which has the ability to optimize the vortex tube design.

As it was mentioned in the introduction part of this chapter the numbers of researches on the comparison between the experiments and CFD results are the strong reasons to make the use of this new technology as a necessary part of each research to minimize the restrictions of CFD.

Chapter 3

METHODOLOGY

3.1 Introduction

The analysis needed to find a particular turbulent system that is legitimate in the computational flow dynamics in the upsurge of bluff bodies, in addition to the impacts of variety in the separating proportion in these bodies which are in a fluid. A quantifiable examination carried out on the wake properties of the 2D flow, was from two typical level plates arranged behind each other with different gap ratio and angle. Control volume strategy tried to change with the differentiable equations with the algebraic ones computing them arithmetically and achieving a result that fits fulfilling an administering conditions for each and every component of grid. The structural study utilized the perception of computational flow dynamic information methods with guides of its diagrams/outlines to examine stream qualities keeping in mind the end goal is to contrast the outcomes and the past experiment. In order to create the consequences of the observational study practically, identical to past investigations was used as a kind of perspective by Hasan Hacisevkis‟s test [28] (Appendix A). The test examination was carried out in an open sort of low velocity wind tunnel with a space for testing measuring $0.5 \times 0.5\ m^2$ and a dimension of 1.5m. Two plates were found typical to the air bearing in passage as vortex shedders with 30mm breadth 500mm, stature 6mm and depth measurements.

The underlying states of the specified investigations, for example, the speed channel, weight of the framework and so forth were expected as info information for the

numerical examination. The research was performed in two stages: pre-preparing by ANSYS/FLUENT 13.0® business framework generator and codes individually, handling with ANSYS/FLUENT13.0® lastly post-preparing by ANSYS/FLUENT13.0®.

3.2 Pre-Processing

3.2.1 Geometry Modeling and Grid Generation

All the chosen bodies as vortex shedders were found in a particular course and the cross sectional zone heading in a steady way with no big difference in the bearing as the stream was typical to the body, It was a two dimensional model because the issue could be portrayed in one plane [29]. Base up methodology was utilized to make the geometry of the model. Vortex's which were produced as low dimensional elements and afterward lines and faces made a high dimensional element. Wind passage was determined to be sufficiently enormous to accommodate the model to keep the impacts of divider obstruction and obstruction to the structure. Obstruction which is the proportion of the models frontal region to the test segment must not be exactly as showed by [4] and it should be under 5% as stated by [30]. Wind passage was drawn as a 2D rectangular geometry with 1.5m×0.5m measurements.

Two level plates with 30mm breadth and 60mm thickness were in the rectangle. Dispersing between the plates was dictated by various crevice proportions.

Gap proportion decided as non-dimensional proportion which is the proportion of gap between the plates to the width of the plates g/d. The crevice proportion ranges from 0.276 to 2 in this study. As the geometry displaying finished, the pre-preparing moved to its next stride which was network era.

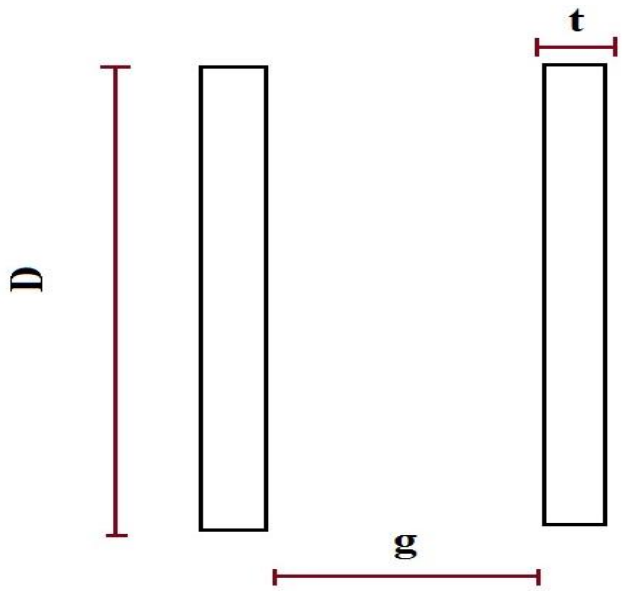

Figure 1.gap ratio definition

The cross section characterized, by point of the venture and the way that stream expected to be investigated. Framework era is an imperative piece of computational fluid dynamics issues that requires a high determination in the areas that the demonstration of stream is touchier with a specific end goal to diminish the blunder, memory squandering and the joining time. High thickness cross section was needed in the bounded layers. The networks must be adequately fine to determine the stream. With a specific end goal to spare memory and time, the quantity of components that are accessible are far from the plates and wake of the bluff bodies, were much lower than the quantity of components in complex parts. Poorly structured quadrilateral matrix innovation was taken into account with nearness of blending component sort. Clearing required for quads production in 2D was naturally executed. Estimations of the mesh quality are not total but could help with the upgrades of the framework. The nature of cross section can be checked in ANSYS/FLUENT 13.0® projects.

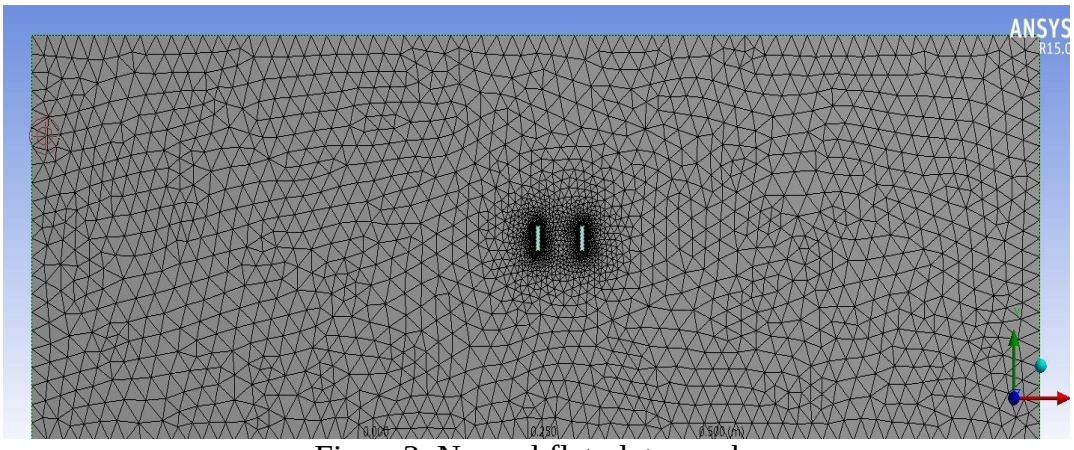

Figure2. Normal flat plate mesh

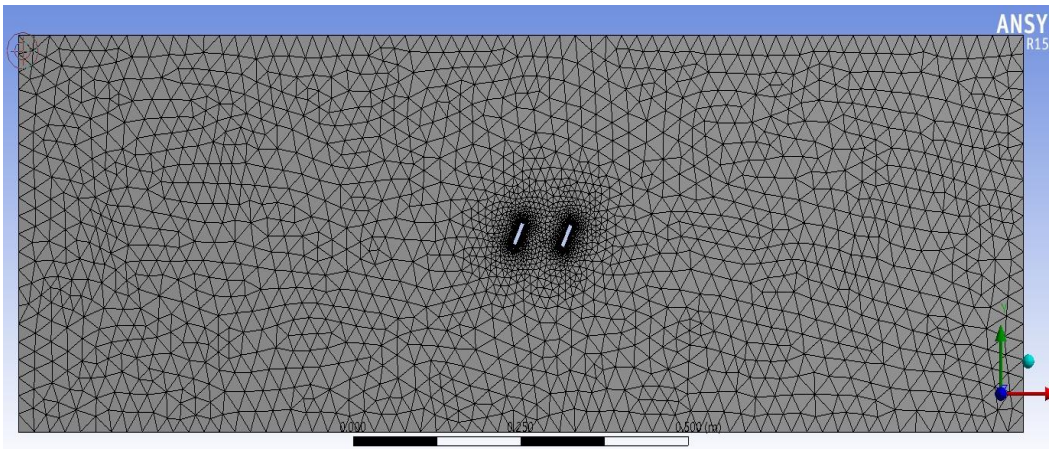

Figure3. Inclined flat plate mesh

Diverse terminologies are accessible for demonstrating the amount of quality for the cross section, for example, skewness, viewpoint proportion and quality of the orthogonal structure. A most extreme satisfactory estimation of the skewness amount is 0.5.A lower the skewness results to a better cross section quality. There are three distinct sorts of limit zones; speed gulf, out stream and divider.

3.2.2 Problem Set Up

Arrangement of the computational flow model depends on an oversight condition for the liquid stream which explains preservation laws of material science numerically. The computational flow dynamics program has been intended to comply with these guidelines which have given results while breaking down the liquid stream [31];

- The mass of liquid is monitored which implies the rate of expansion of mass in liquid component is equivalent to the net rate of stream of mass into liquid component (progression condition is the scientific articulation of this law),

$$\frac{\partial \rho}{\partial t} + \frac{\partial (\rho u)}{\partial x} + \frac{\partial (\rho v)}{\partial y} + \frac{\partial (\rho w)}{\partial z} = 0 \quad (3.1)$$

Where,

ρ is density of the fluid,

u, v, w are the velocities in x, y and z direction, respectively.

- The rate of change of momentum equals the sum of the forces on a fluid particle (Newton"s second law),

x-Momentum

$$\frac{\delta(\rho u)}{\delta t} + \text{div}\,(\rho u u) = -\frac{\partial p}{\partial x} + \text{div}(\mu\ \text{grad}\ u) + S_{Mx} \quad (3.2)$$

y-Momentum

$$\frac{\delta(\rho v)}{\delta t} + \text{div}\,(\rho v u) = -\frac{\partial p}{\partial y} + \text{div}(\mu\ \text{grad}\ v) + S_{My} \quad (3.3)$$

z-Momentum

$$\frac{\delta(\rho w)}{\delta t} + \text{div}\,(\rho w u) = -\frac{\partial p}{\partial y} + \text{div}(\mu\ \text{grad}\ w) + S_{Mz} \quad (3.4)$$

Where, P = Pressure,

S_{Mx}, S_{My}, S_{Mz} are total force on the element due to body forces in x, y and z directions, respectively.

- The branch of physical science that deals with the relations between heat and other forms of energy (such as mechanical, electrical, or chemical energy),

and, by extension, of the relationships between all forms of energy. (first law of thermodynamics).

$$\rho C_P \left(u\frac{\partial t}{\partial x} + v\frac{\partial t}{\partial y} + w\frac{\partial t}{\partial z}\right) = \beta T \left(u\frac{\partial p}{\partial x} + v\frac{\partial p}{\partial y} + w\frac{\partial p}{\partial z}\right) + div\ (k\ divT) + \phi \qquad (3.5)$$

Where, C_P = Specific heat at constant

T = Temperature

β = Coefficient of thermal expansion

Φ = Dissipation function

3.2.3 Turbulence Modeling

Determining the thickness model of this flow was the next stage. For the most parts, three sorts of gooey model exist; laminar, inviscid, and turbulent, their choices on them relies upon the estimation of their Reynold's value. Vortices which is the arrangement and shedding of moving liquid pieces as the flow goes through long cylinders, for Reynolds more prominent than 90 (the Reynolds number for the under scrutiny stream is 33000). Speed vacillations brought about by vortices result in the ascent in extra weights on the liquid which are called Reynolds focuses on that could be recreated by the turbulent gooey model. More transport conditions must be understood as the stream get to be turbulent to speak to the turbulent properties of the stream. Distinctive sorts of turbulence models are accessible in the ANSYS/FLUENT 13.0 ® program that is displayed in the Appendix E. These models are arranged by nearness of transport conditions in every model. Sadly, there is no single turbulence model that is all around acknowledged to be unrivaled for all classes of the issues. Distinctive variables, for example, the material science covering the stream, the accessible measure of time, required level of exactness and the available computational assets, impacts the decision of turbulence models. Also, comprehending the capacities and impediments of the different choices could help select the most proper models. The $k-\omega$ shear-stress transport (SST) model and the straight weight strain Reynolds stress model were chosen for this issue. The $k-\omega$ model comprises of two transport conditions for turbulent dynamic vitality with a particular dissemination rate that is analyzed in Appendix B.

The $k-\omega$ SST model is great in anticipating the antagonistic weight inclinations in limit layers and isolating streams. What's more, there is no compelling reason to demonstrate any additional damping capacities as they could be utilized as a low-Reynolds turbulence models. These reasons together with, the vigor and broadly use of this turbulence model in streamlined streams brought on the usage of this model in this study.

The RSM turbulence model comprises of five transport conditions in 2-D streams which are the vehicle conditions for the Reynolds, focuses together with one condition for the scattering rate. The primary reason for applying the RSM model as a gooey model was the immediate calculation of the Reynolds stresses in its methodology. Reynolds stresses $u'^2, v'^2, u'v'$ could be surveyed by the guide of this model. Weight strain Reynolds stress model (RSM) together with the improved divider treatment (EWT) approach performed to figure the Reynolds stresses. The vehicle conditions utilized for this model have been exhibited in the Appendix B. The weight inclination impacts choice were additionally empowered as the upgraded divider treatment choices to give more precise results in divider limit layers. Since there is no variety in thickness of the stream, there is no relationship between the vitality condition and protection of mass and energy. Be that as it may, the choice which empowers the count of the vitality condition was turn on so as to get data in regards with energy.

3.2.4 Initial and Boundary Conditions

The following stride was to characterize the underlying and limit states of computational fluid dynamics issue which are vital to be spoken to precisely in the model for computation. The limit conditions were utilized by ANSYS/FLUENT 13.0® to consider the mass stream along with the area, fluxes of force, vitality, and species through the channel. As it was specified, three limit zones were recognized in the Gambit 2.2.30 ® program. The underlying states of this study are same as the accessible information from the test that was under scrutiny. In the speed channel limit zone the greatness of the air speed was considered as $16.4 \pm 0.02\ (m/s)$ ordinary to the limit and in X-heading. The turbulence determination strategy indicated 0.8% turbulent force together with 0.0021 (m) turbulent length scale. The underlying temperature was taken at 289.75K. No slip conditions were resolved for the dividers that were stationary. Also, the stream rate weighting was considered as 1 since there was stand out surge in the limit zone.

3.3 Processing

The achievement in the CFD can be controlled by three scientific ideas called, joining, consistency and solidness. Arrangement setup and the computation undertakings are composed at this part to fulfill these contemplations. The joining is characterized as a property of numerical strategy that achieves the accurate arrangement as the separation of matrix diminished to zero. In other word, the model is numerically merged as the estimations of the whole under scrutiny space encounter no noteworthy changes from the present cycle to the following. Consistency in numerical plans results in the arrangement of frameworks of mathematical conditions that are similarly as the first overseeing conditions as the mesh distances reduces to zero. The last numerical idea which manages damping the mistakes as the issue is in its handling level is its resilience.

3.3.1 Spatial Discretization Scheme

The velocity which confluences and the required memory space for the code are more than the isolated ones. As per the dimension of the mesh and the accessible memory of the PC, the isolated calculation was favored over the coupled calculation for the weight speed coupling technique in the weight based solver. The ANSYS/FLUENT13.0® project is fit for performing three isolated speed coupling calculations. The Pressure-Implicit with Splitting of Operators (PISO) was chosen over the other weight speed coupling plans as it is prescribed for every single transient stream. This plan depends on the higher level of the inexact connection between the remedies for weight and speed.

The PISO calculation created two extra revision, neighbor amendment and skewness redress, to enhance the effectiveness of the computation of force. Force redress or "neighbor revision" diminish the quantity of rehashed counts, in the arrangement phase of weight rectification condition, required by other weight speed coupling plans to fulfill the congruity and energy conditions all the more nearly. The PISO calculation devours more CPU time per solver cycle and lessens the quantity of emphases to accomplish the joining. Another iterative procedure comparative to the neighborو amendment is required to recognize the segments of the pressure coefficient average as they are not known on cell faces. This procedure is called "skewness correction" lessens the issues connected with union with exceedingly mutilated cross sections. One more emphasis of skewness remedy executed over the neighbor redress for every different cycle to acquire high exactness modification of the face mass flux revision in the ordinary weight rectification slope.

Discretization plans were distinguished to unravel the substitution and dispersion terms in the way the equation dealt with the conservative law of science. The minimum square cell-base technique gave an answer for slopes. This technique is widely accepted in view of its high exactness and minimal effort (as far as calculation) and its ability to perform on improper lattices. The "normal" strategy connected for the additional weight plan as it is adequate for generally cases. A 2nd request up-wind discretization’s were chosen for the force plus energy conditions due to the more exact results that are acquired from this plan. Transient definition was made by iterative time-headway plan. This strategy unravels every condition on characterizing a time frame, necessary to meet the joining criteria. Accordingly, quantities of external cycles were needed for every time-step.

The limited second request understood was chosen as transient detailing, which gives preferable solidness over alternate definitions. Transient formulation was selected as implicitly second bounded order that produces greater balance over alternate definitions. The limited second request is in arrangement with the second request verifiable regarding precision.

The under-unwinding elements, which have been identified with every amount of the vehicle conditions, relating with time and step size are alternate variables which have impact on the joining troubles. Little changes in the elements results in adjustments in joining velocity. These under unwinding components are recognized to be near the ideal qualities to accelerate the joining. The supreme joining measure which thinks about the remaining of every condition in emphasis with a client indicated esteem at the introduction part was chosen together with the scaled leftover. Moderately little stride size ($2e-4second$) was represented as the time-step size to meet the joining and dependability criteria. The level required for residual changes as per the predetermined system. Information was auto-stored after every hundred minutes in order to have the adjustments in each 0.02 second.

3.4 Post-Processing

Post preparing which depicts the flows conduct by the guide of diagrams, reports and graphs is the last stage of the system. We can see how the project is continuing through reports, for instance the estimations of many stream rate must be equivalent in extent at in and out limits which is acquired in every dissected model of this research.

3.5 Verification of CFD Codes

The CFD program checked the residual, meeting of cycles at an interval were represented which is the declaration of fulfilling the idea for convergence. The protection laws of material science were fulfilled which demonstrates the compatibility in the outcomes.

Chapter 4

RESULTS

4.1-Introduction

Utilization of Computational Flow Dynamics and correlation of test information for verification and validation of the method used is the point of this research and it is completed in the following way:

- Accessible exploratory information is as a result of consequences on examinations of two sound and muddled geometry of stream behind two couple level plates.

- Computational flow dynamics examination was done with similar issue taking after gap proportions:

  g/d = 0.267, 05, 1.0 , 1.5 and 2.0

  The consequences of this research includes;

- Outcomes for the crevice proportions of 0.5, 1.0 and 2.0 could be contrasted and the accessible exploratory information that was exhibited in the following segments. The correlation demonstrates a capacity of the computational flow dynamics in similar ways.

4.2 Analysis Results

The program that made use of the pre-mentioned research is the ANSYS/FLUENT 13.0®.The reliable program generates important results which are in graphical forms, that provide a better comprehension of the flows attitude. This research encompasses the investigation of the flow of around bluff bodies with 6 varying space proportions. Portraying a general result is avoided except in situations where there is a 0.267 gap proportion which is examined by the $k-\omega$ SST system as most outcomes, results from graphs are represented below.

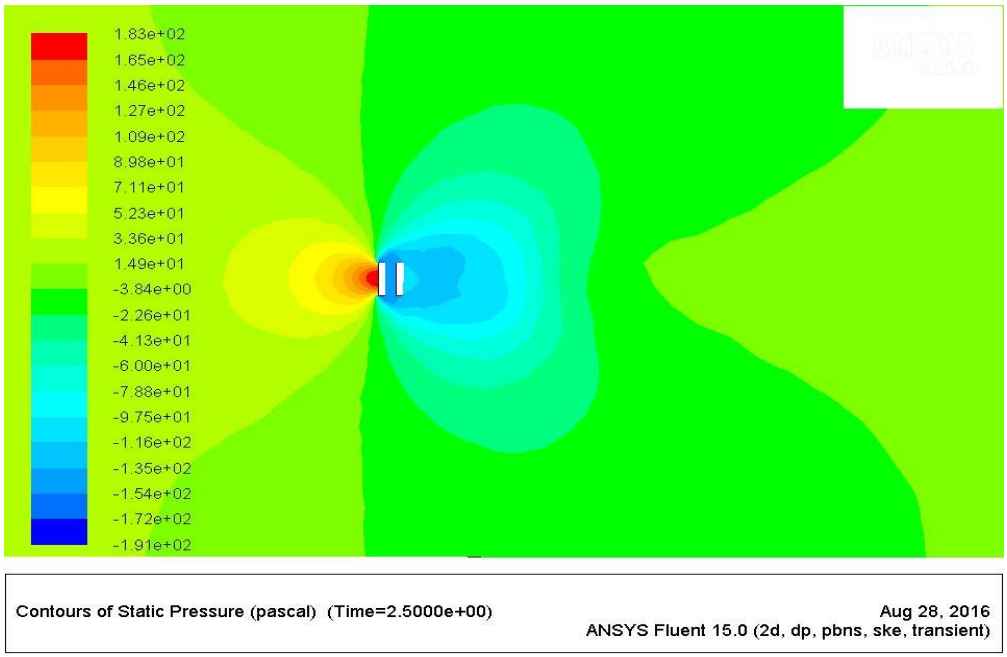

Figure 4. Contours of Static Pressure (Pa), at gap ratio=0.276

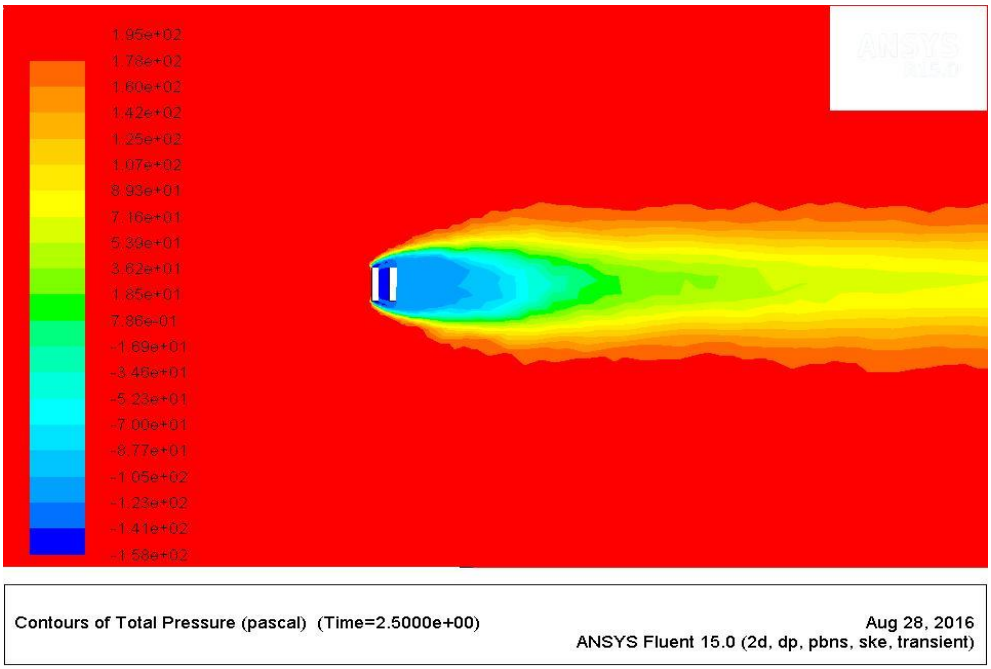

Figure 5. Contours of Total Pressure (Pa), at gap ratio =0.276

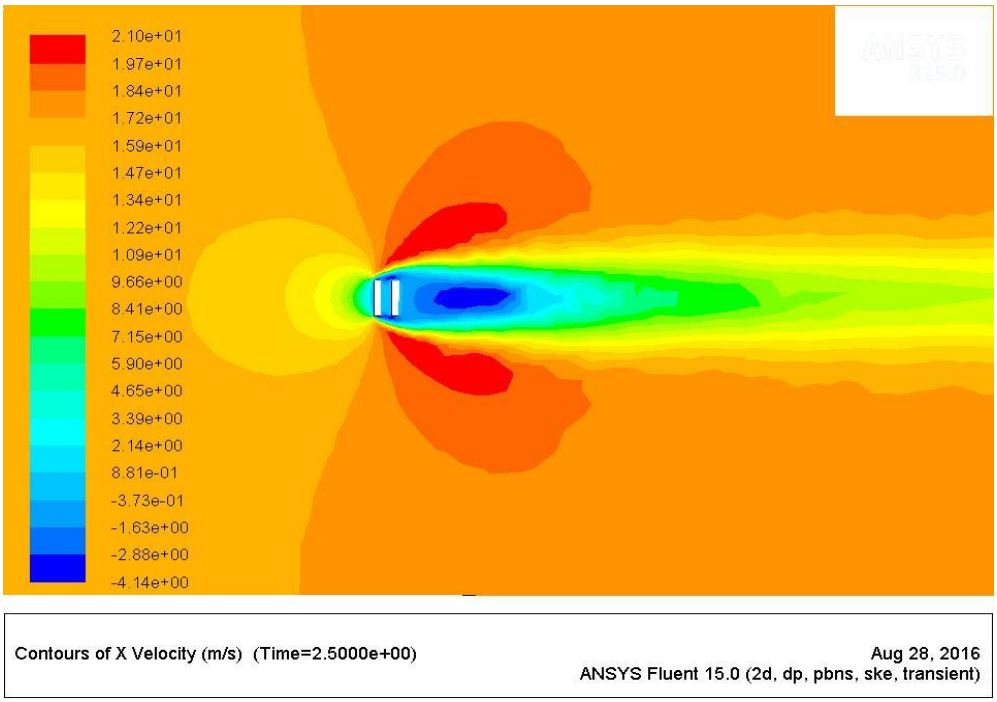

Figure 6. Contours of X-Velocity (m/s) , at gap ratio =0.276

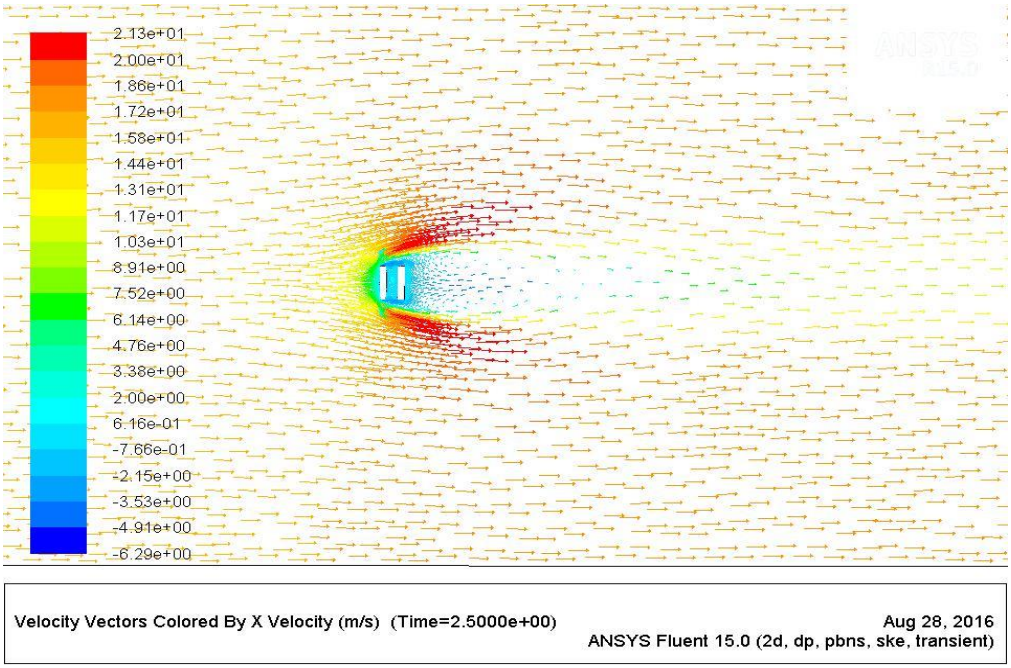

Figure 7. Velocity Vectors Colored by X-Velocity, at gap ratio =0.276

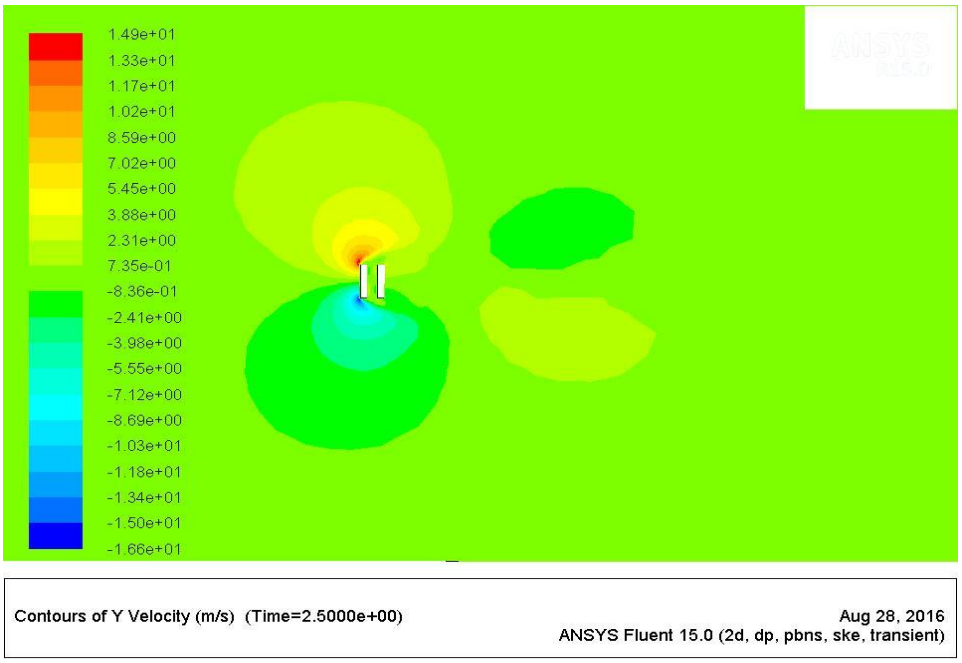

Figure 8. Contours of Y-Velocity (m/s) , at gap ratio =0.276

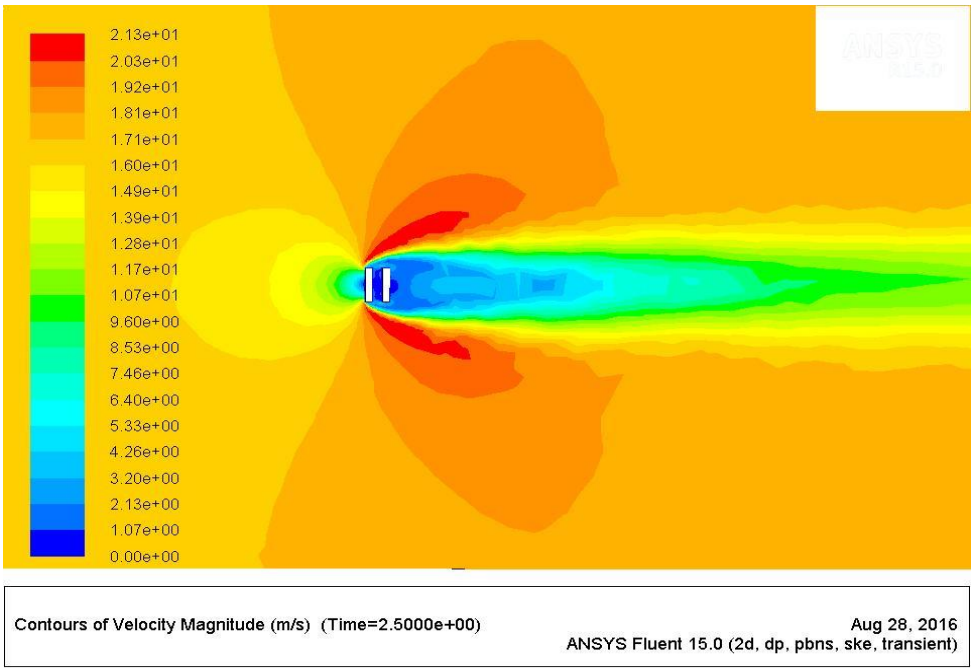

Figure 9. Contours of Velocity Magnitude (m/s), at gap ratio =0.276

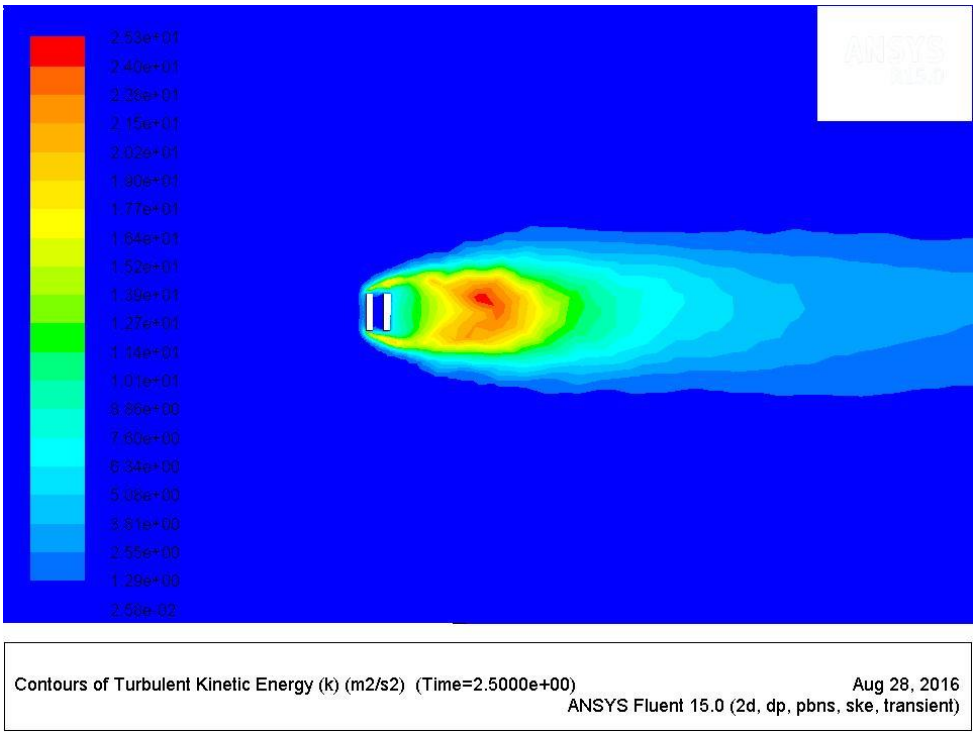

Figure 10. Contours of Turbulent Kinetic Energy (k) (m^2/s^2), at gap ratio =0.276

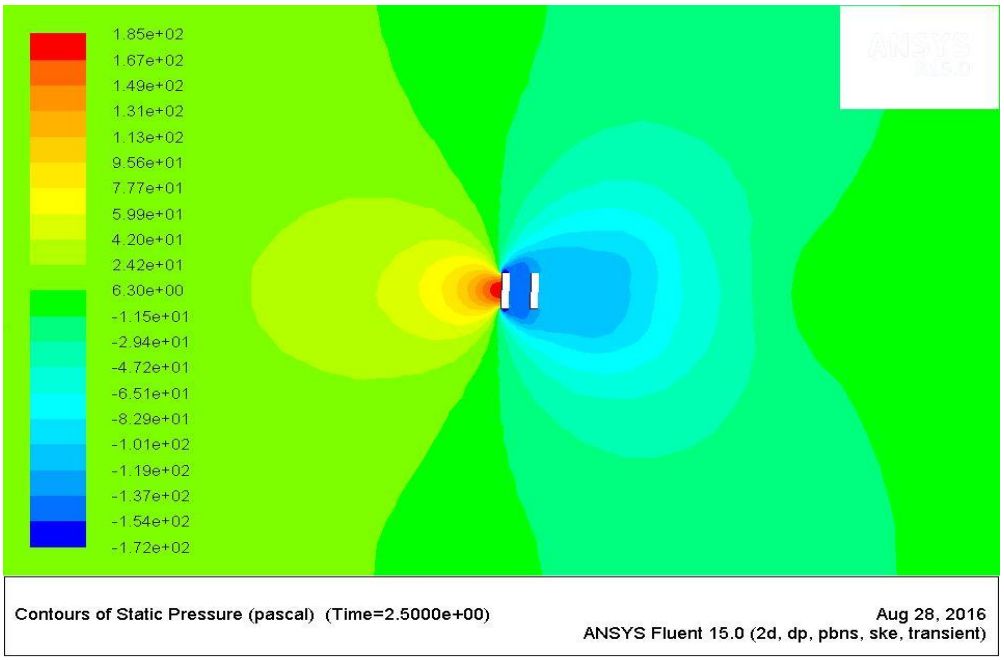

Figure 11. Contours of Static Pressure (Pa), at gap ratio=0.5

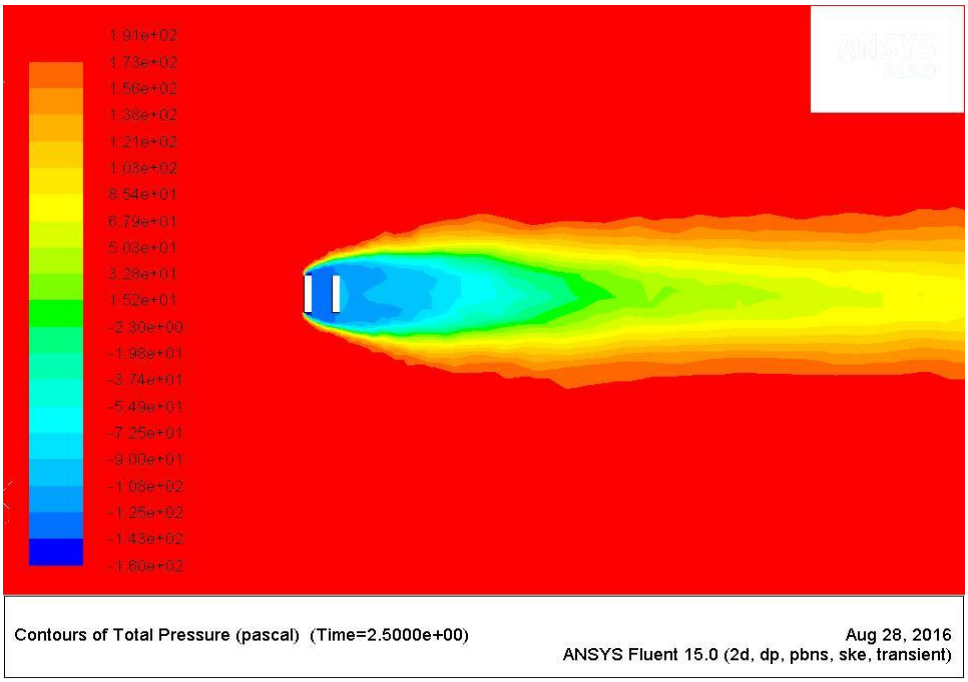

Figure 12. Contours of Total Pressure (Pa), at gap ratio=0.5

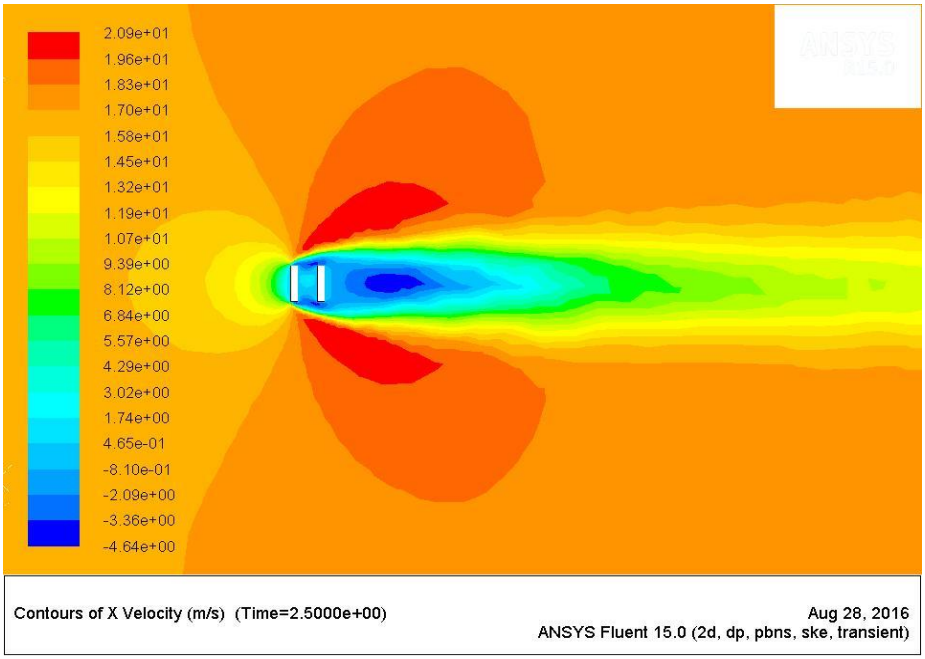

Figure 13. Contours of X-Velocity (m/s) , at gap ratio =0.5

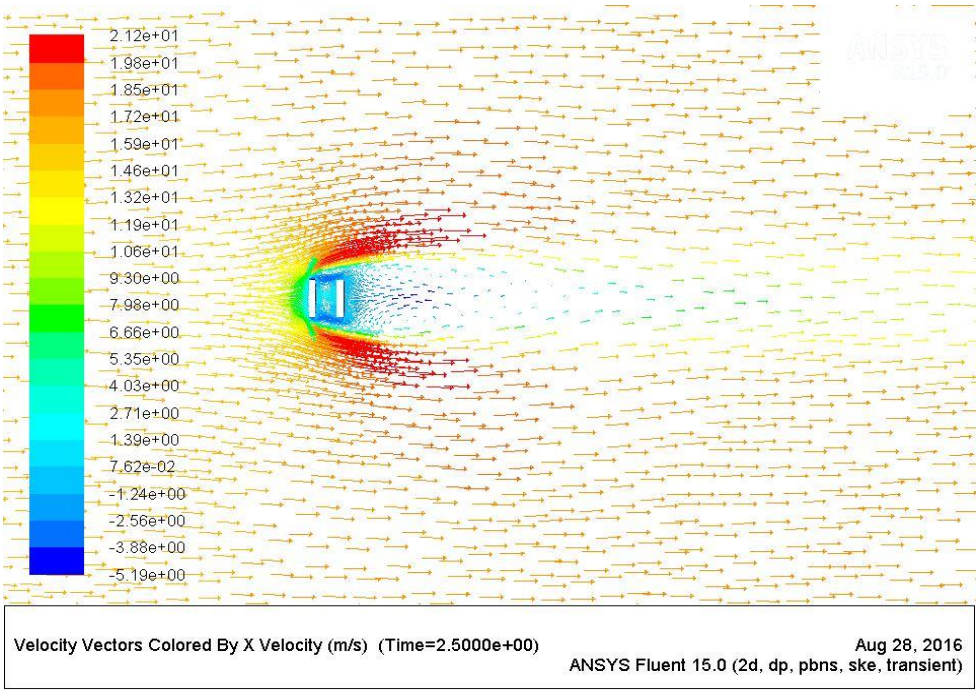

Figure 14. Velocity Vectors Colored by X-Velocity, at gap ratio =0.5

Figure 15. Contours of Y-Velocity (m/s) , at gap ratio =0.5

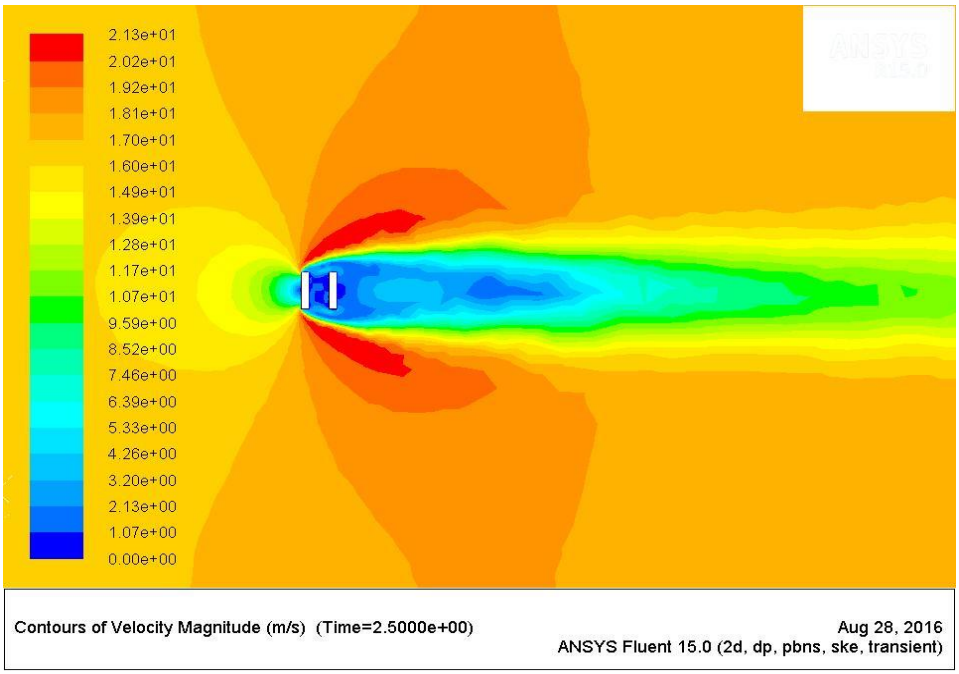

Figure 16. Contours of Velocity Magnitude (m/s), at gap ratio =0.5

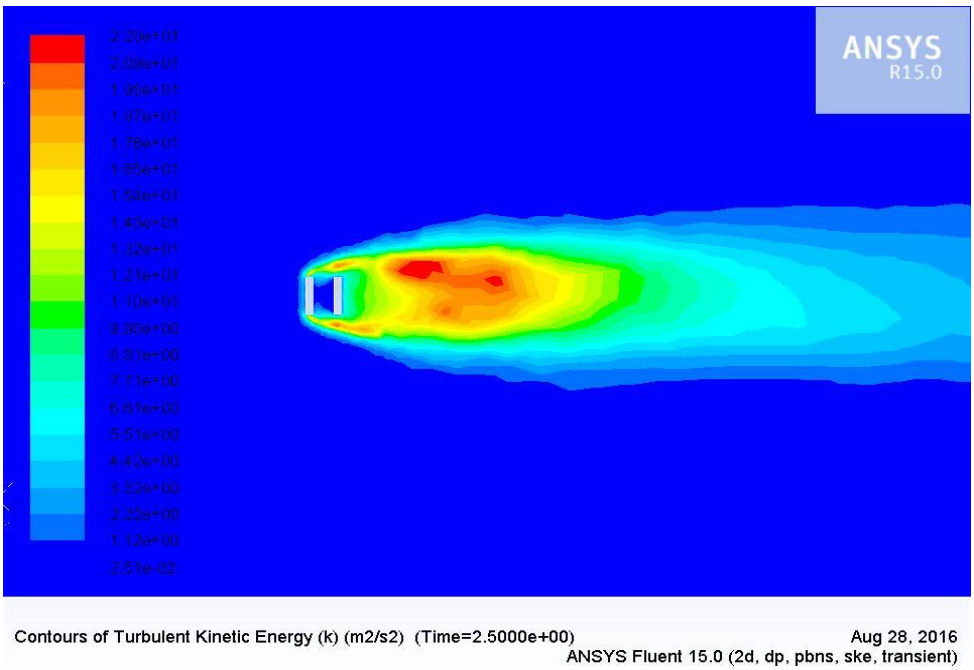

Figure 17. Contours of Turbulent Kinetic Energy (k) (m^2/s^2), at gap ratio =0.5

In figure 4 – 17 shows the normal flat plate by gap ratio 0.276 and 0.5 because of the distance between two plates there are no vortex shedding behind the second plate also in gap ratio 0.276 vortex is not developed between two plates but in gap ratio 0.5 there is more development as this is shown in vector x - velocity.

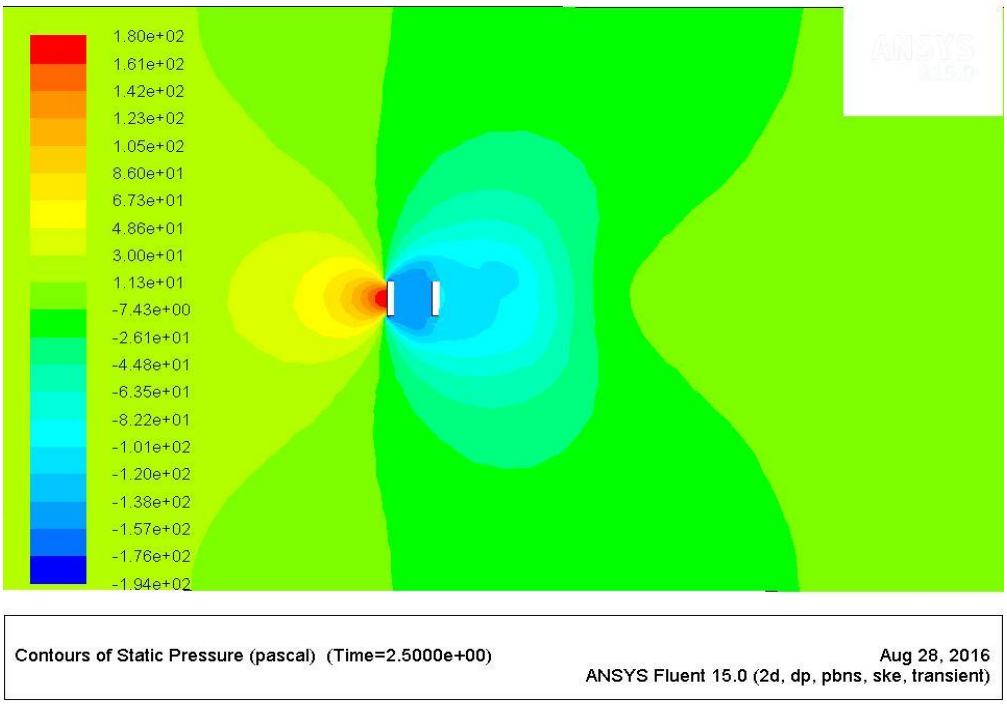

Figure 18. Contours of Static Pressure (Pa), at gap ratio=1.0

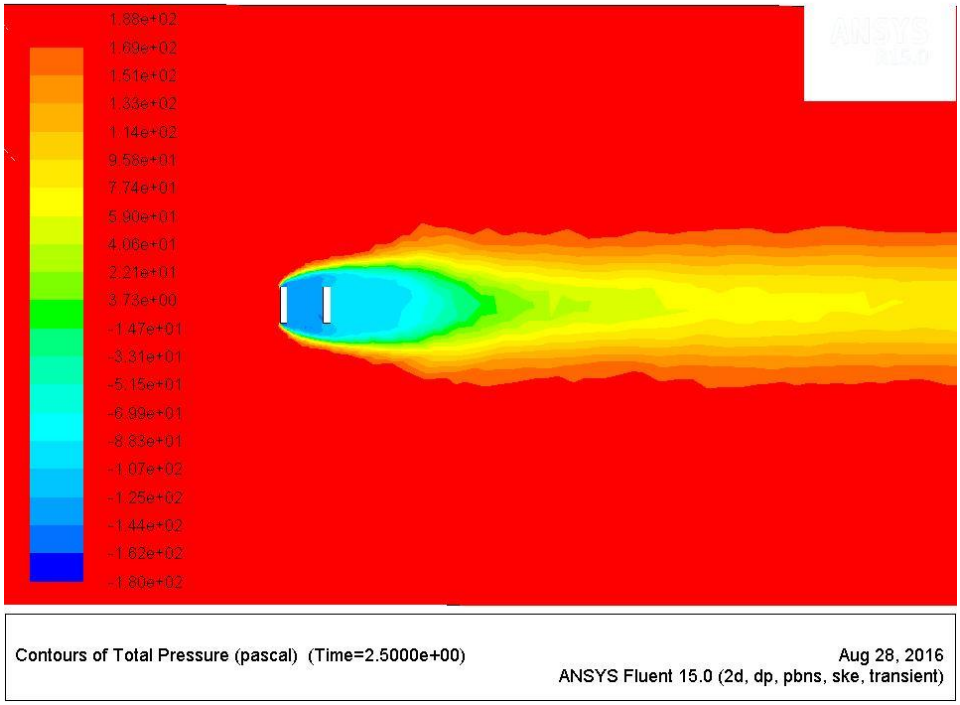

Figure 19. Contours of Total Pressure (Pa), at gap ratio=1.0

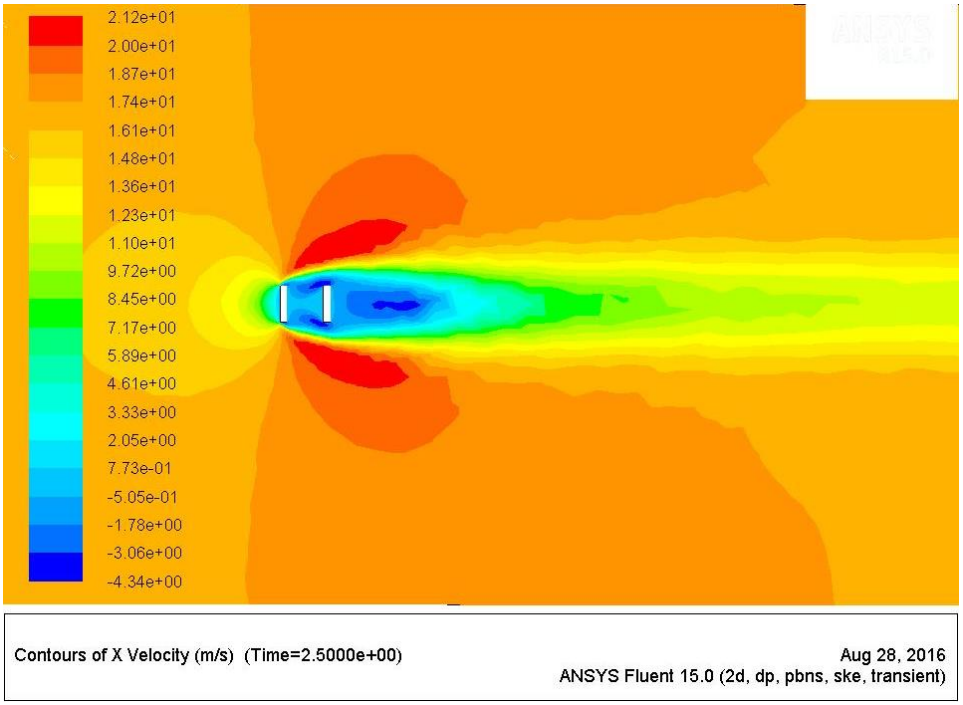

Figure 20. Contours of X-Velocity (m/s) , at gap ratio =1.0

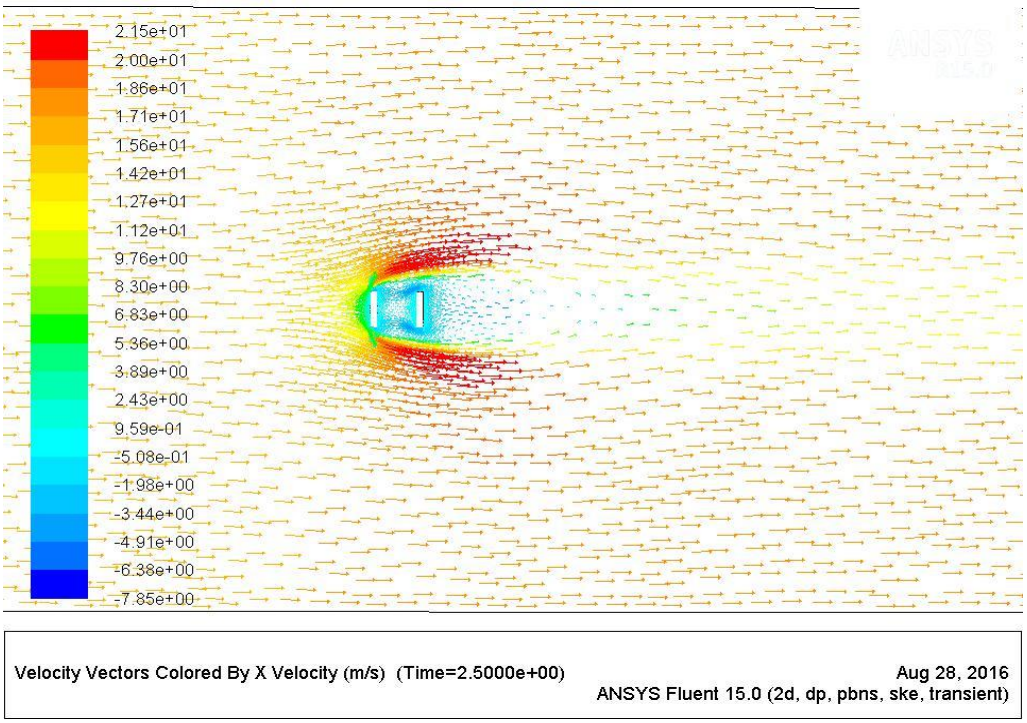

Figure 21. Velocity Vectors Colored by X-Velocity , at gap ratio =1.0

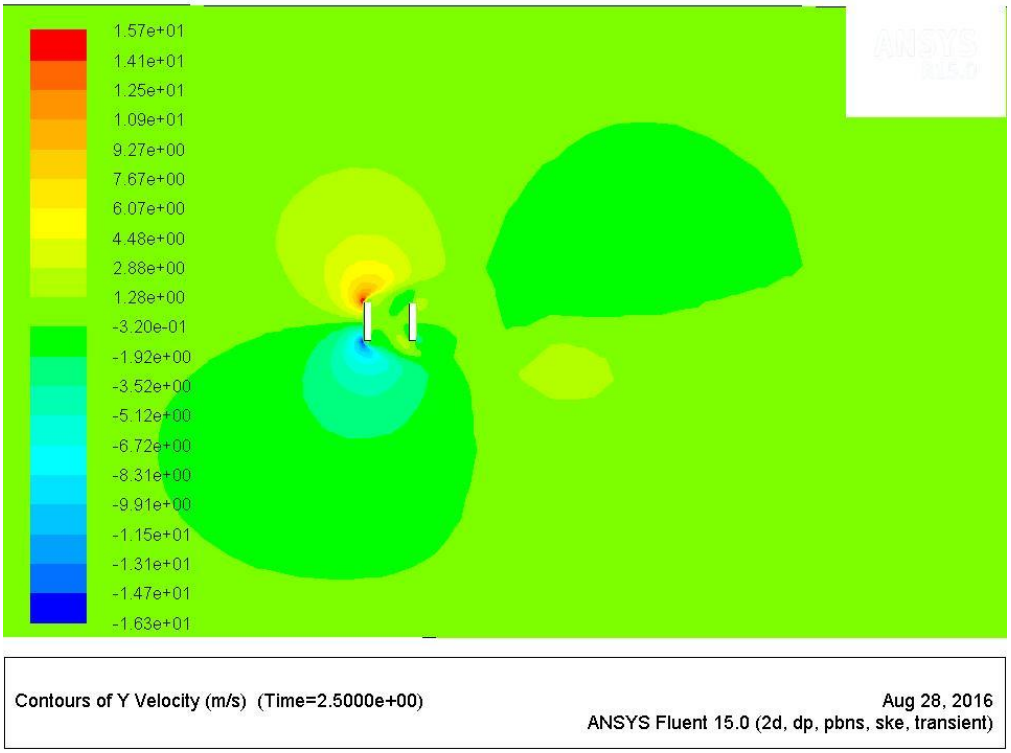

Figure 22. Contours of Y-Velocity (m/s), at gap ratio =1.0

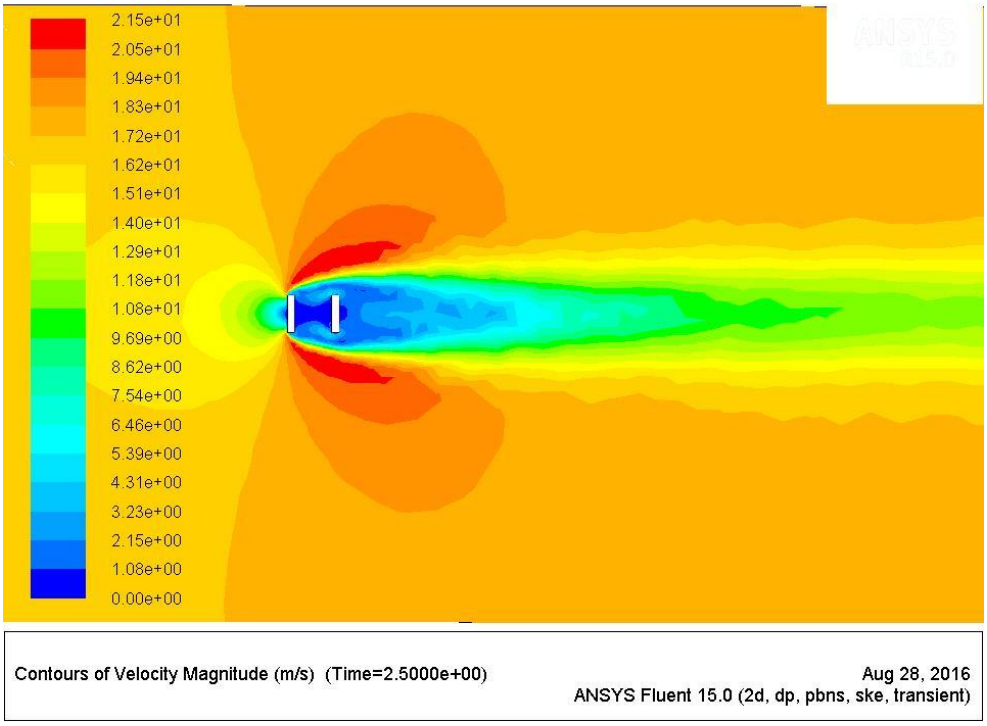

Figure 23. Contours of Velocity Magnitude (m/s), at gap ratio =1.0

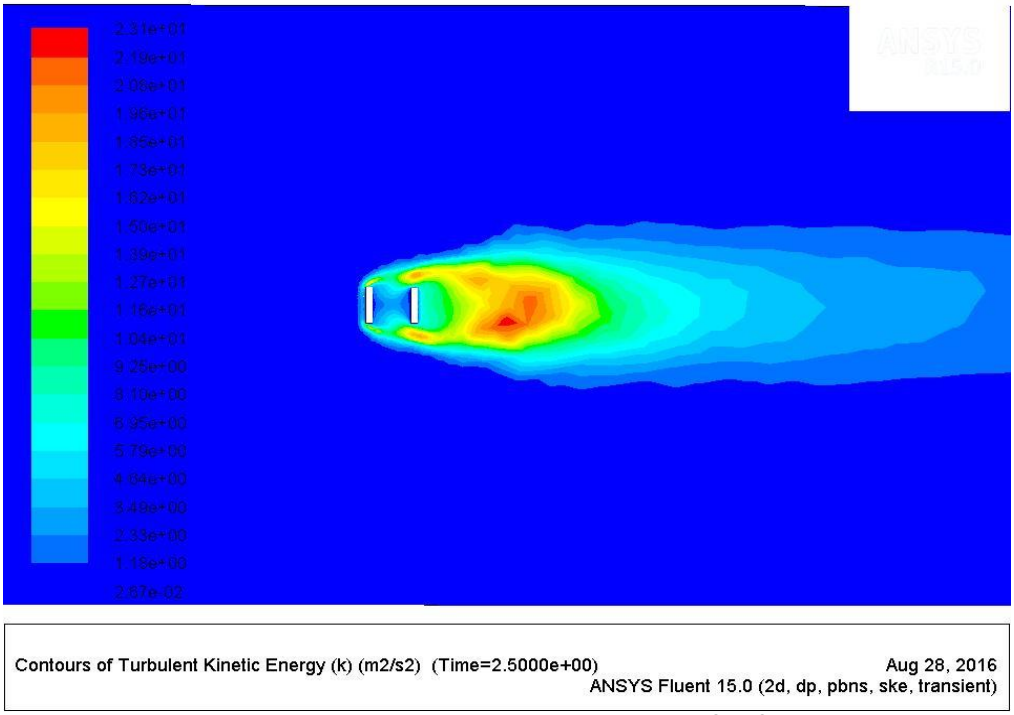

Figure 24. Contours of Turbulent Kinetic Energy (k) (m^2/s^2), at gap ratio =1.0

Last figures 18 – 24 shows two normal flat plates by gap ratio 1.0, between two plates vortex shedding also appears behind the second plate in figure 24. Contours of turbulent kinetic energy is found behind the second plate as there is still no developed vortex shedding.

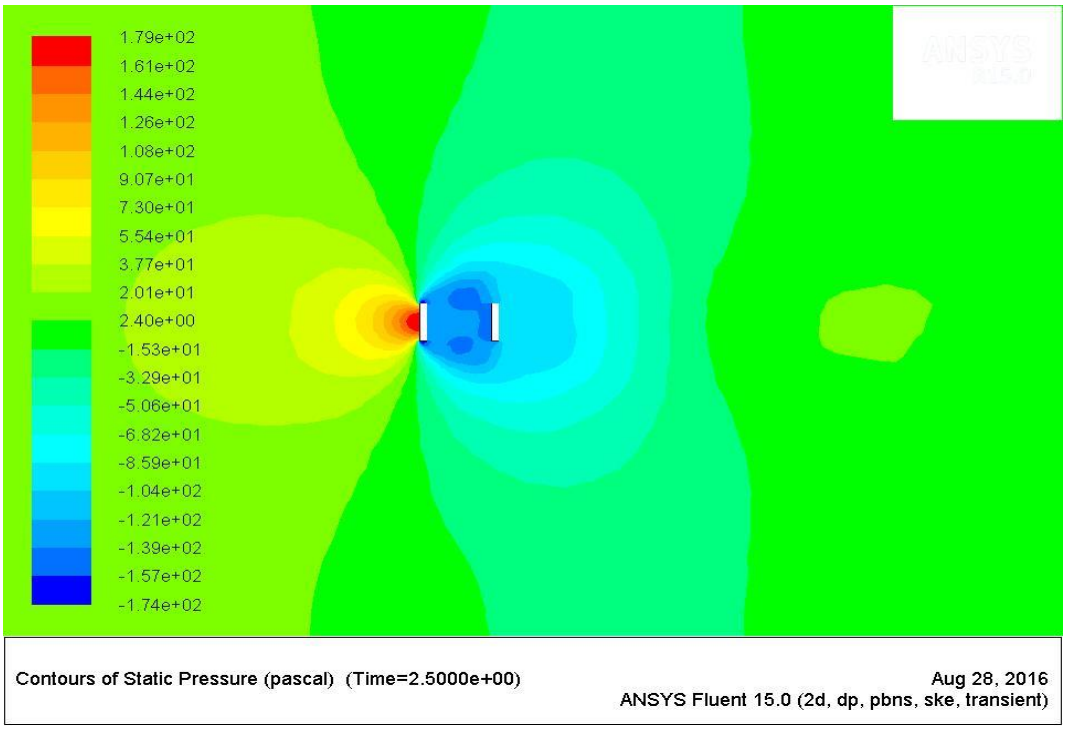

Figure 25. Contours of Static Pressure (Pa), at gap ratio=1.5

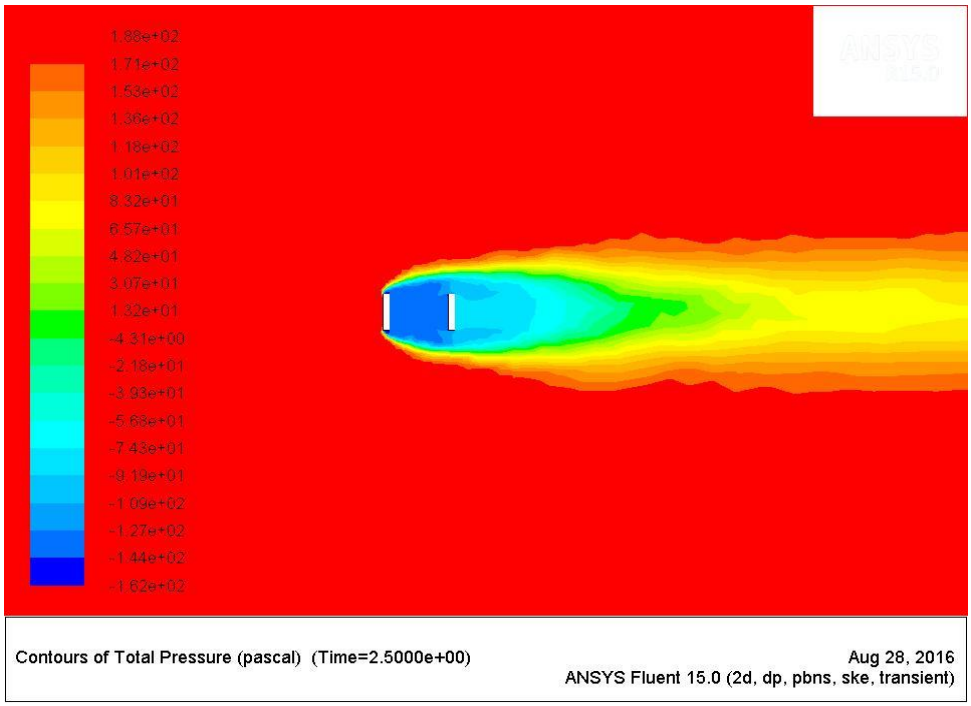

Figure 26. Contours of Total Pressure (Pa), at gap ratio=1.5

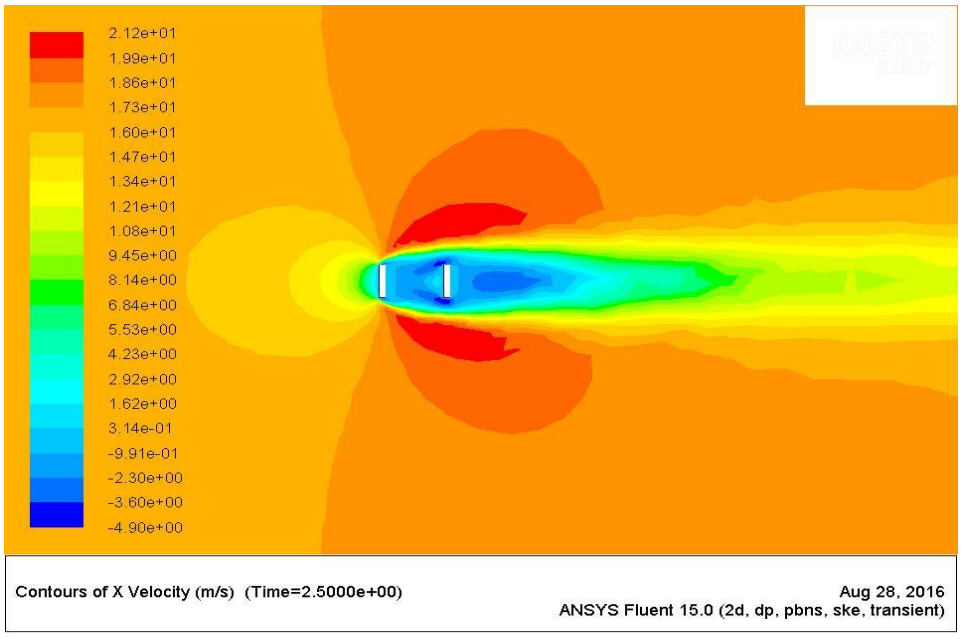

Figure 27. Contours of X-Velocity (m/s) , at gap ratio =1.5

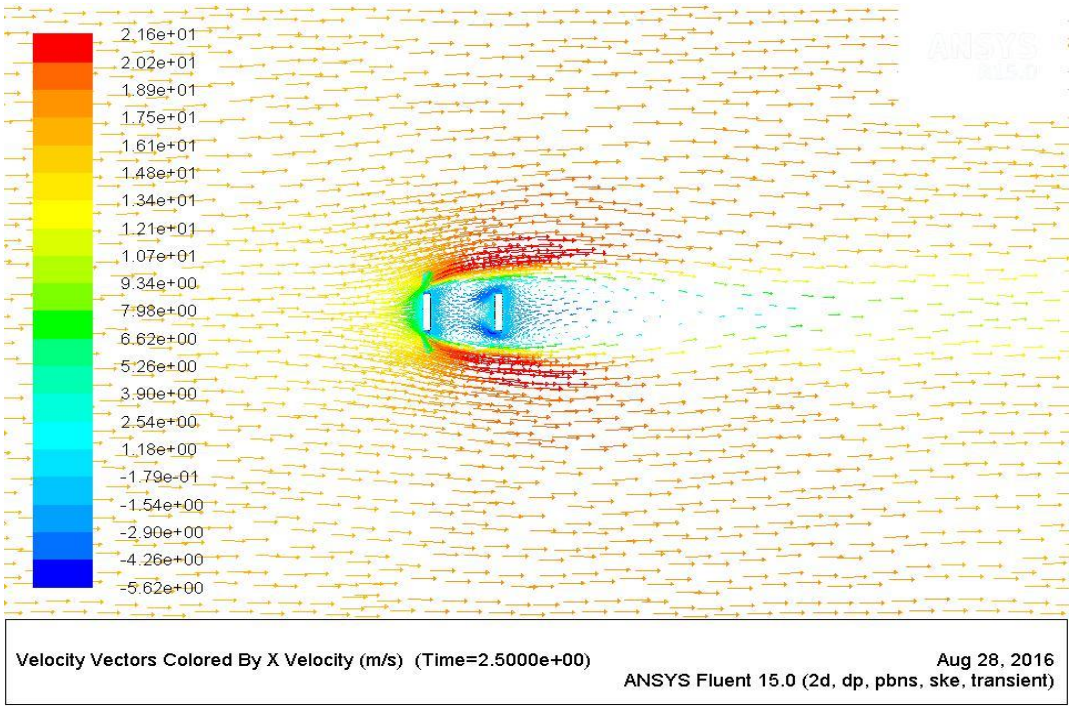

Figure 28. Velocity Vectors Colored by X-Velocity, at gap ratio =1.5

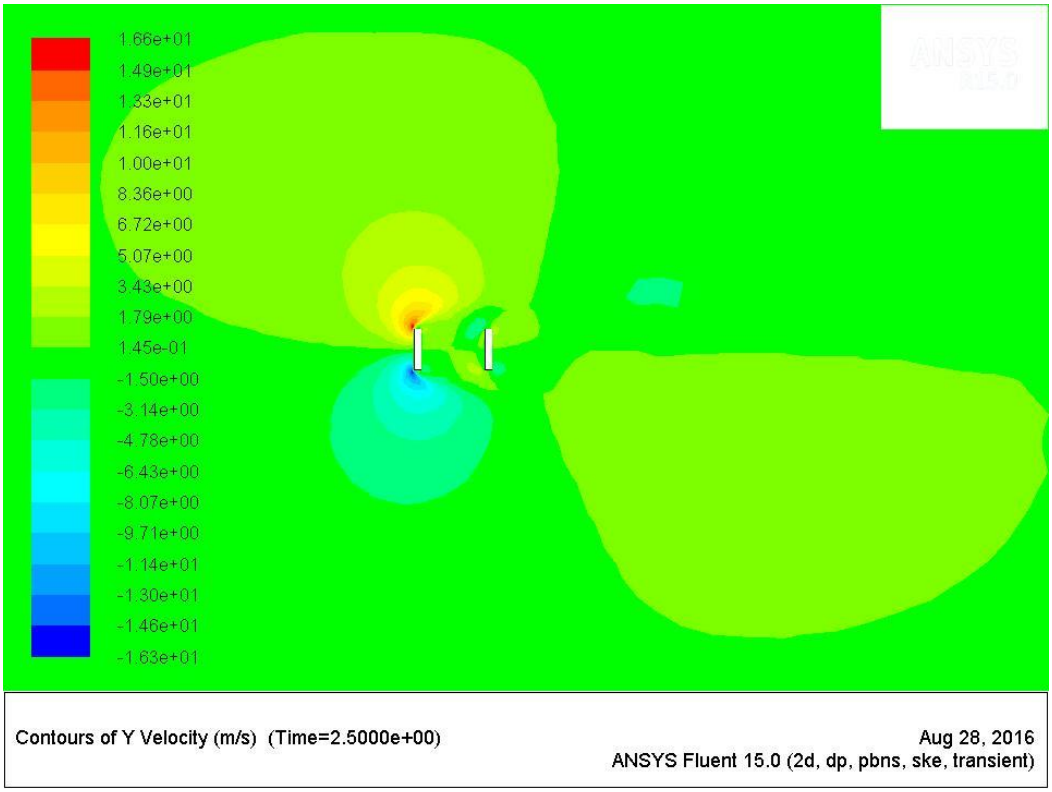

Figure 29. Contours of Y-Velocity (m/s) , at gap ratio =1.5

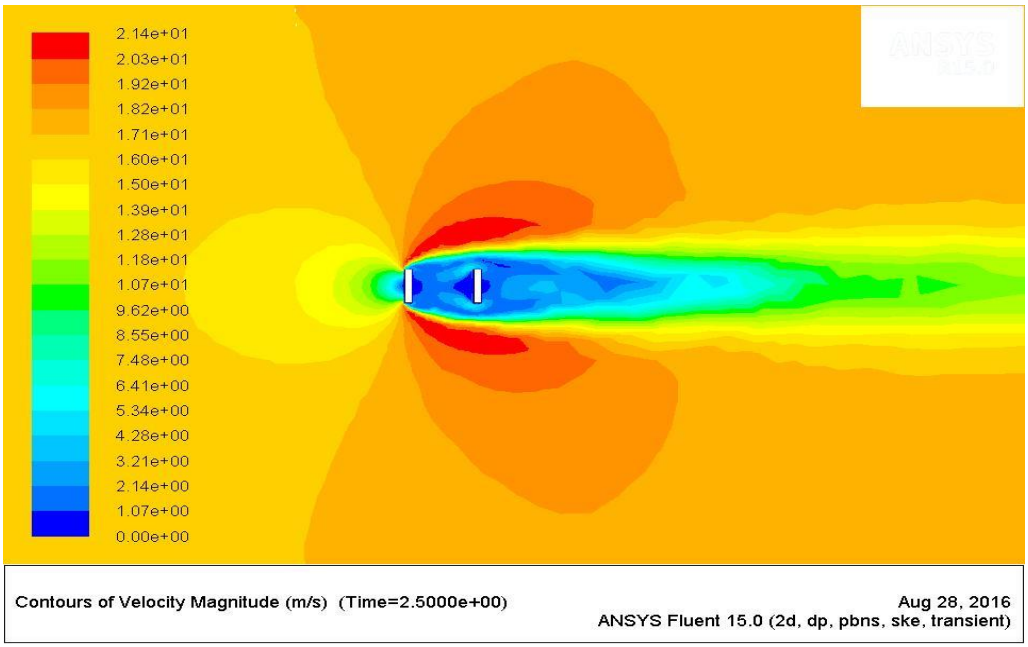

Figure 30. Contours of Velocity Magnitude (m/s), at gap ratio =1.5

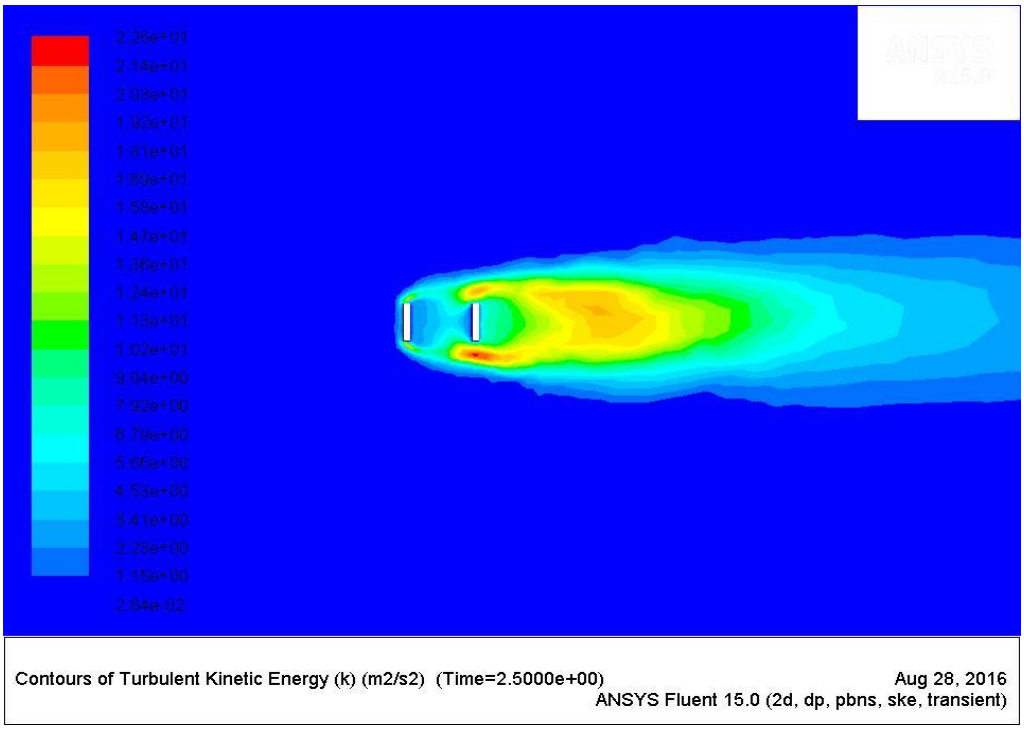

Figure 31. Contours of Turbulent Kinetic Energy (k) (m^2/s^2), at gap ratio =1.5

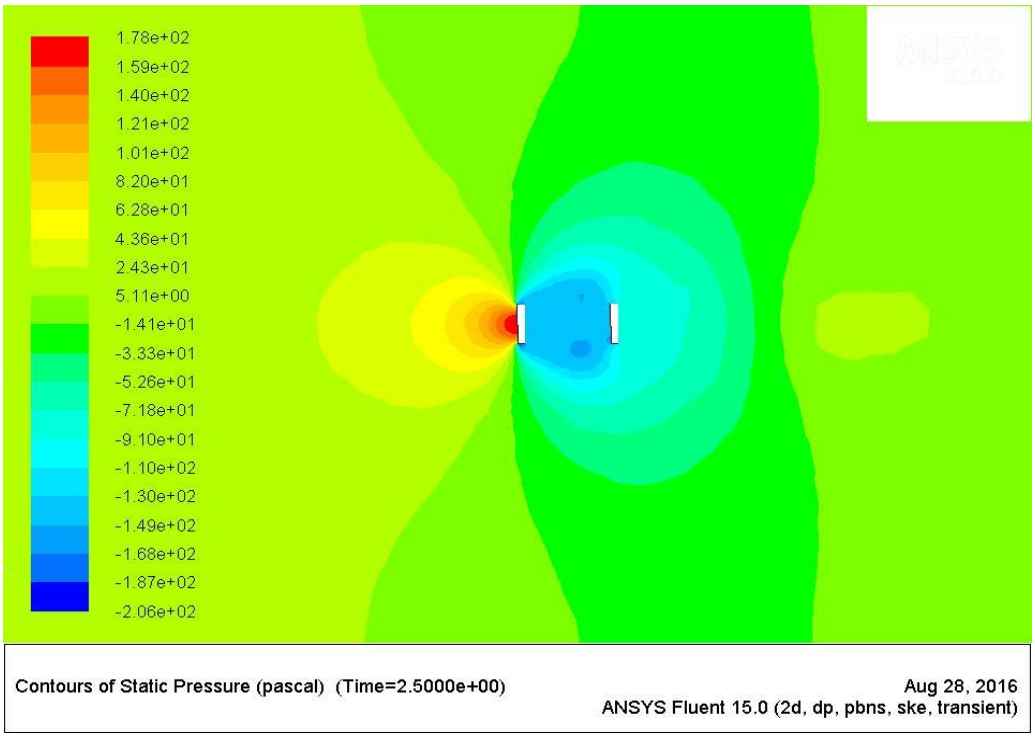

Figure 32. Contours of Static Pressure (Pa), at gap ratio=2.0

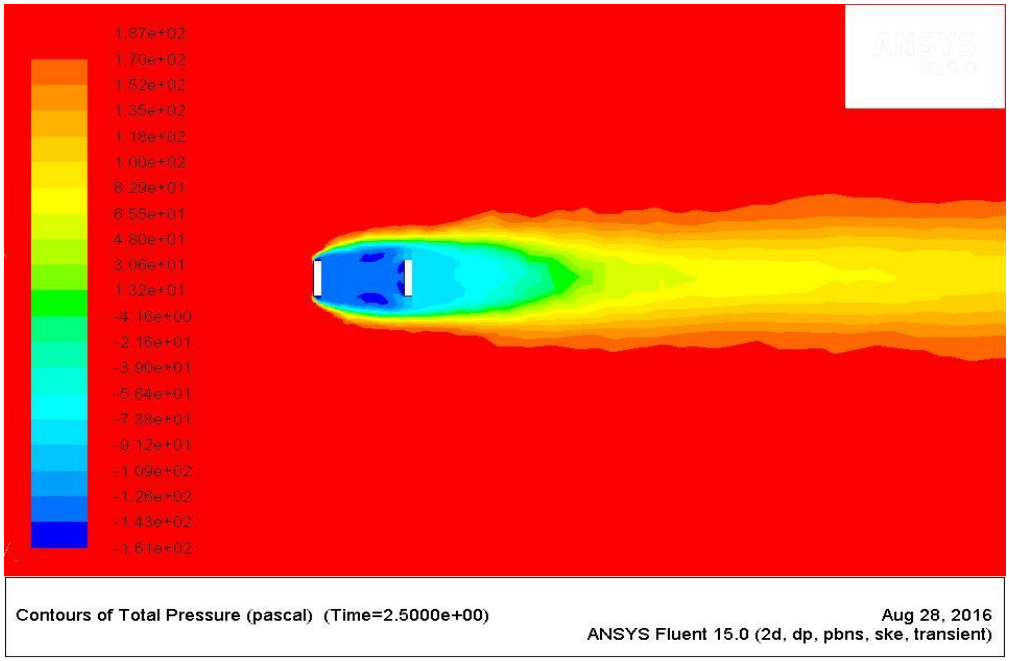

Figure 33. Contours of Total Pressure (Pa), at gap ratio=2.0

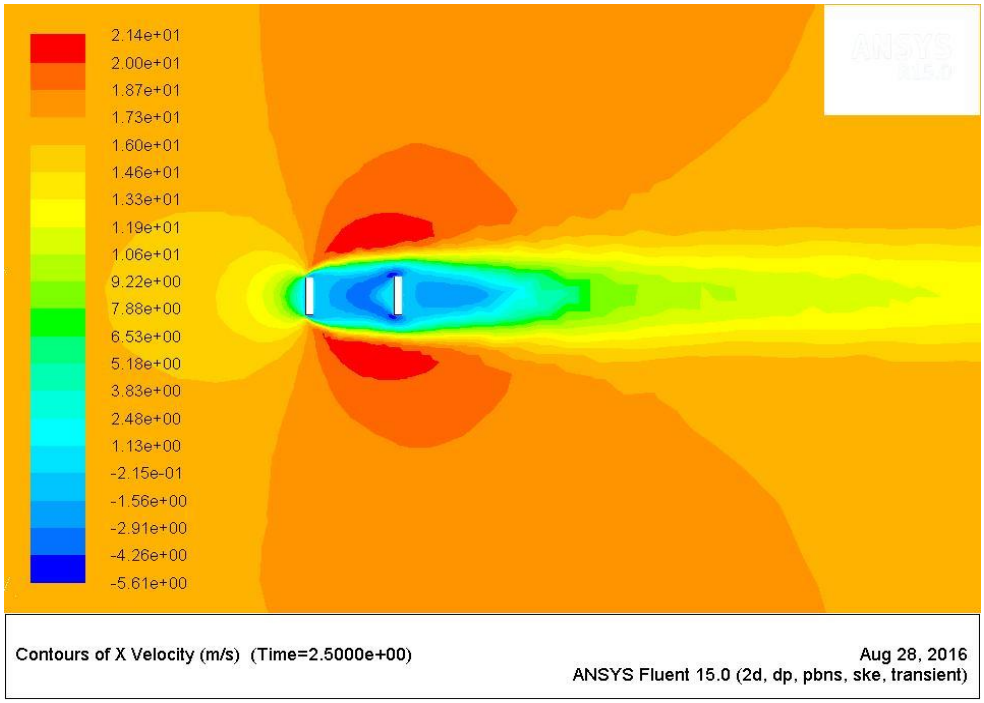

Figure 34. Contours of X-Velocity (m/s) , at gap ratio =2.0

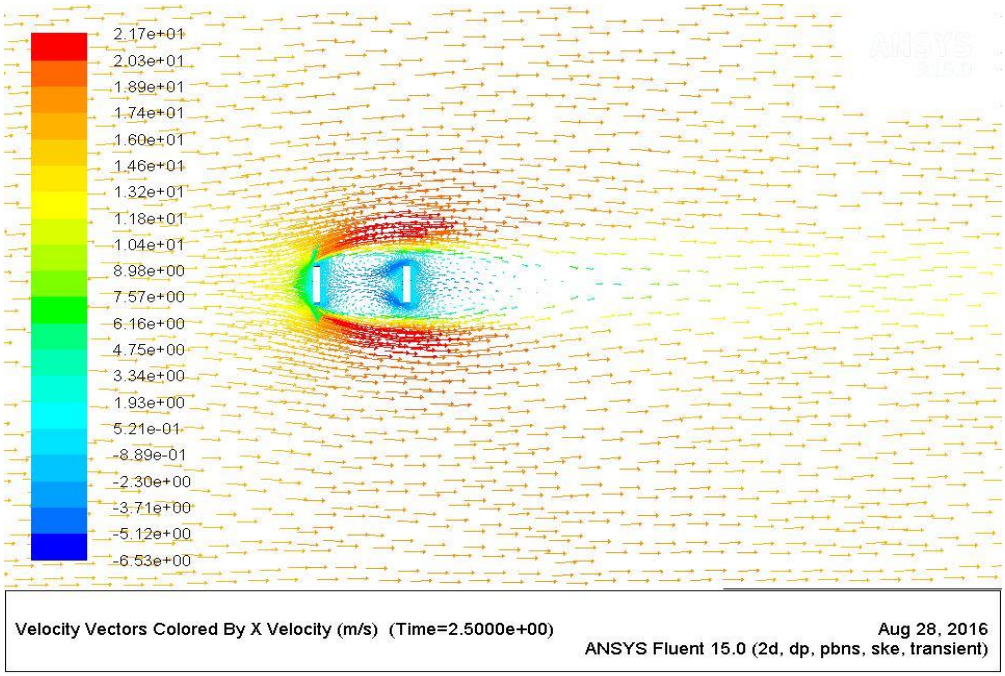

Figure 35. Velocity Vectors Colored by X-Velocity, at gap ratio =2.0

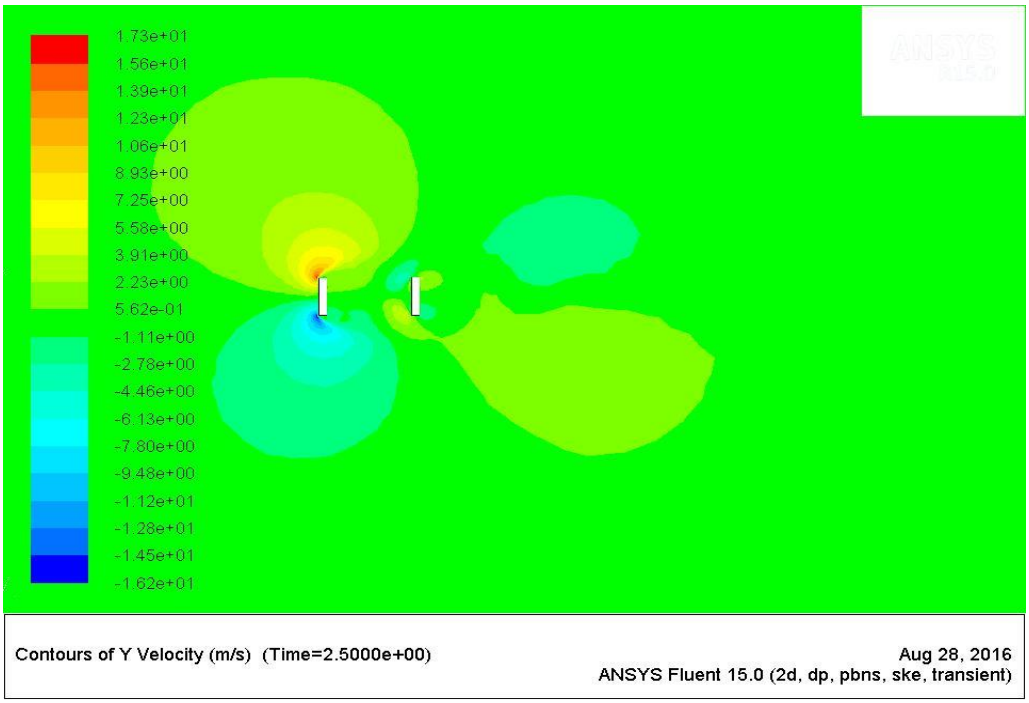

Figure 36. Contours of Y-Velocity (m/s) , at gap ratio =2.0

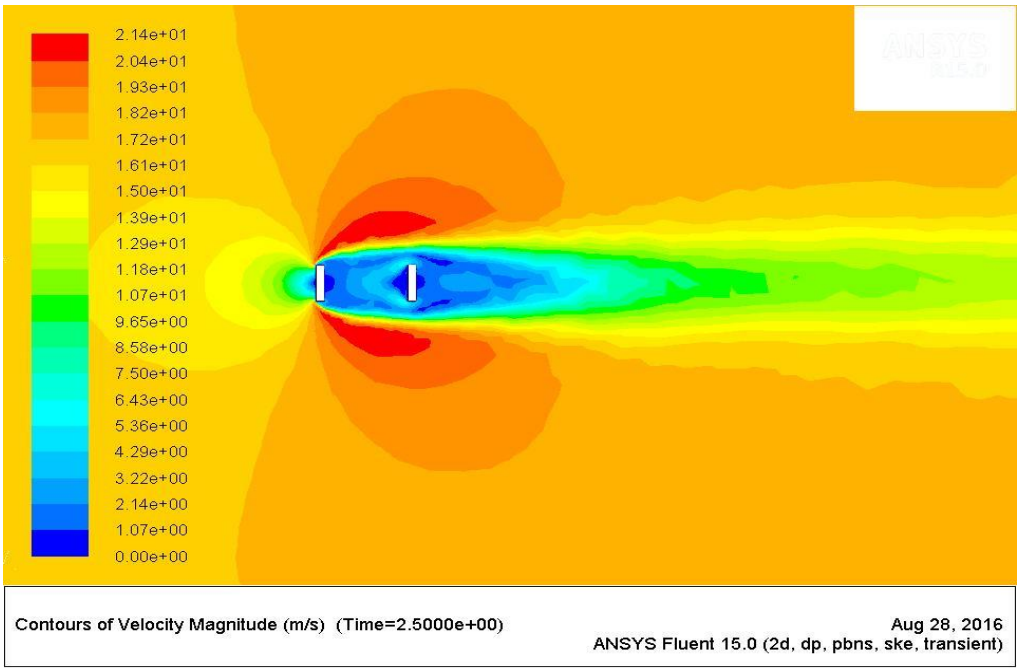

Figure 37. Contours of Velocity Magnitude (m/s), at gap ratio =2.0

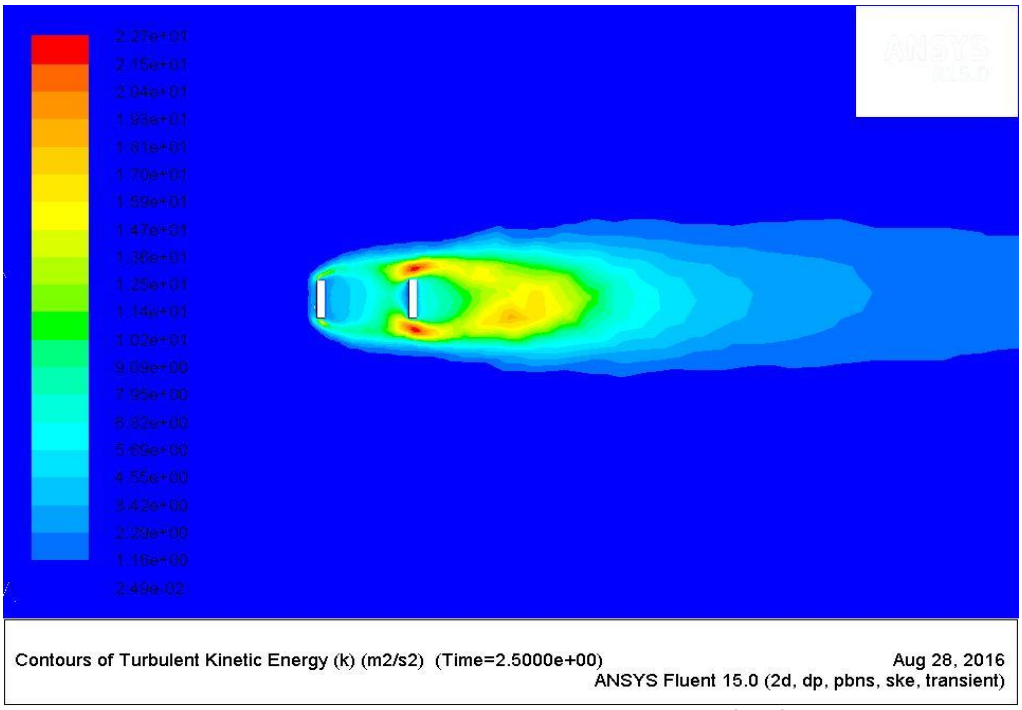

Figure 38. Contours of Turbulent Kinetic Energy (k) (m^2/s^2), at gap ratio =2.0

For gap ratio 1.5,2.0 shown in figures 25 – 38 vortex is developed behind the second plate and also between two plates vortex appears and in the vector x, the velocity is clearly shown.

For the inclined plate these graphical outputs consisting of x-velocity contours, y-velocity, contoured kinetic turbulence and contours and vorticity contours are presented in sequence:

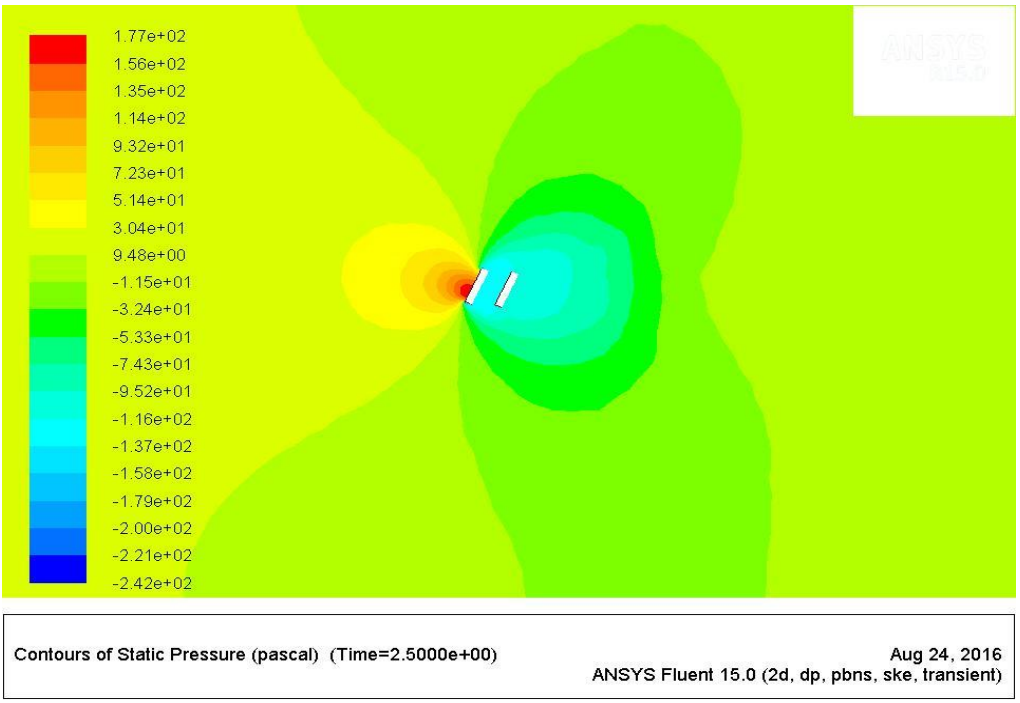

Figure 39. Contours of Static Pressure (Pa), at gap ratio=0.5 and75 degree

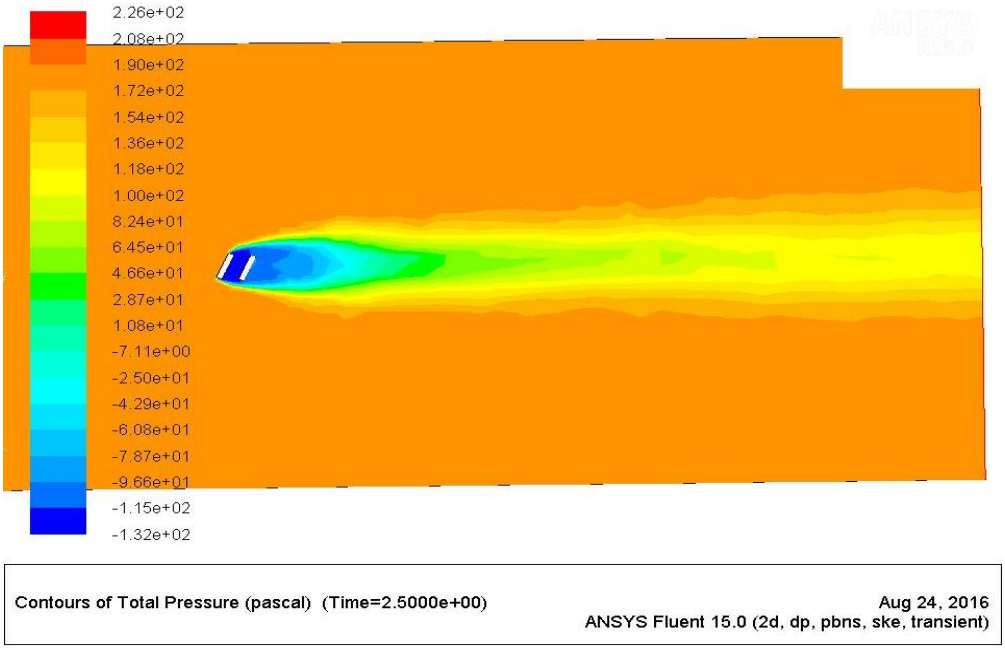

Figure 40. Contours of Total Pressure (Pa), at gap ratio=0.5 and 75 degree

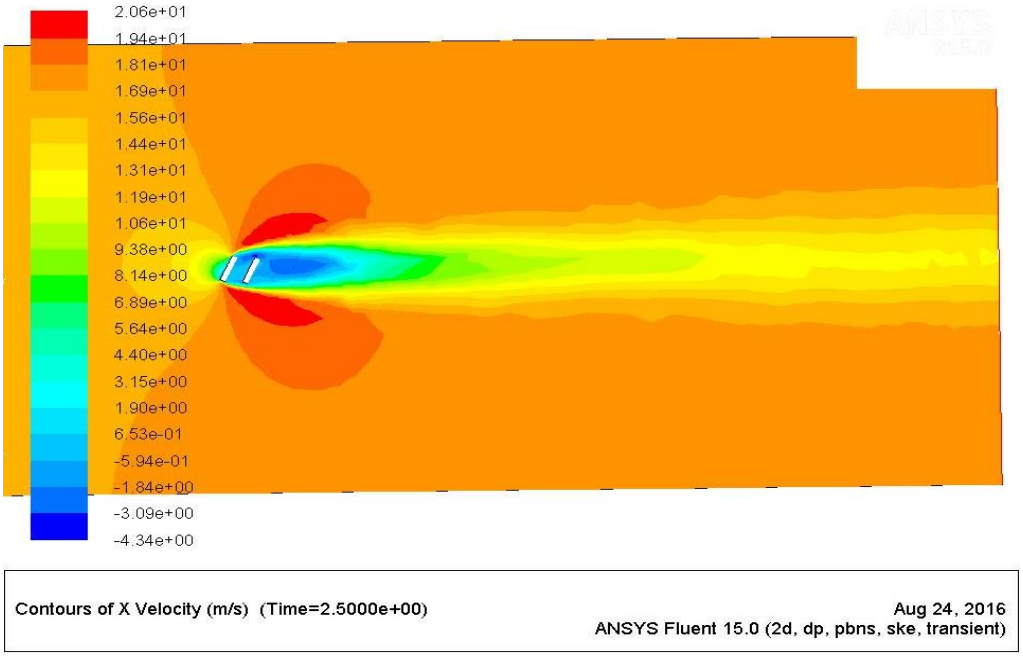

Figure 41. Contours of X-Velocity (m/s) , at gap ratio =0.5 and 75 degree

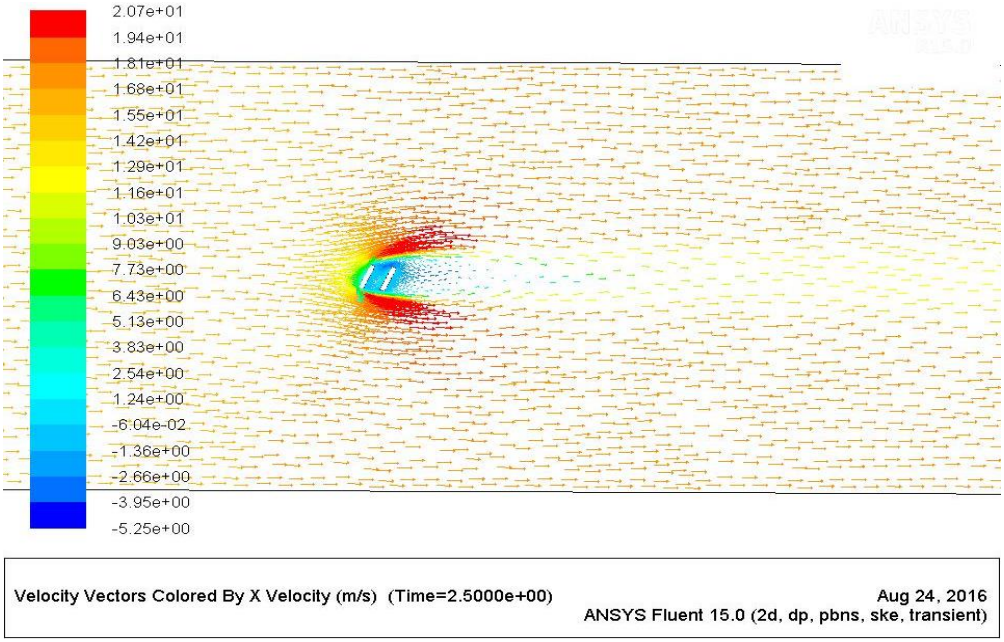

Figure 42. Velocity Vectors Colored by X-Velocity, at gap ratio =0.5 and 75 degree

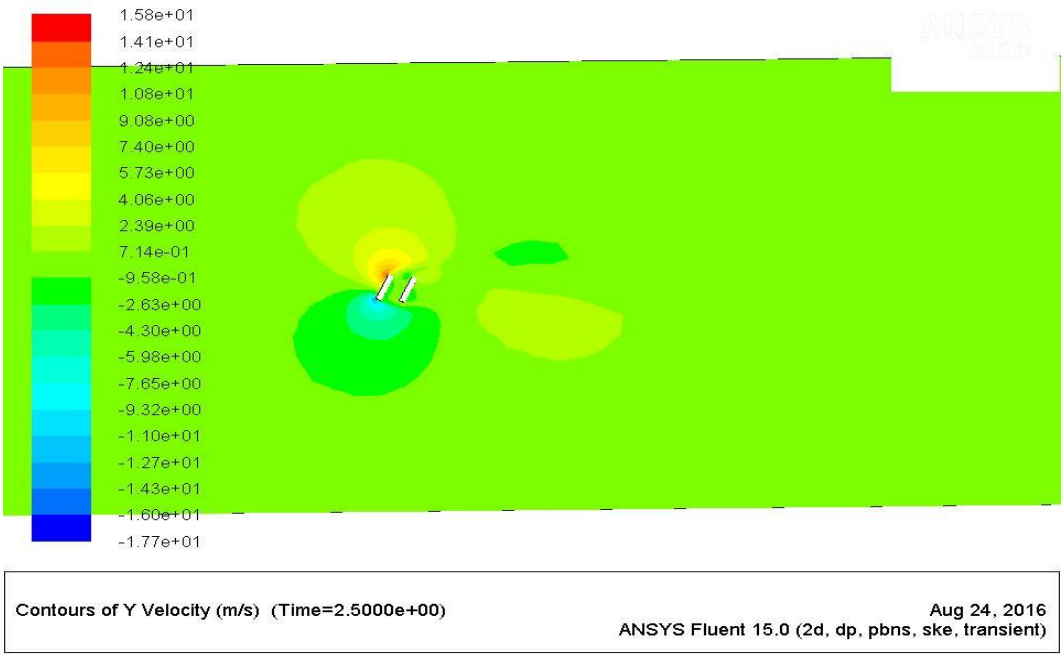

Figure 43. Contours of Y-Velocity (m/s), at gap ratio =0.5 and 75 degree

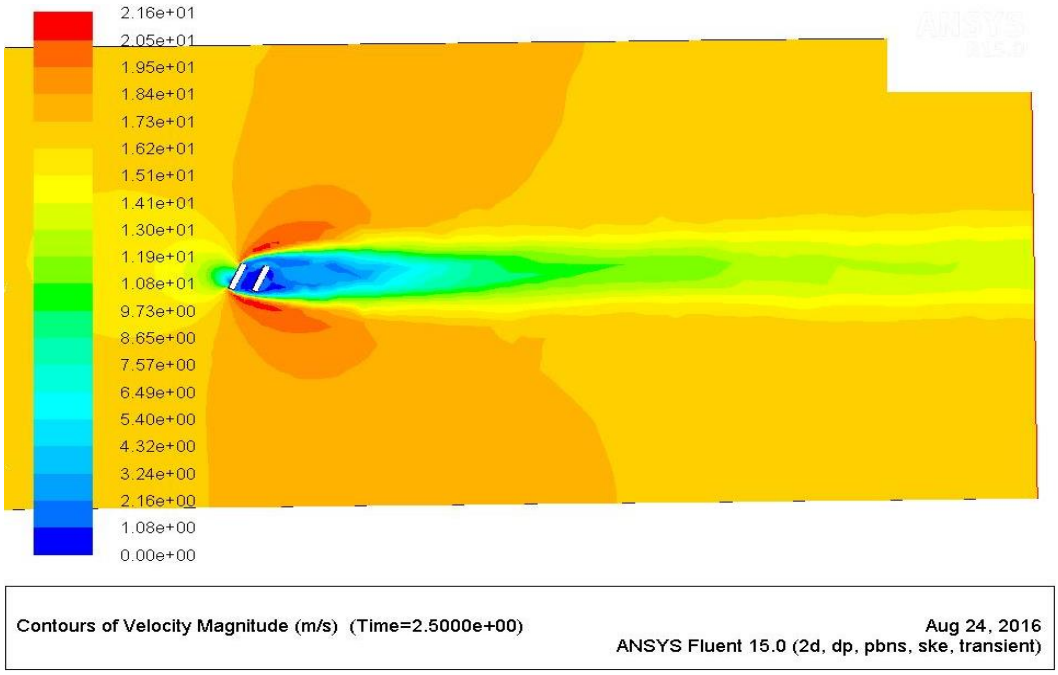

Figure 44. Contours of Velocity Magnitude (m/s), at gap ratio =0.5 and 75 degree

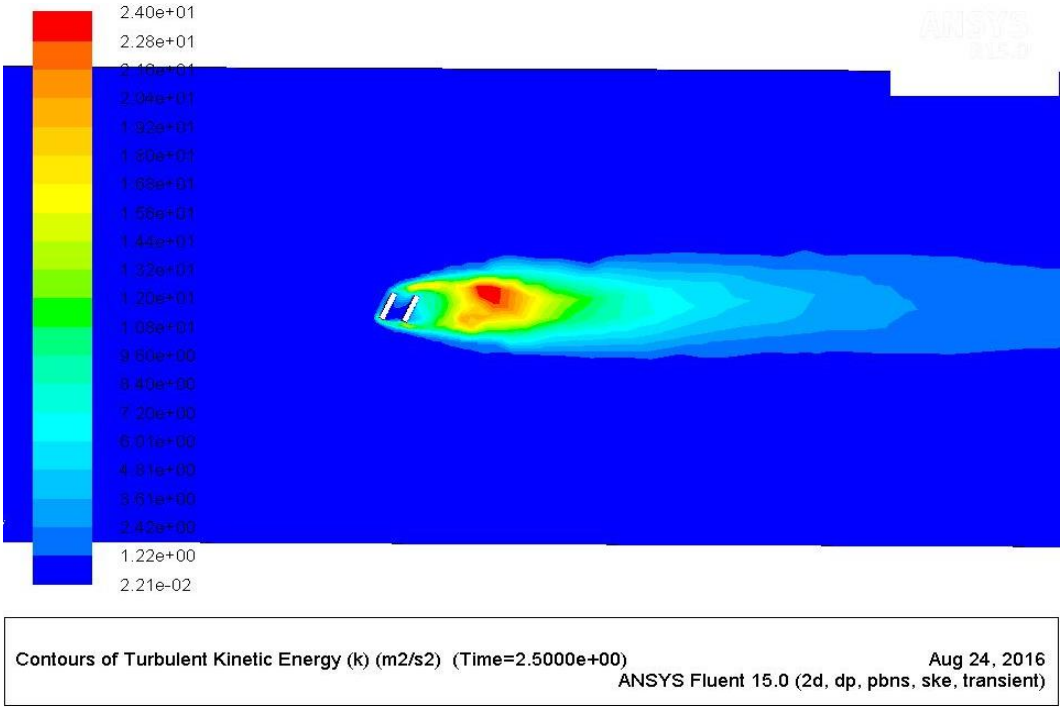

Figure 45. Contours of Turbulent Kinetic Energy (k) (m^2/s^2), at gap ratio =0.5 75 degree

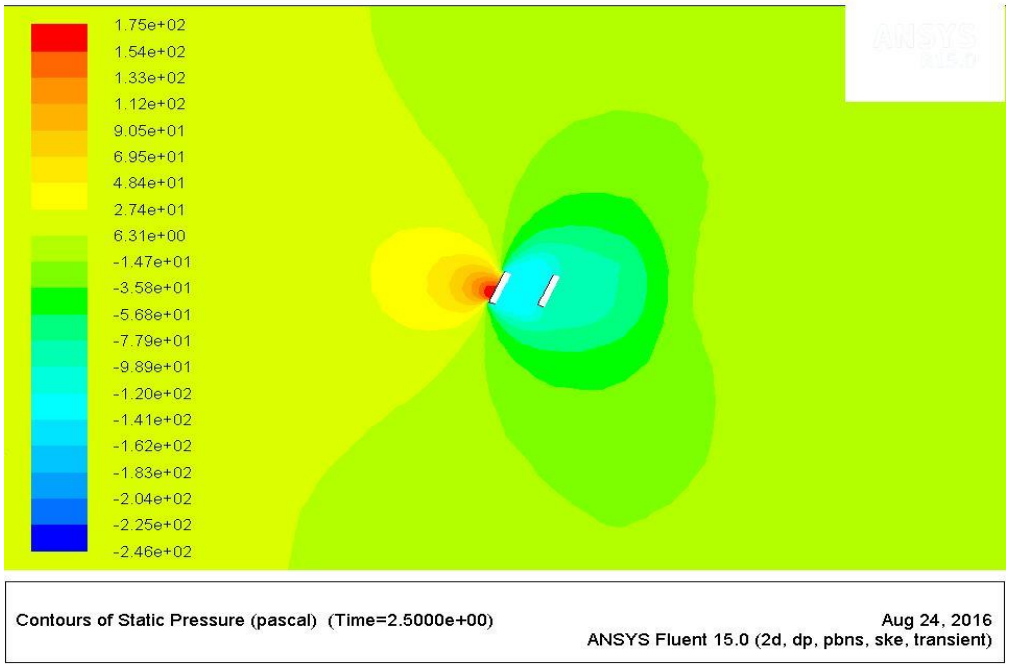

Figure 46. Contours of Static Pressure (Pa), at gap ratio=1.0 and 75 degree

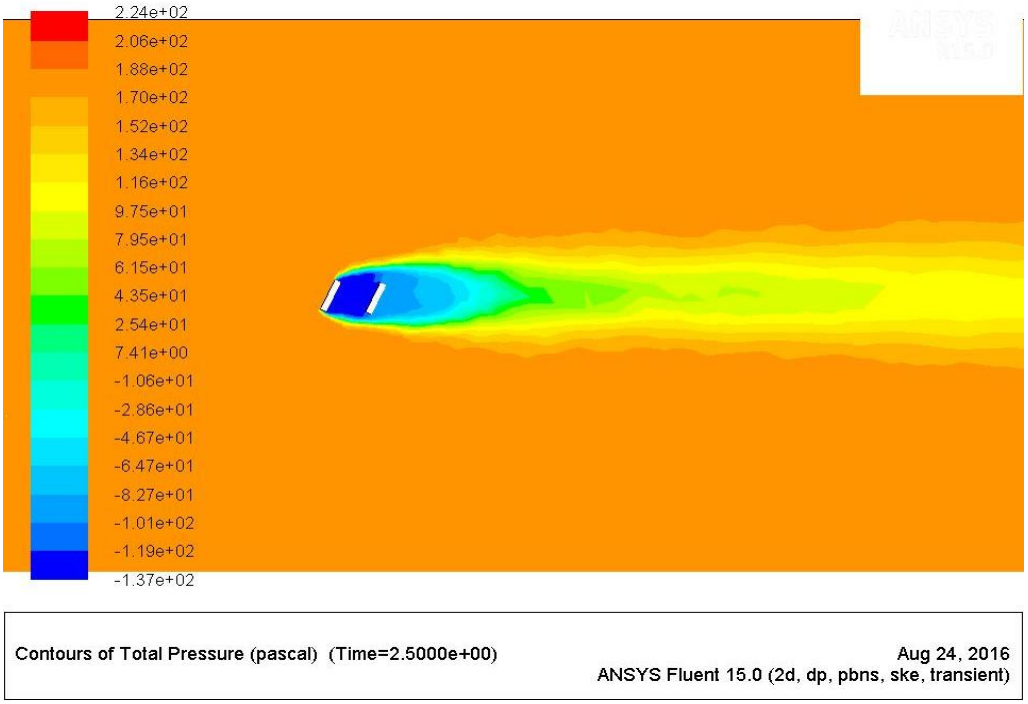

Figure 47. Contours of Total Pressure (Pa), at gap ratio=1.0 and 75 degree

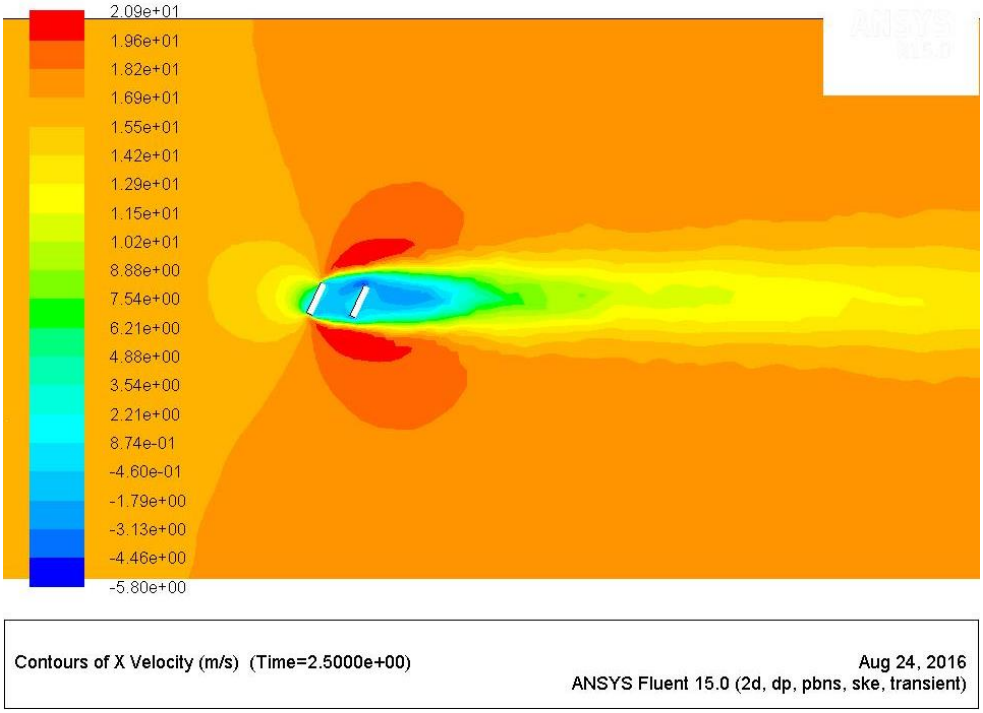

Figure 48. Contours of X-Velocity (m/s) , at gap ratio =1.0 and 75 degree

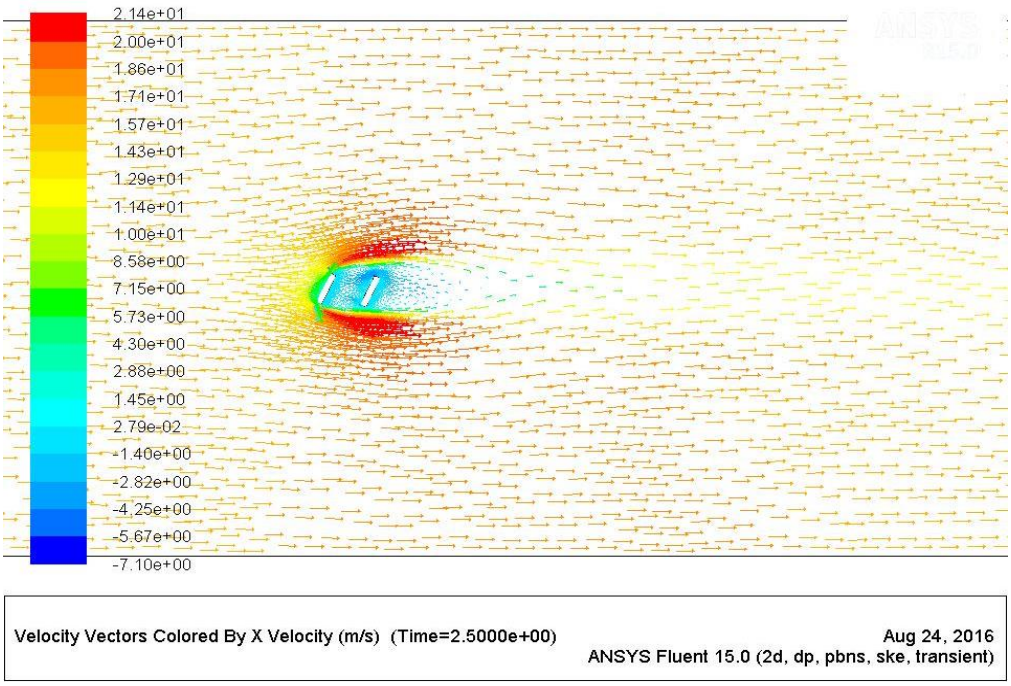

Figure 49. Velocity Vectors Colored by X-Velocity, at gap ratio =1.0 and 75 degree

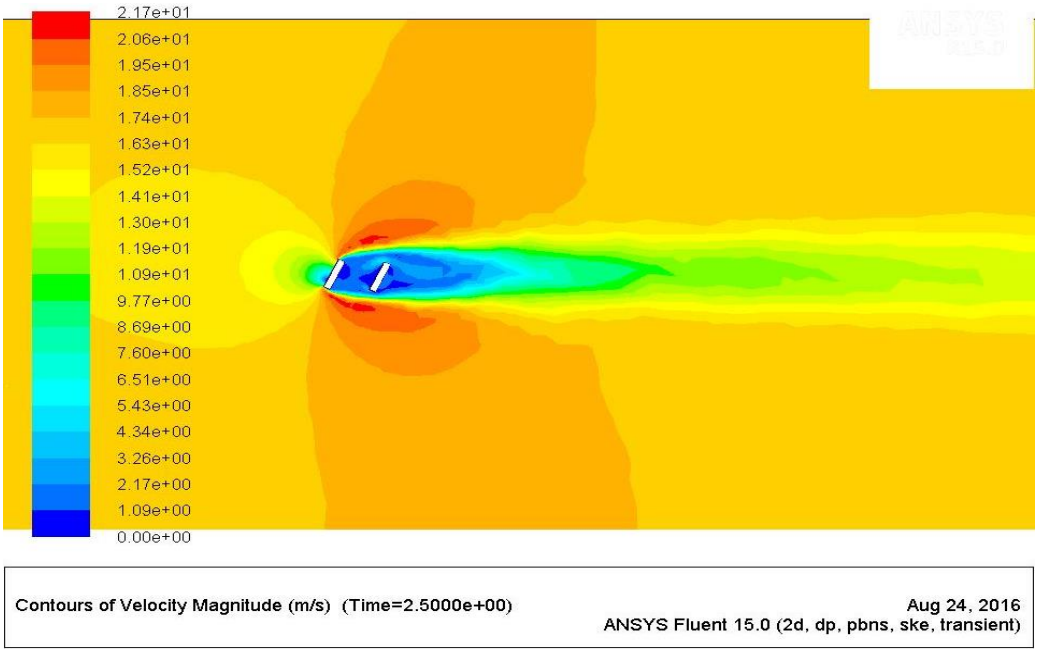

Figure 50. Contours of Velocity Magnitude (m/s), at gap ratio =1.0 and 75 degree

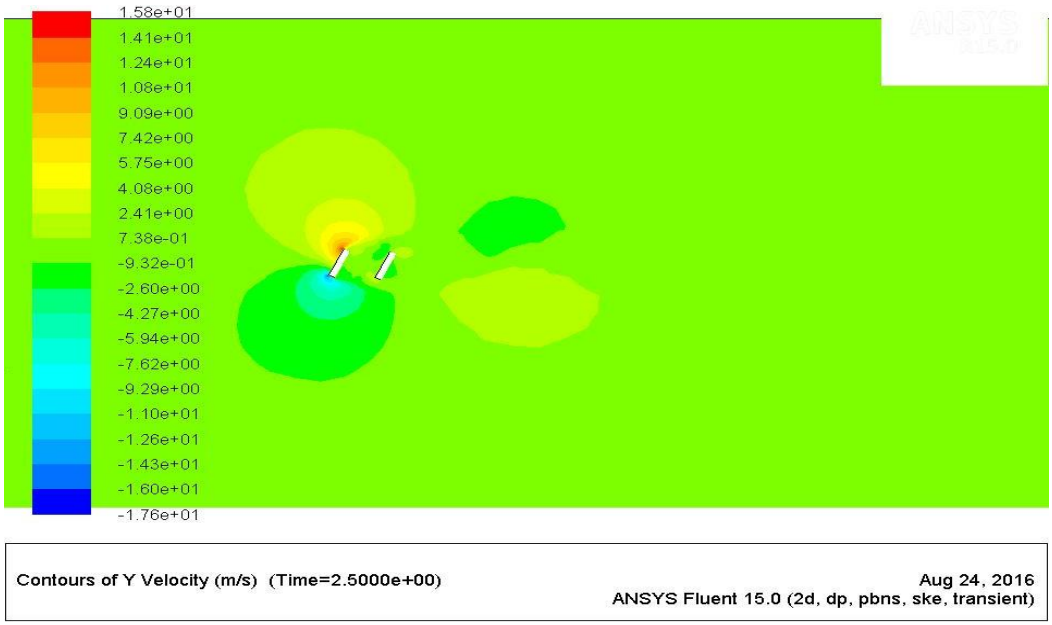

Figure 51. Contours of Y-Velocity (m/s) , at gap ratio =1.0 and 75 degree

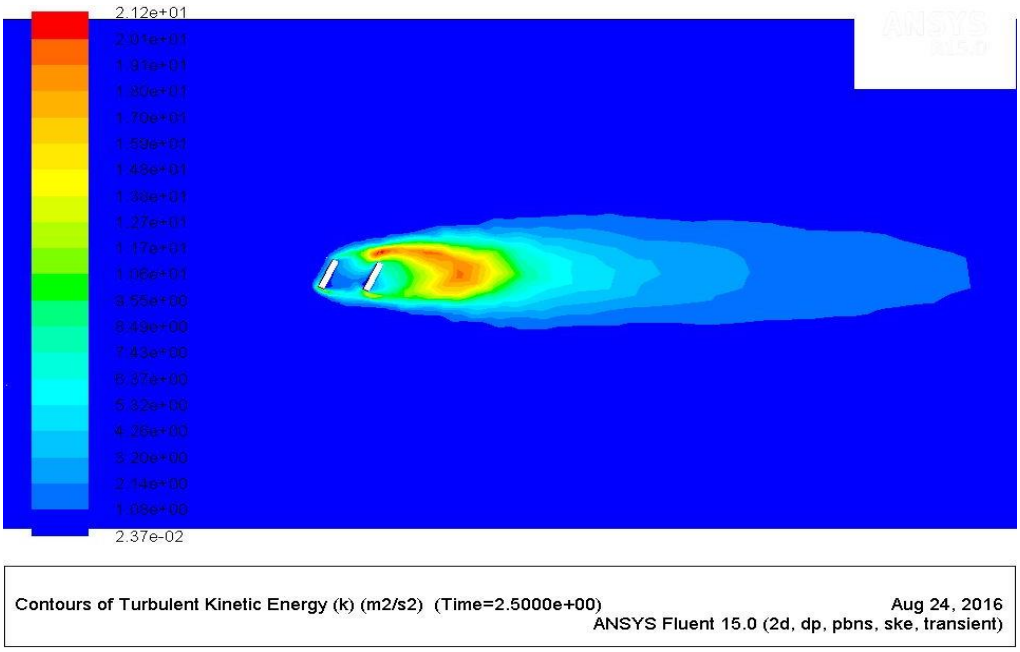

Figure 52. Contours of Turbulent Kinetic Energy (k) (m^2/s^2), at gap ratio =1.0 and 75 degree

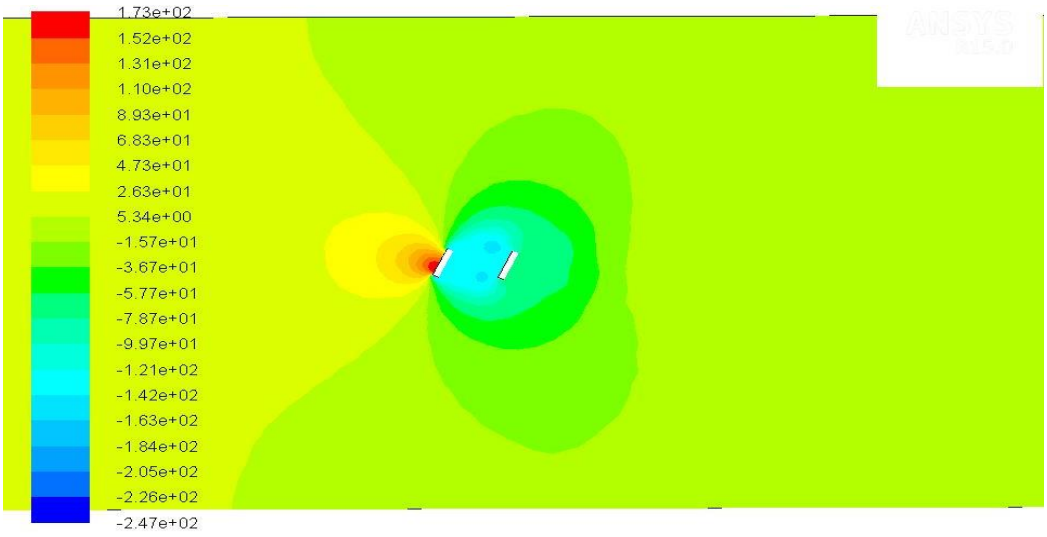

Figure 53. Contours of Static Pressure (Pa), at gap ratio =1.5 and 75 degree

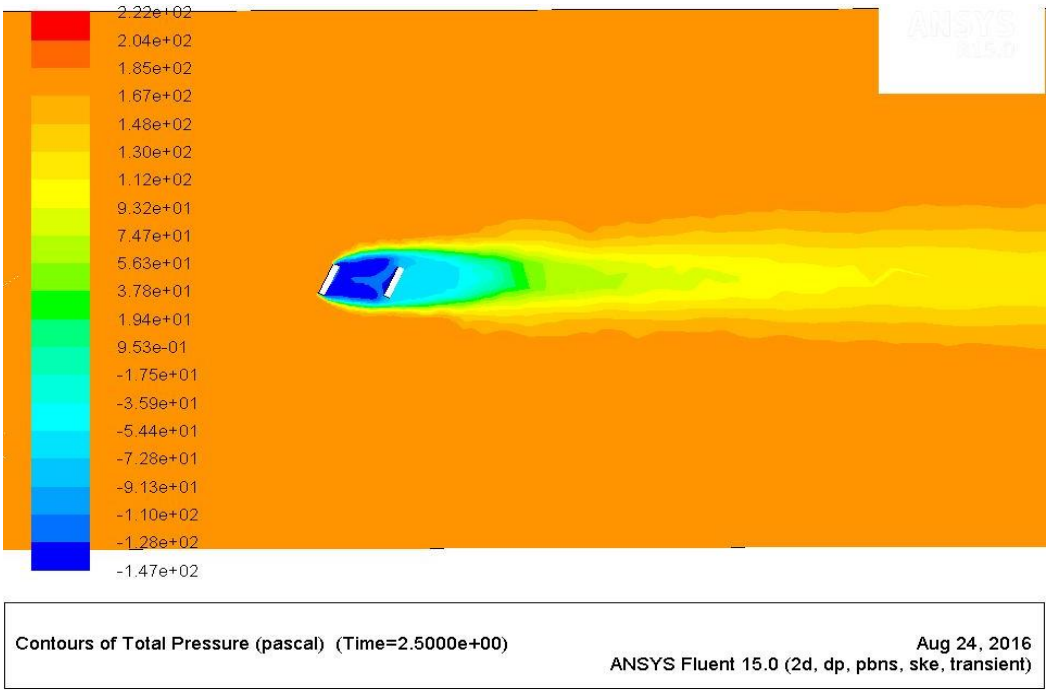

Figure 54. Contours of Total Pressure (Pa), at gap ratio=1.5 and 75 degree

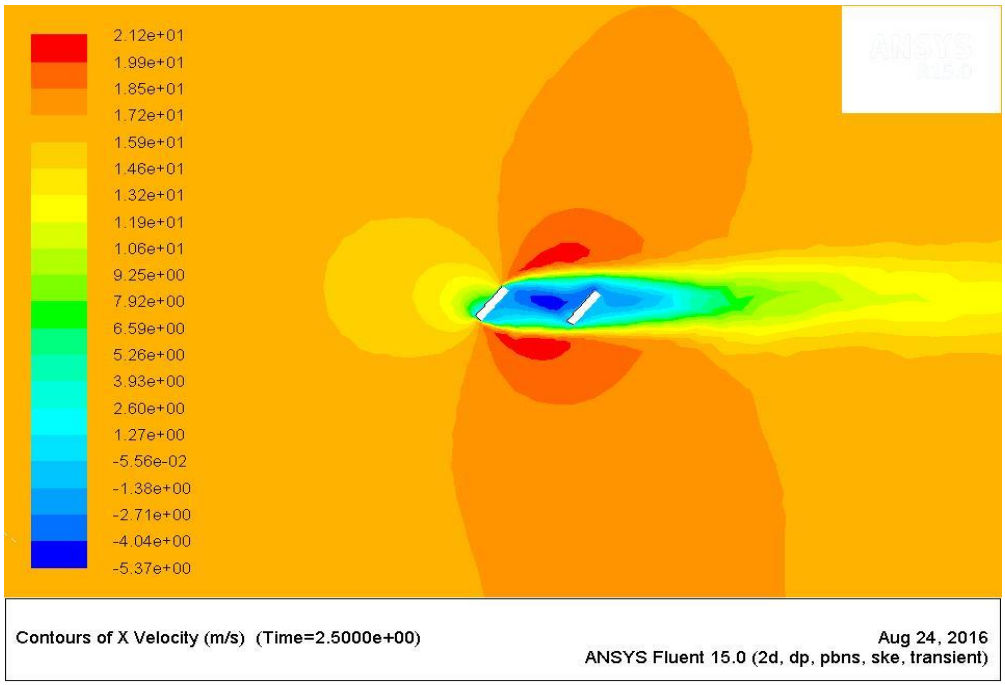

Figure 55. Contours of X-Velocity (m/s) , at gap ratio =1.5 and 75 degree

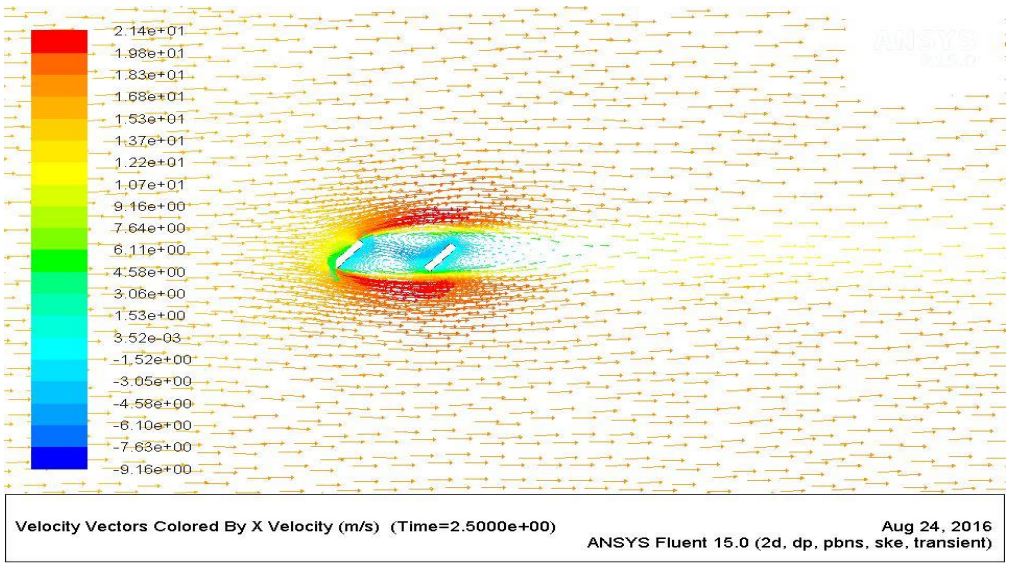

Figure 56. Velocity Vectors Colored by X-Velocity, at gap ratio =1.5 and 75 degree

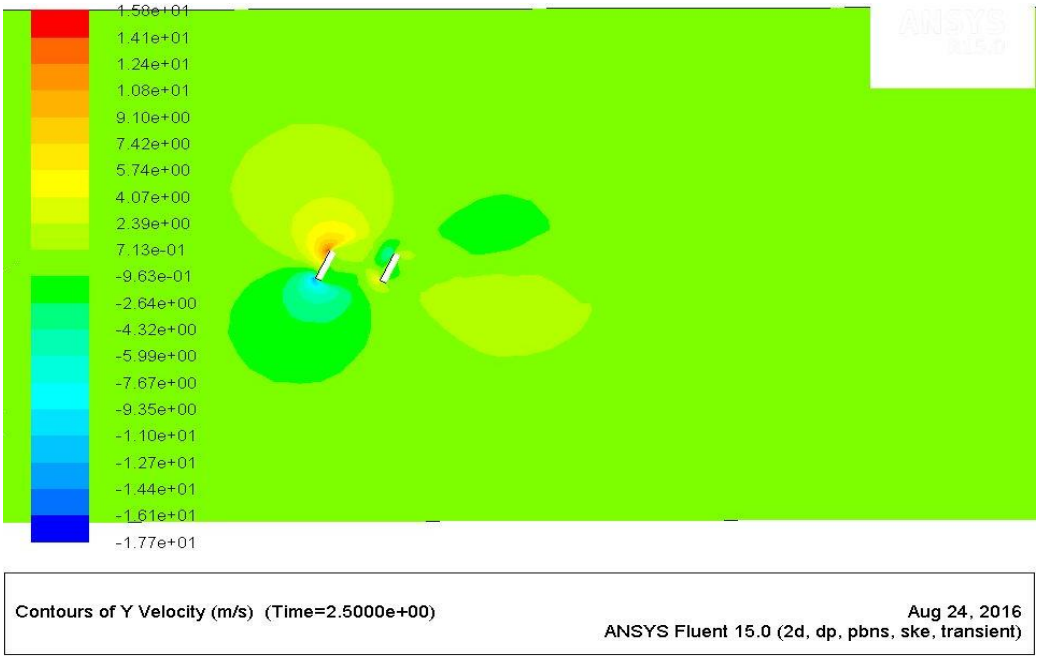

Figure 57. Contours of Y-Velocity (m/s) , at gap ratio =1.5 and 75 degree

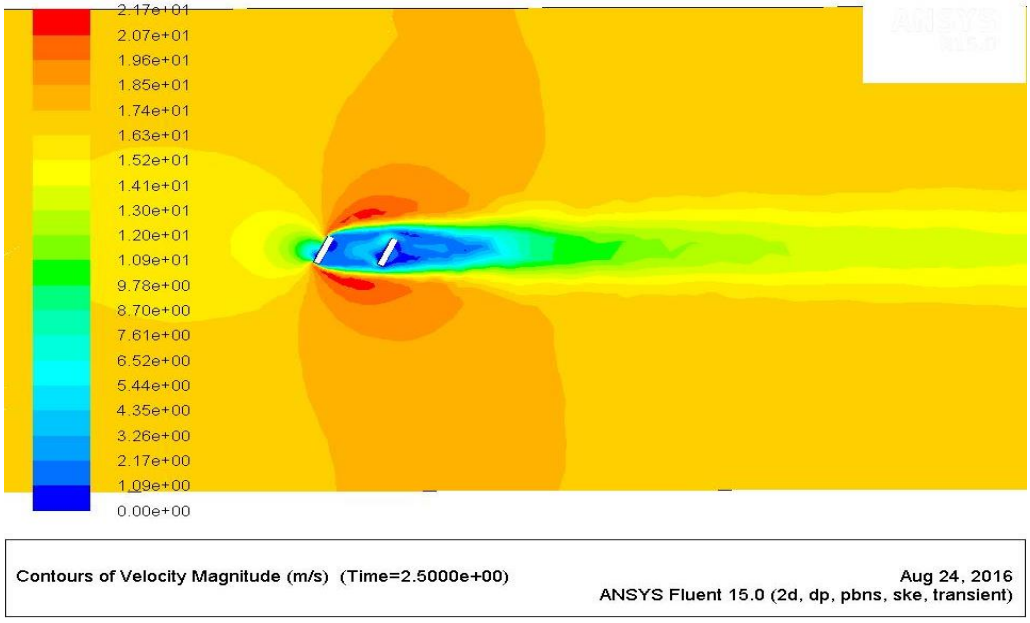

Figure 58. Contours of Velocity Magnitude (m/s), at gap ratio =1.5 and 75 degree

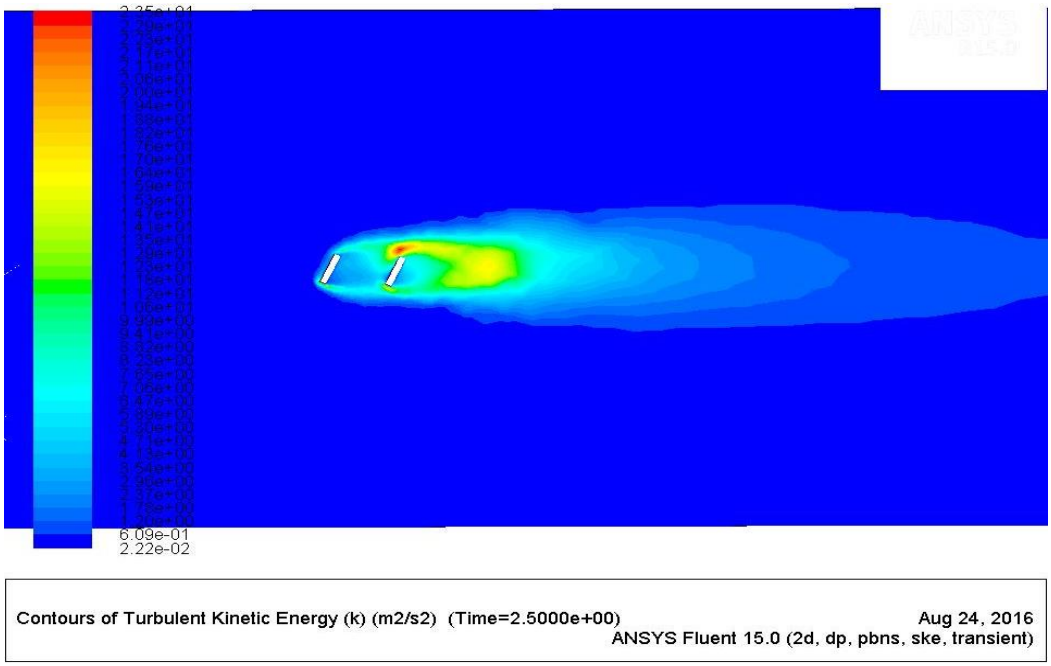

Figure 59. Contours of Turbulent Kinetic Energy (k) (m^2/s^2), at gap ratio =1.5 and 75 degree

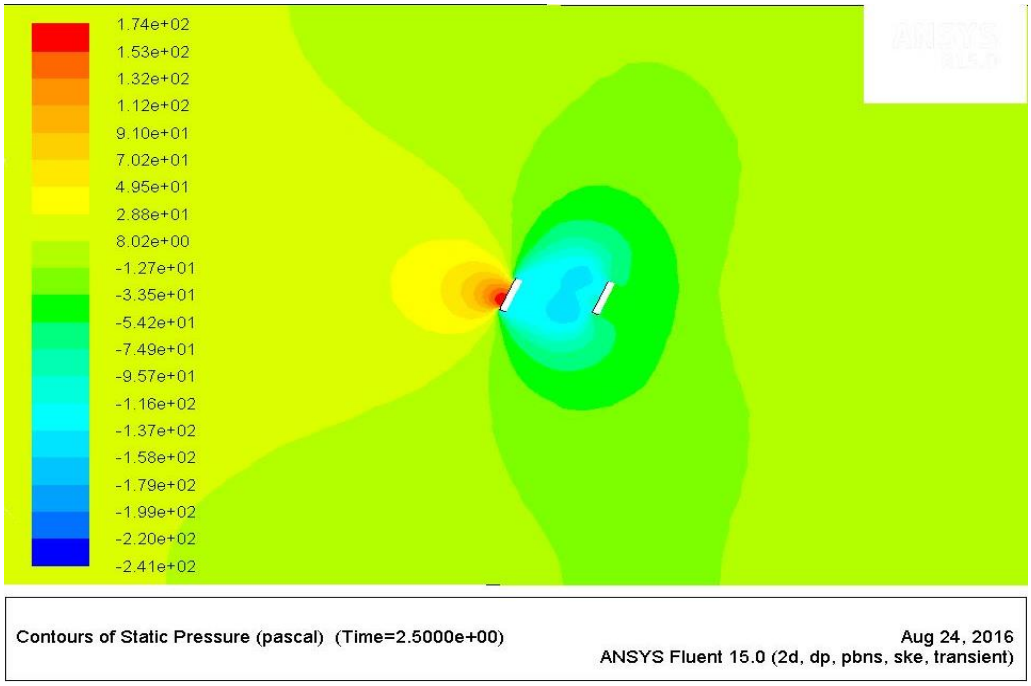

Figure 60. Contours of Static Pressure (Pa), at gap ratio=2.0 and 75 degree

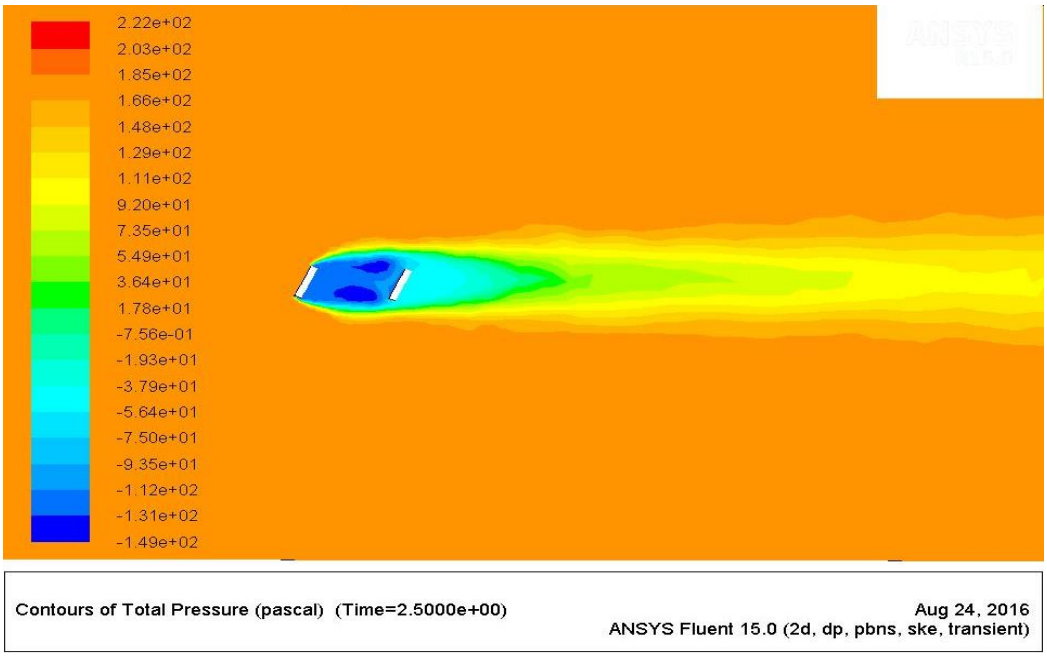

Figure 61. Contours of Total Pressure (Pa), at gap ratio=2.0 and 75 degree

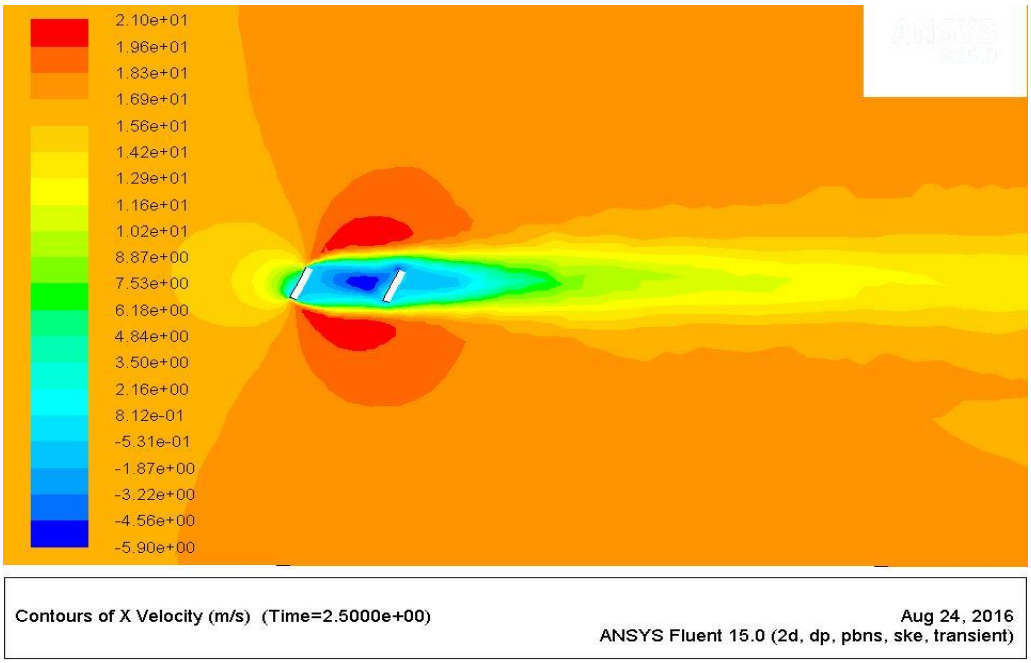

Figure 62. Contours of X-Velocity (m/s) , at gap ratio =2.0 and 75 degree

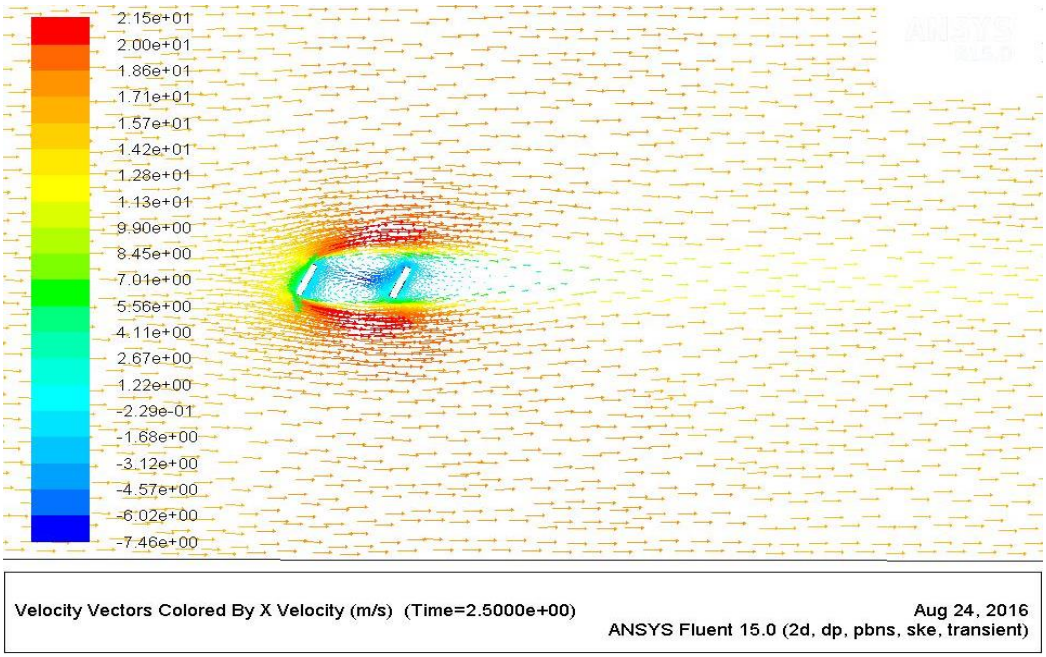

Figure 63. Velocity Vectors Colored by X-Velocity , at gap ratio =2.0 and 75 degree

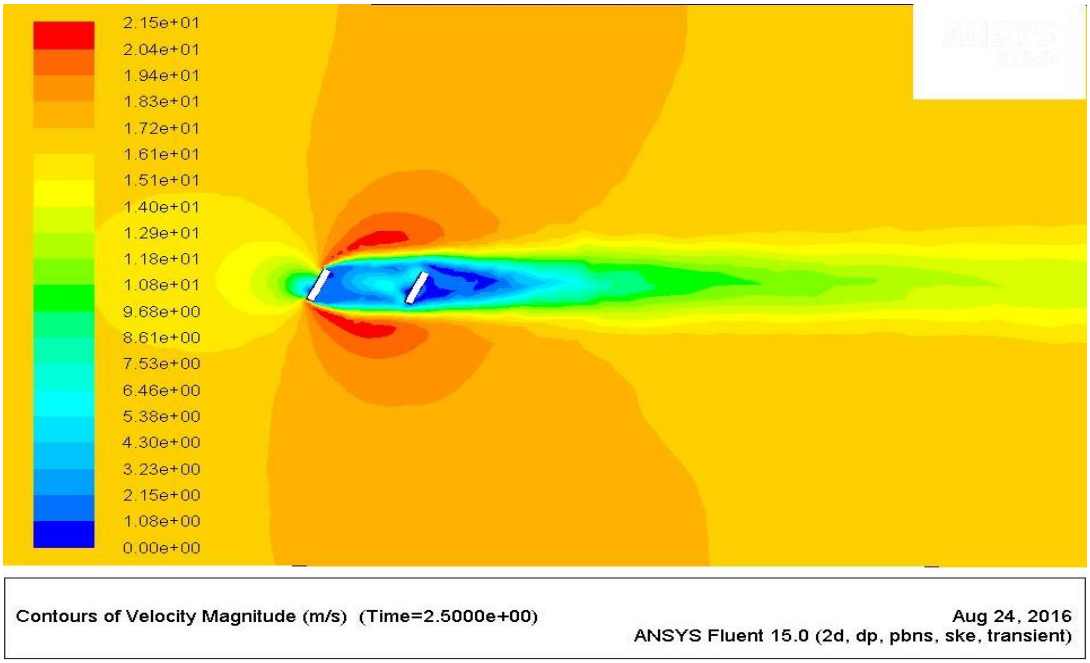

Figure 64. Contours of Velocity Magnitude (m/s), at gap ratio =2.0 and 75 degree

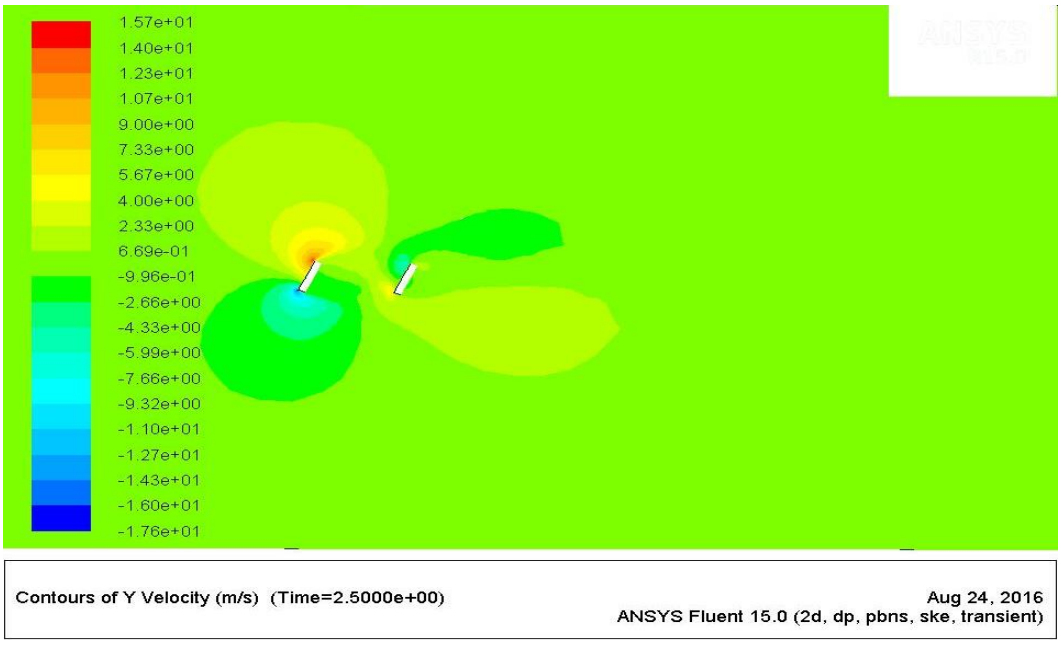

Figure 65. Contours of Y-Velocity (m/s), at gap ratio =2.0 and 75 degree

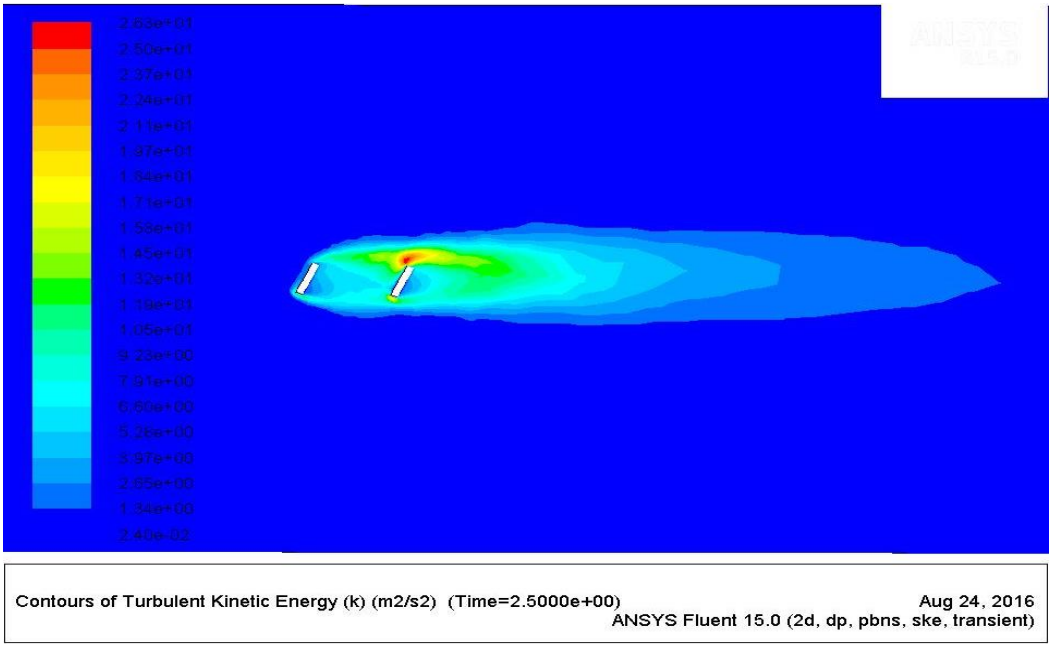

Figure 66. Contours of Turbulent Kinetic Energy (k) (m^2/s^2), at gap ratio =2.0 and 75 degree

As shown in figures 39 – 66 in the declined flat plates by gap ratio 0.5, 1.0, 1.5 and 2.0 also the 75 degree pressure is same in all domain except behind the plates as they also demonstrated the same Strouhal number. Vortex appears just between two plates, in the upstream angle of attack. The kinetic turbulent energy is increased for gap ratio 0.5 and 1.0 however by increasing the gap ratio vortex is developed behind the second plate and it is shown in vector velocity.

In below shown inclined plate by 60 degree contours: static pressure, total pressure, x-velocity and vector x-velocity, contour of y-velocity and kinetic energy by order:

Gap ratio 0.5

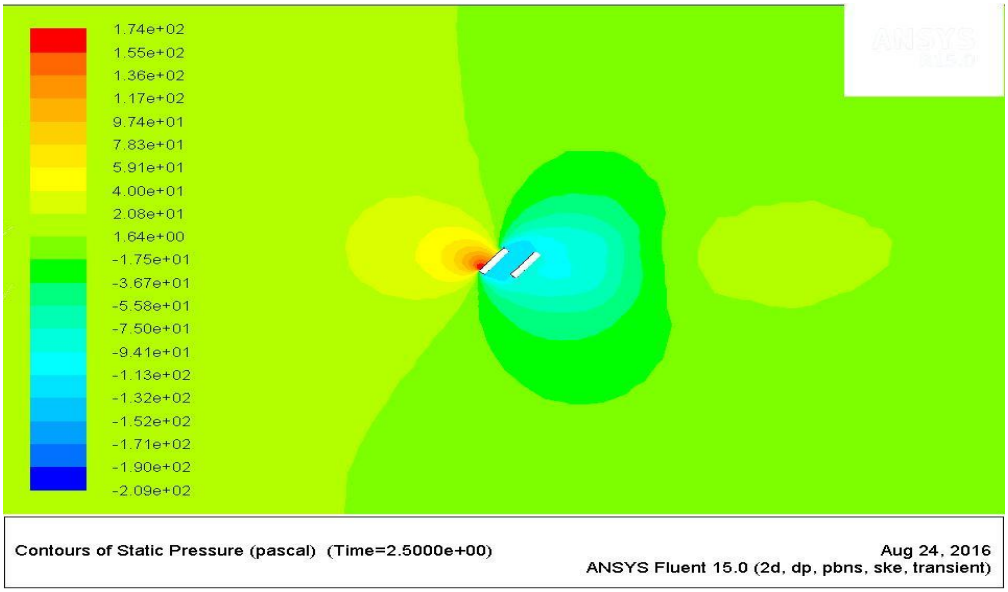

Figure 67. Contours of Static Pressure (Pa), at gap ratio=0.5 and 60 degree

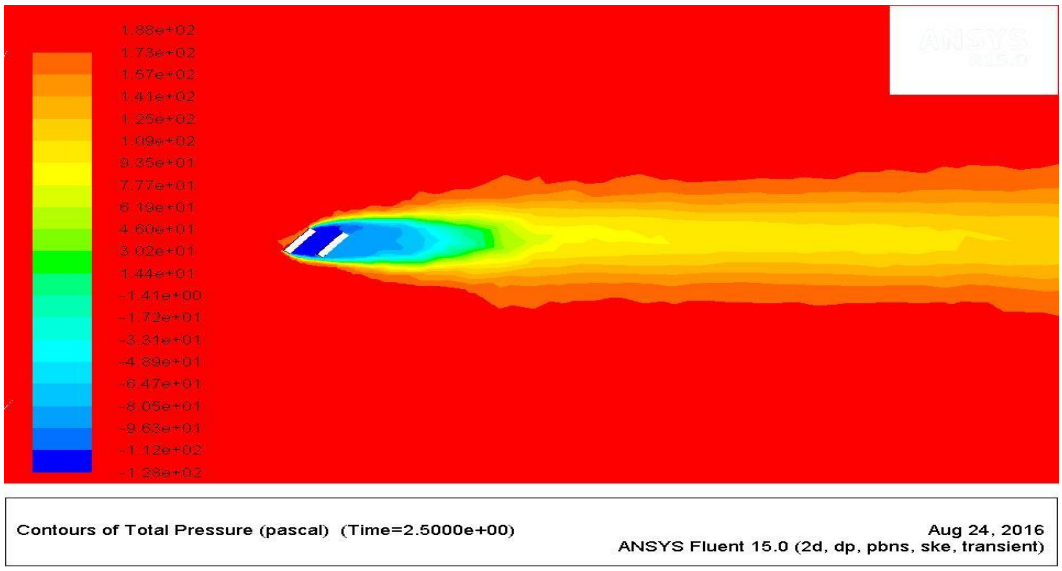

Figure 68. Contours of Total Pressure (Pa), at gap ratio=0.5 and 60 degree

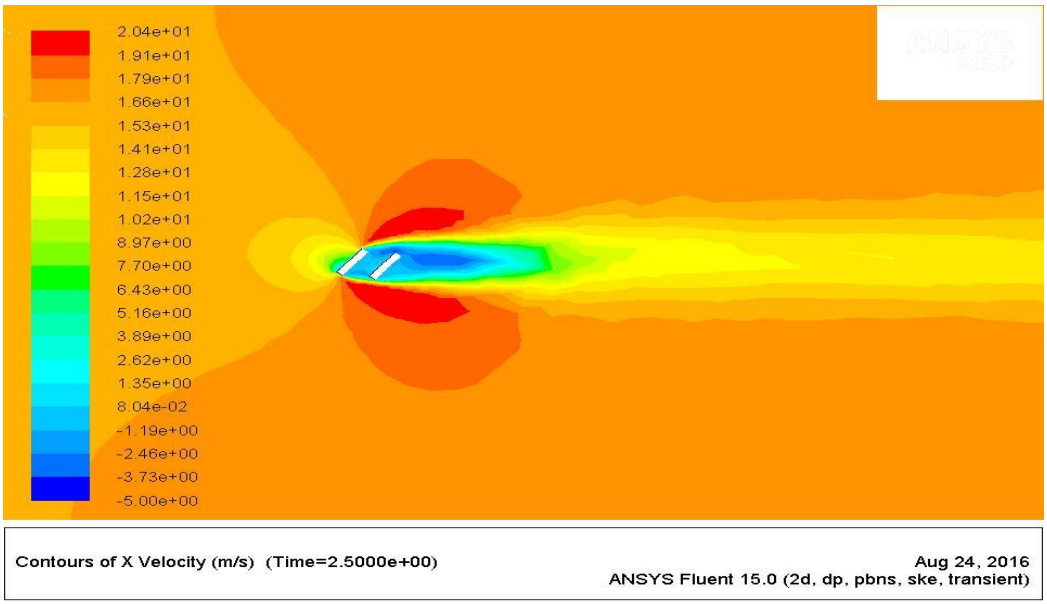

Figure 69. Contours of X-Velocity (m/s), at gap ratio =0.5 and 60 degree

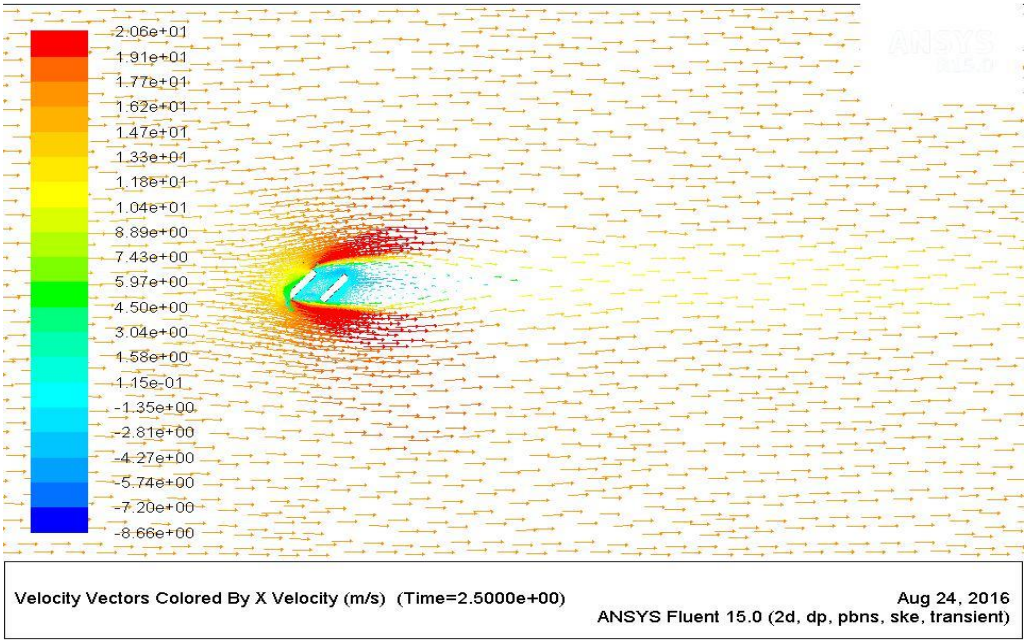

Figure 70. Velocity Vectors Colored by X-Velocity , at gap ratio =0.5 and 60 degree

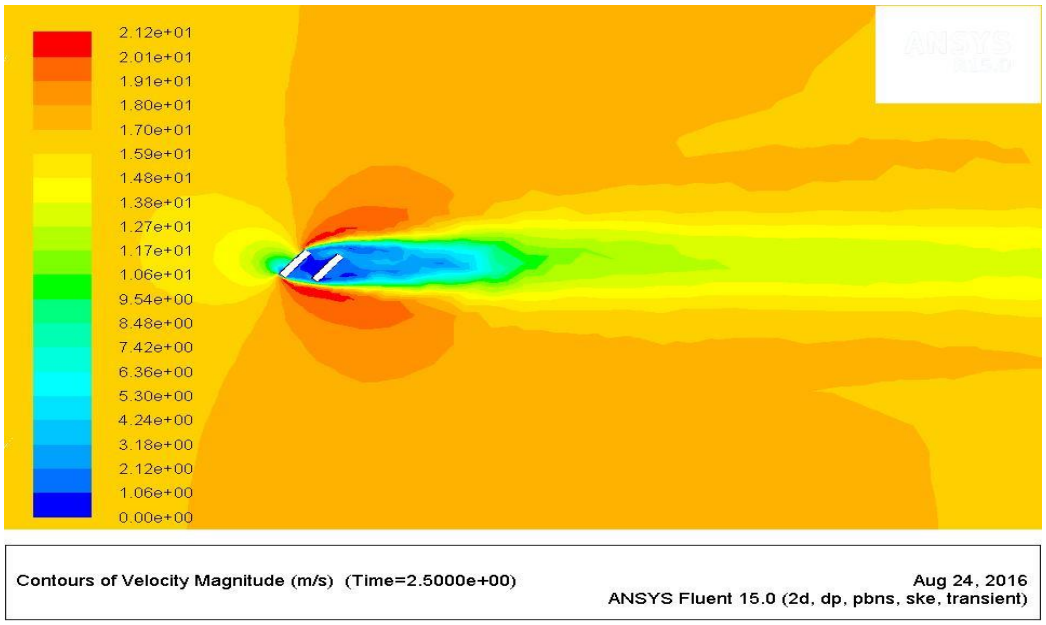

Figure 71. Contours of Velocity Magnitude (m/s), at gap ratio =0.5 and 60 degree

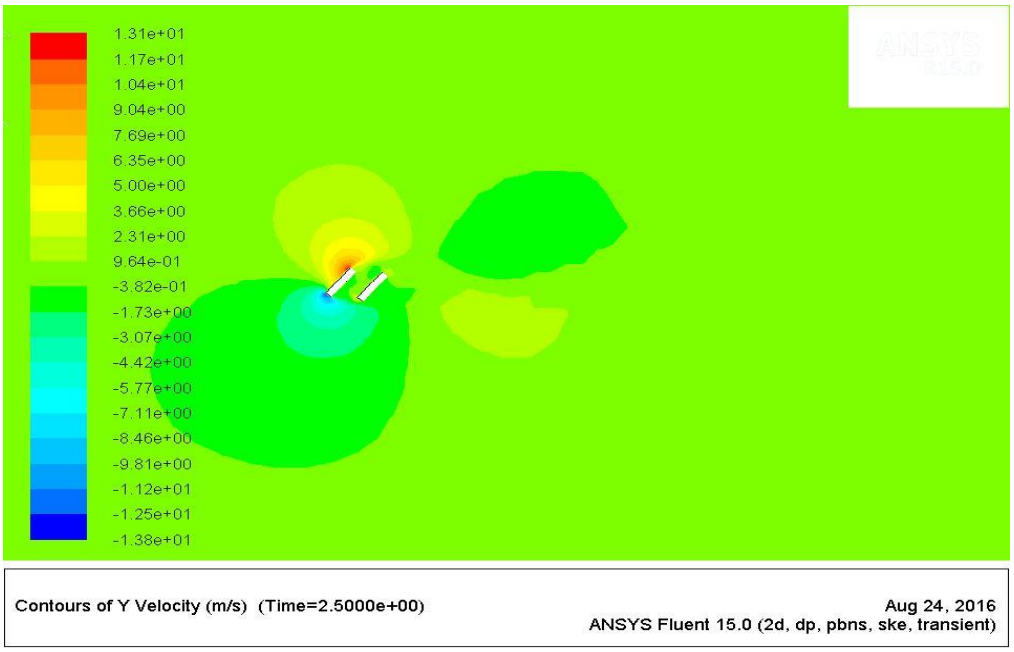

Figure 72. Contours of Y-Velocity (m/s), at gap ratio =0.5 and 60 degree

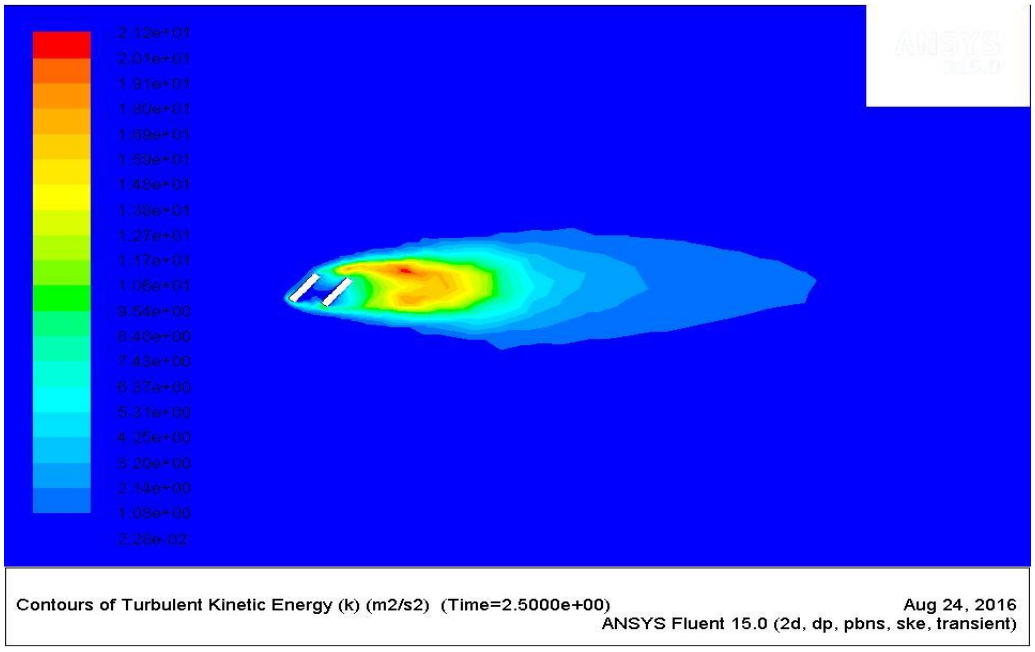

Figure 73. Contours of Turbulent Kinetic Energy (k), at gap ratio =0.5 and 60degree

Gap ratio 1:

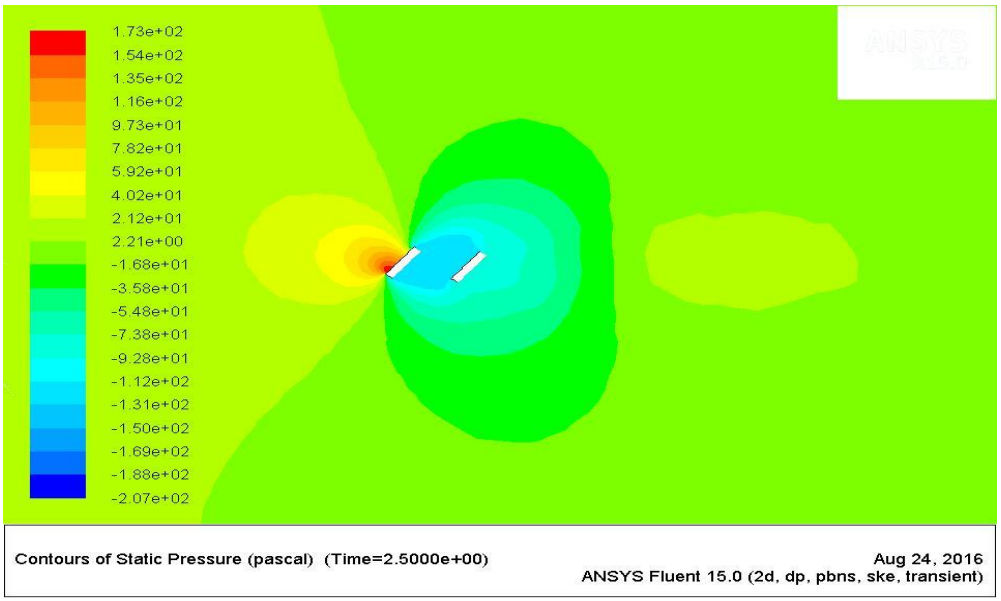

Figure 74. Contours of Static Pressure (Pa), at gap ratio=1.0 and 60 degree

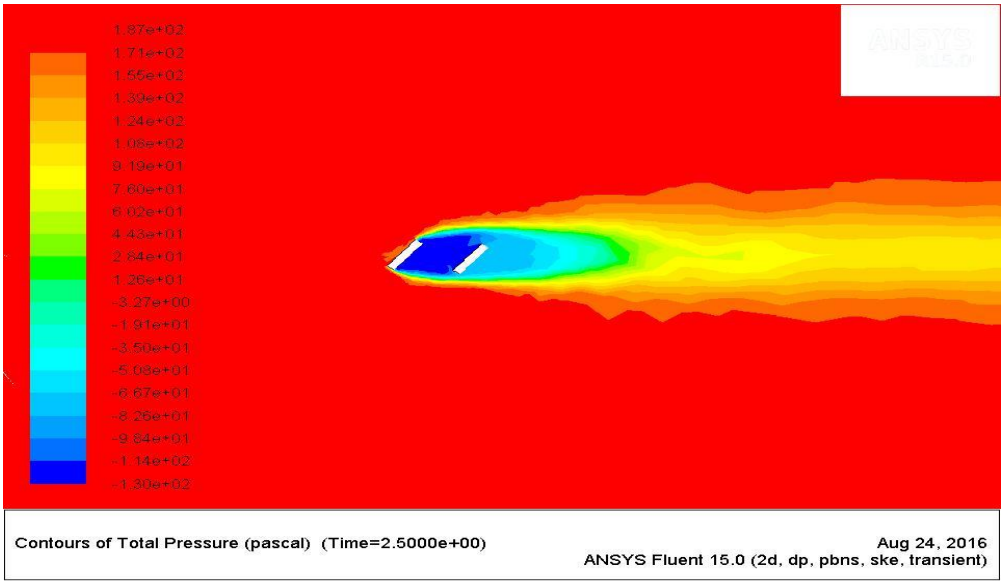

Figure 75. Contours of Total Pressure (Pa), at gap ratio=1.0 and 60 degree

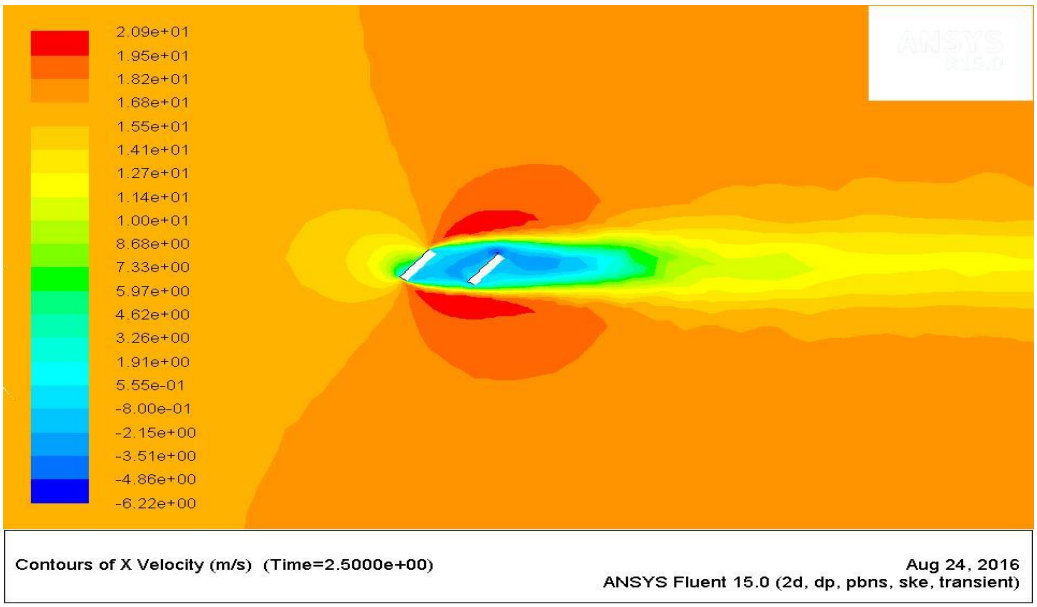

Figure 76. Contours of Total Pressure (Pa), at gap ratio=1.0 and 60 degree

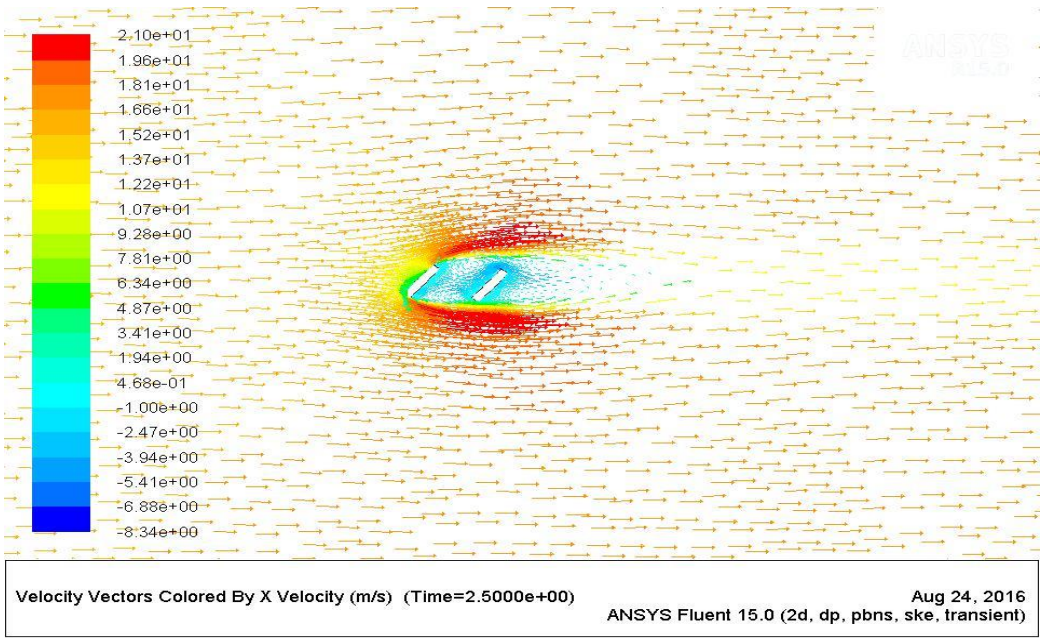

Figure 77. Velocity Vectors Colored by X-Velocity, at gap ratio =1.0 and 60 degree

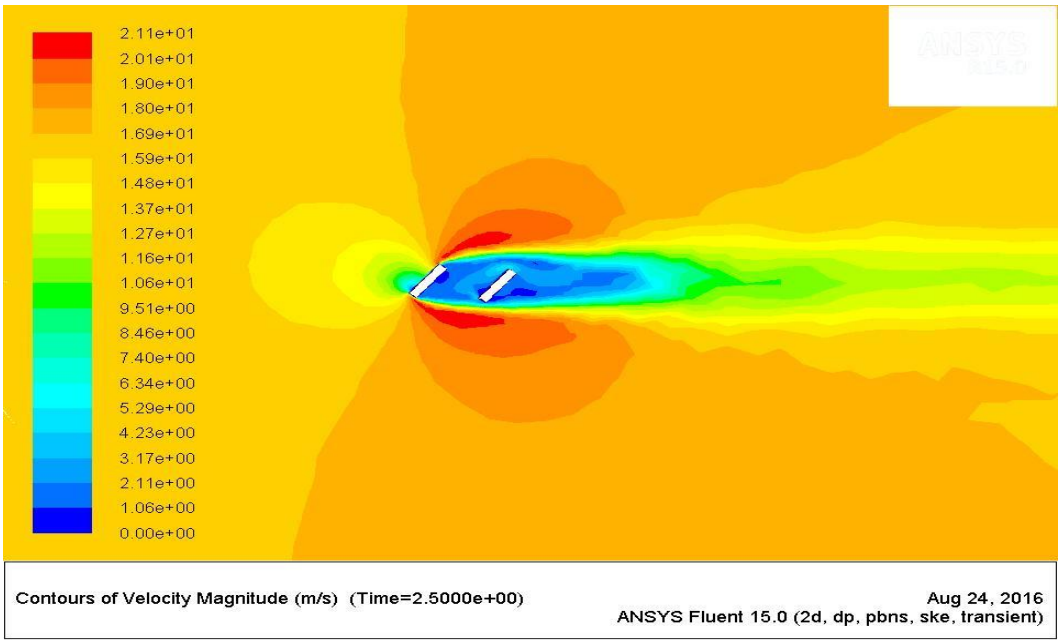

Figure 78. Contours of Velocity Magnitude (m/s), at gap ratio =1.0 and 60 degree

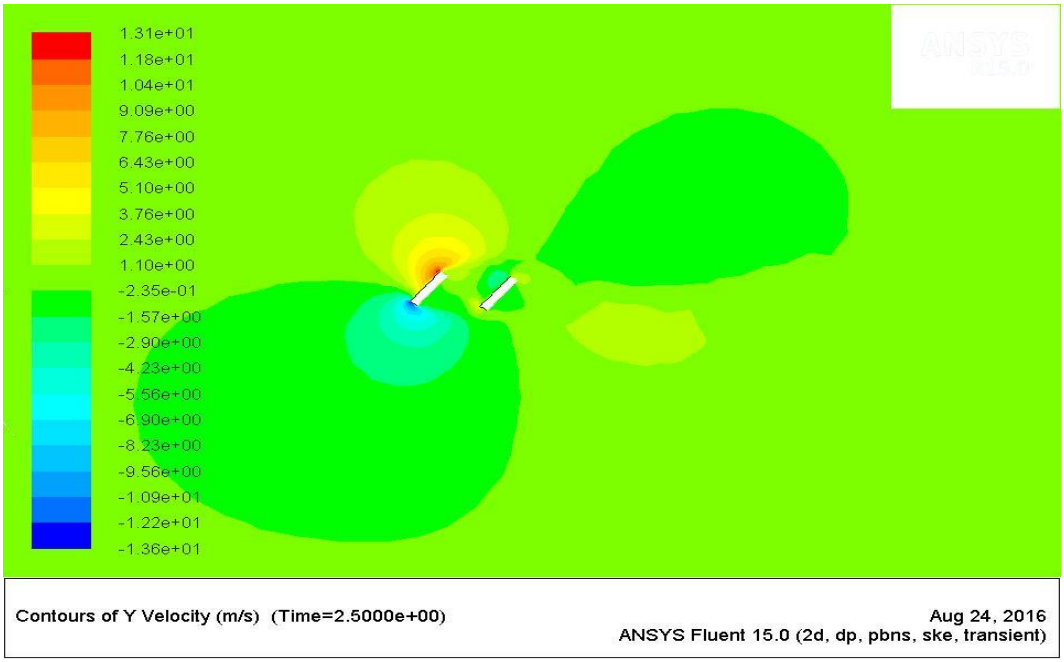

Figure 79. Contours of Y-Velocity (m/s) , at gap ratio =1.0 and 60 degree

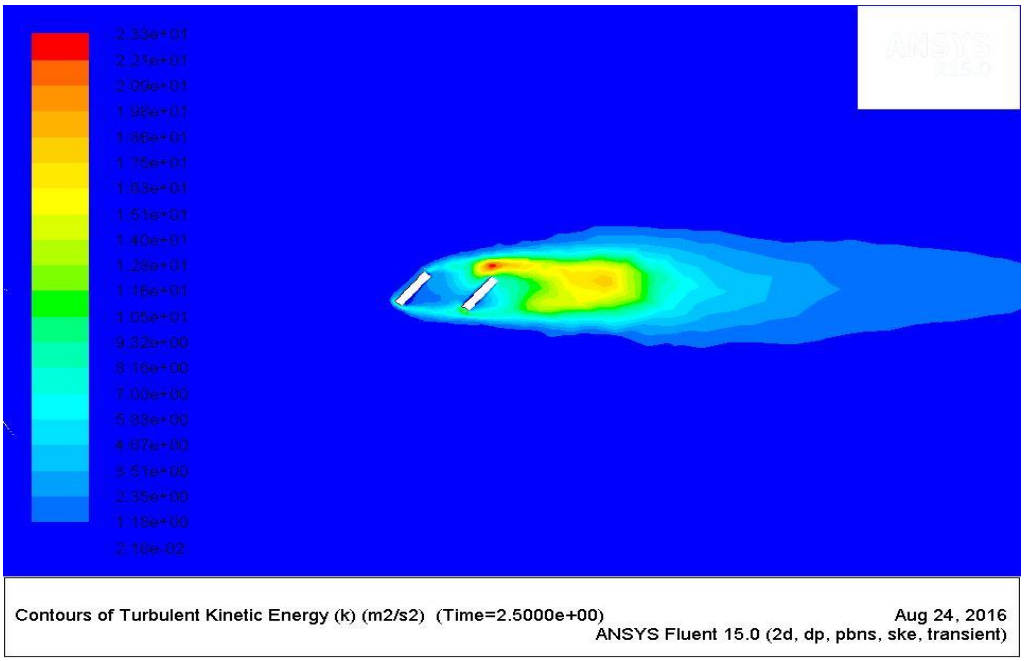

Figure 80. Contours of Turbulent Kinetic Energy (k), at gap ratio =1.0 and 60 degree

Gap ratio 1.5:

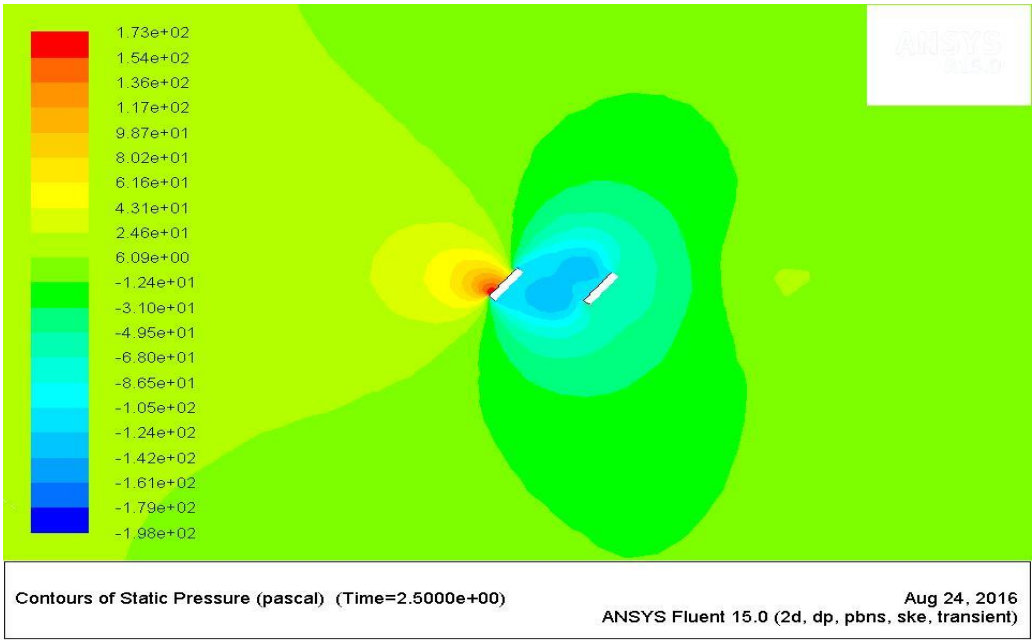

Figure 81. Contours of Static Pressure (Pa), at gap ratio=1.5 and 60 degree

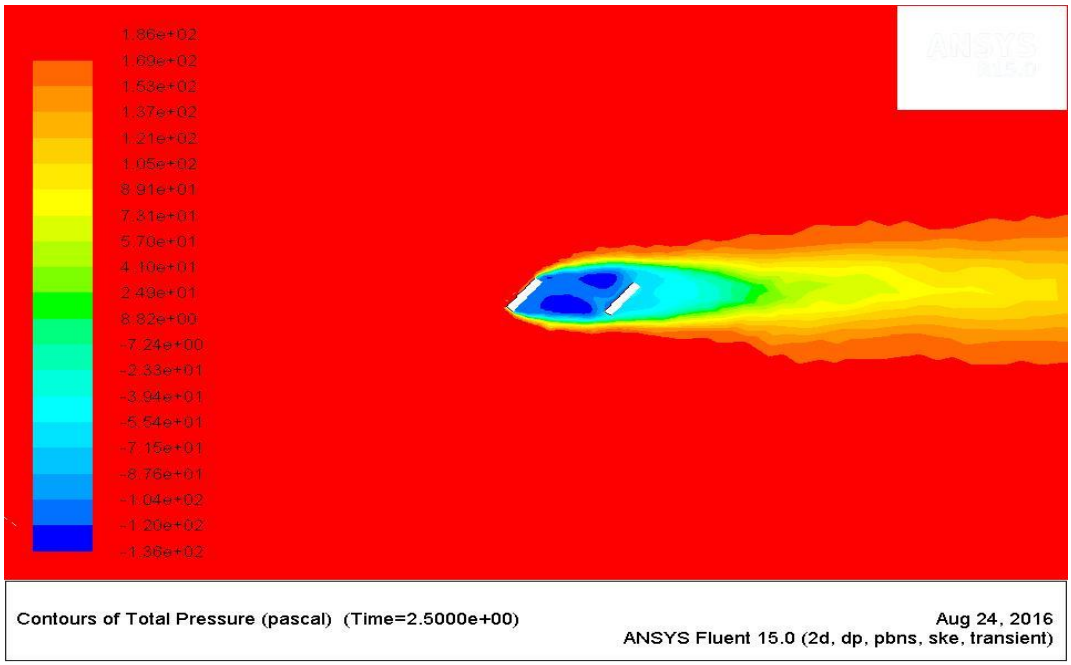

Figure 82. Contours of Total Pressure (Pa), at gap ratio=1.5 and 60 degree

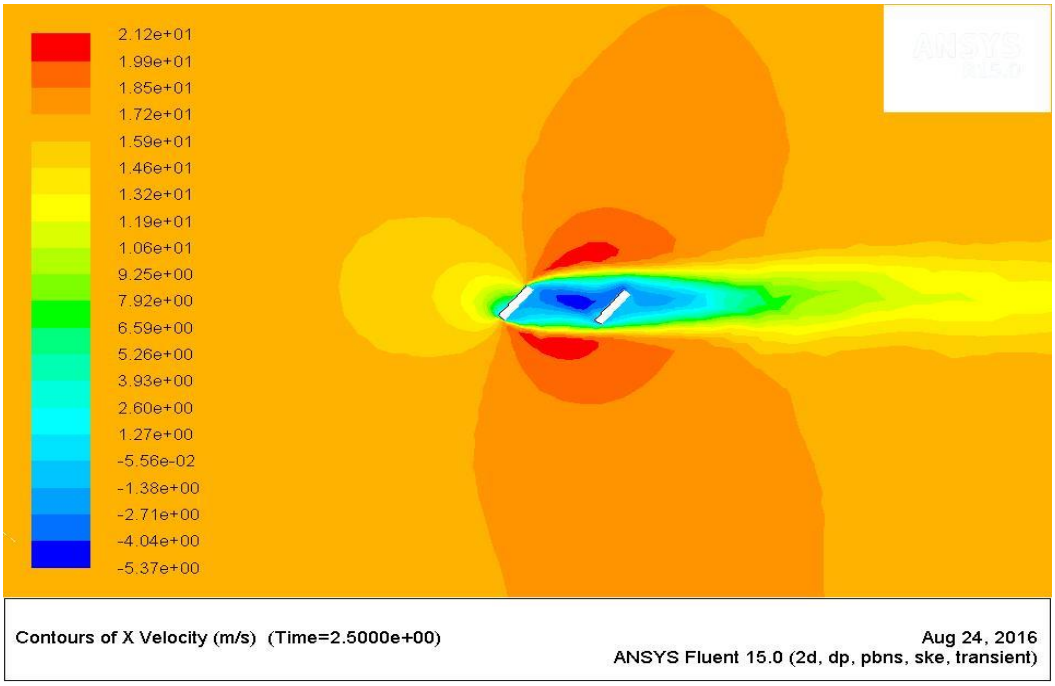

Figure 83. Contours of X-Velocity (m/s), at gap ratio =1.5 and 60 degree

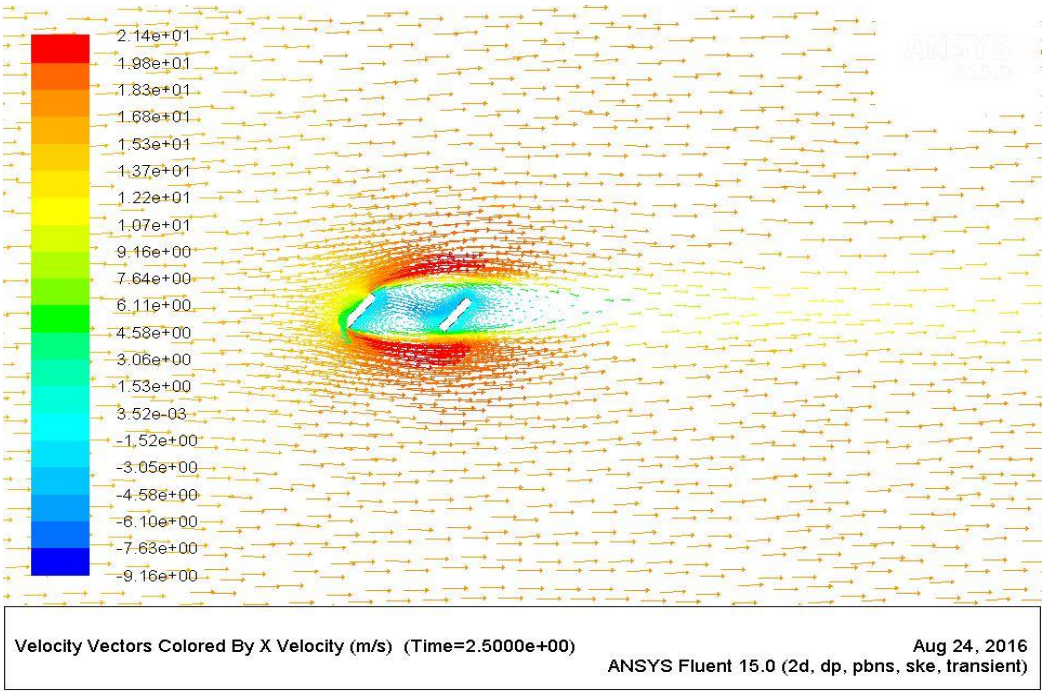

Figure 84. Velocity Vectors Colored by X-Velocity, at gap ratio =1.5 and 60 degree

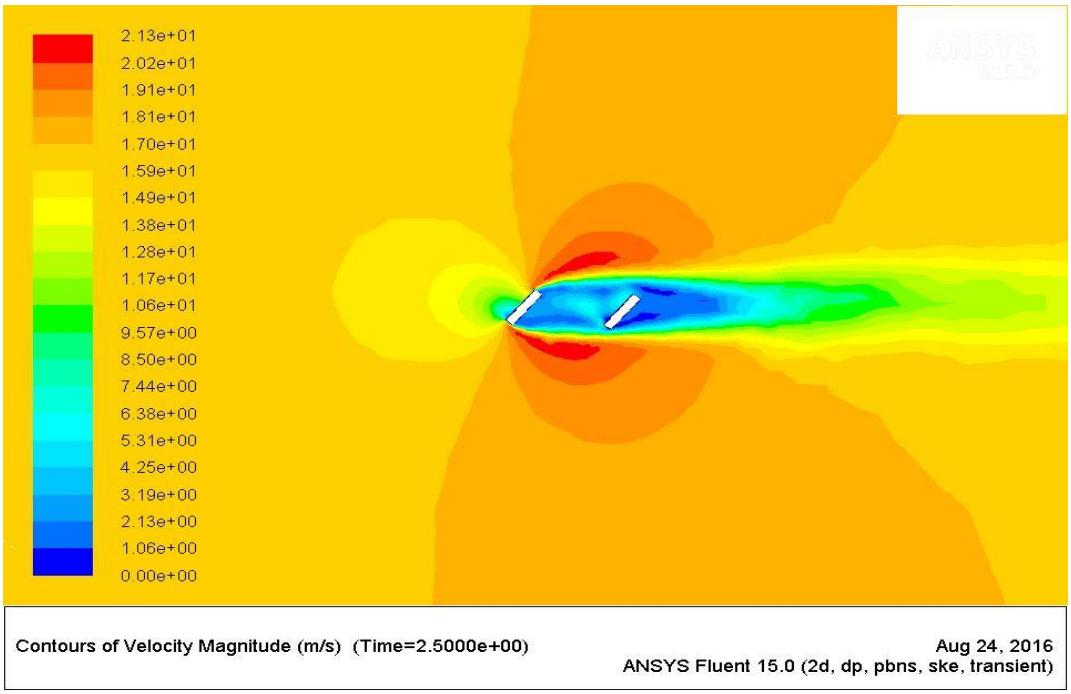

Figure 85. Contours of Velocity Magnitude (m/s), at gap ratio =1.5 and 60 degree

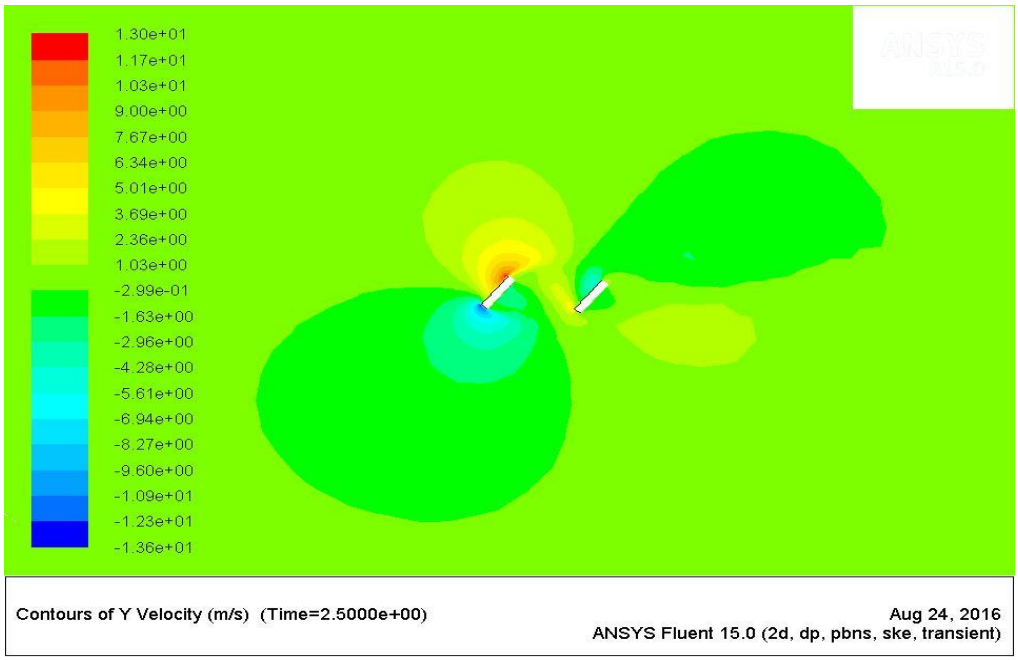

Figure 86. Contours of Y-Velocity (m/s), at gap ratio =1.5 and 60 degree

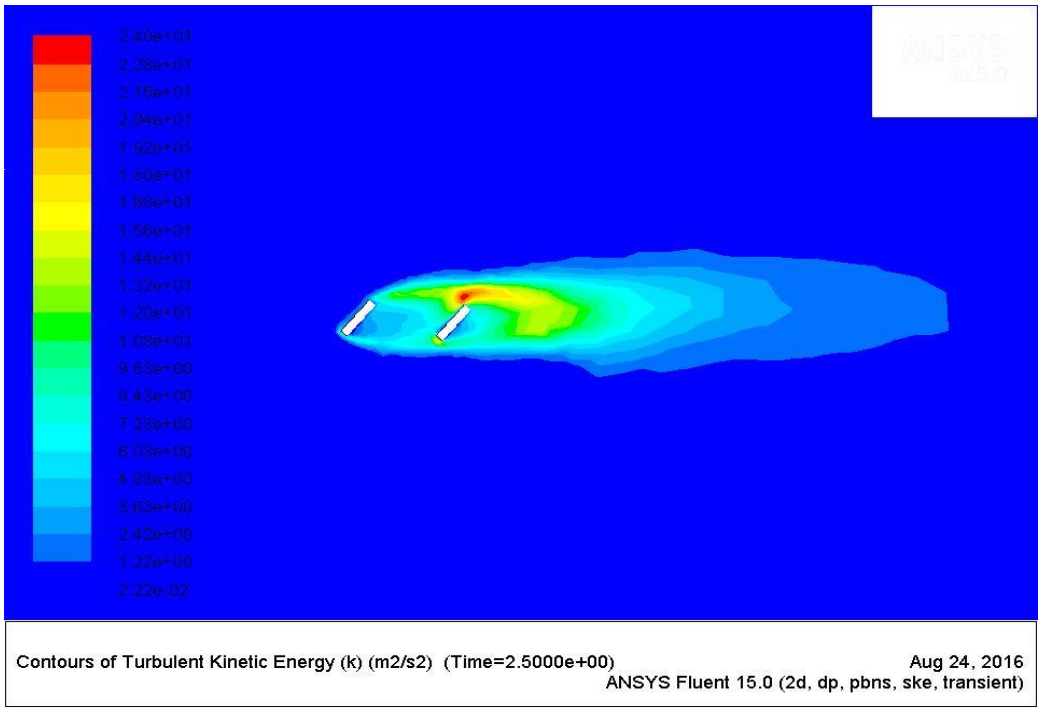

Figure 87. Contours of Turbulent Kinetic Energy (k), at gap ratio =1.5 and 60 degree

Gap ratio 2:

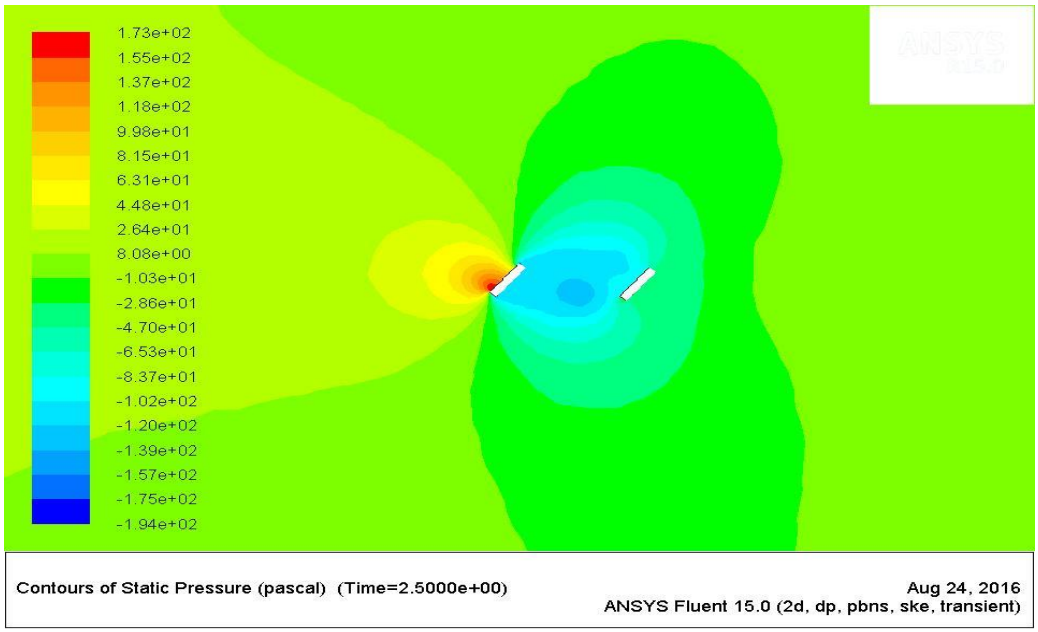

Figure 88. Contours of Static Pressure (Pa), at gap ratio=2.0 and 60 degree

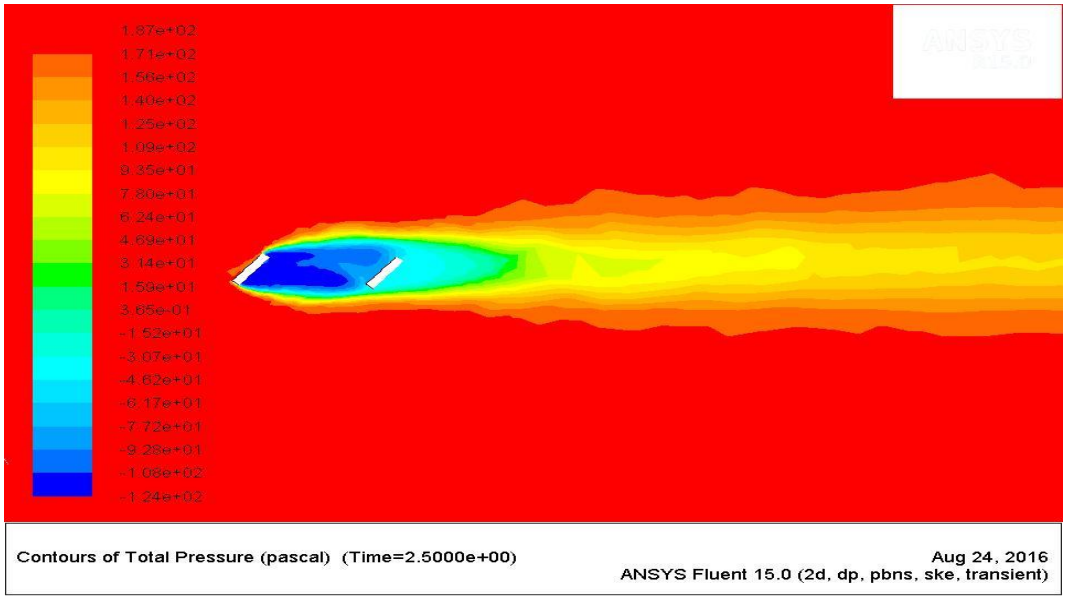

Figure 89. Contours of Total Pressure (Pa), at gap ratio=2.0 and 60 degree

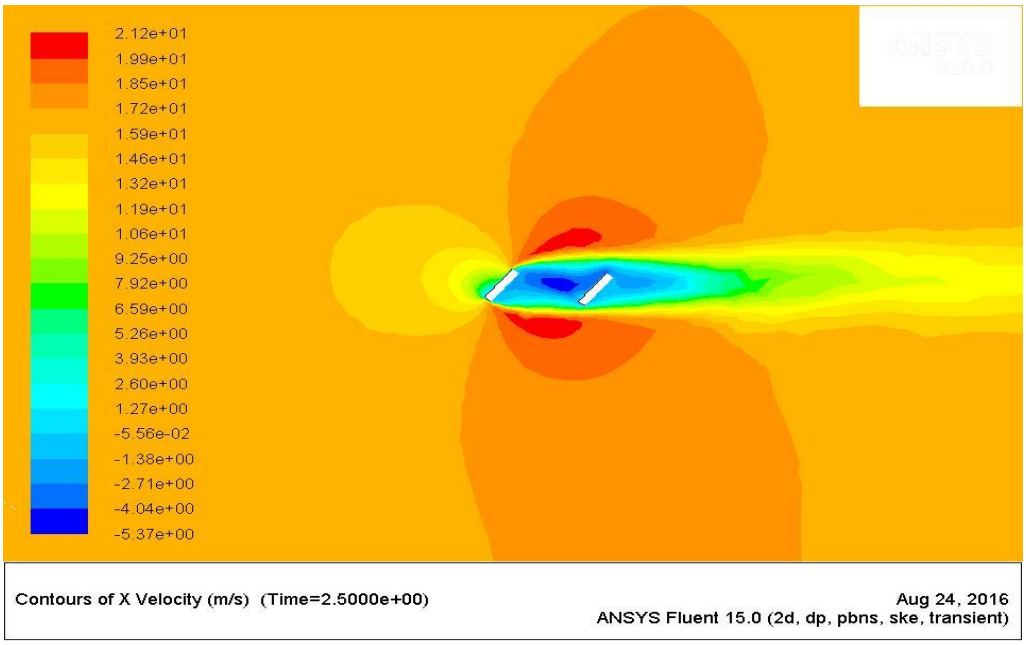

Figure 90. Contours of X-Velocity (m/s), at gap ratio =2.0 and 60 degree

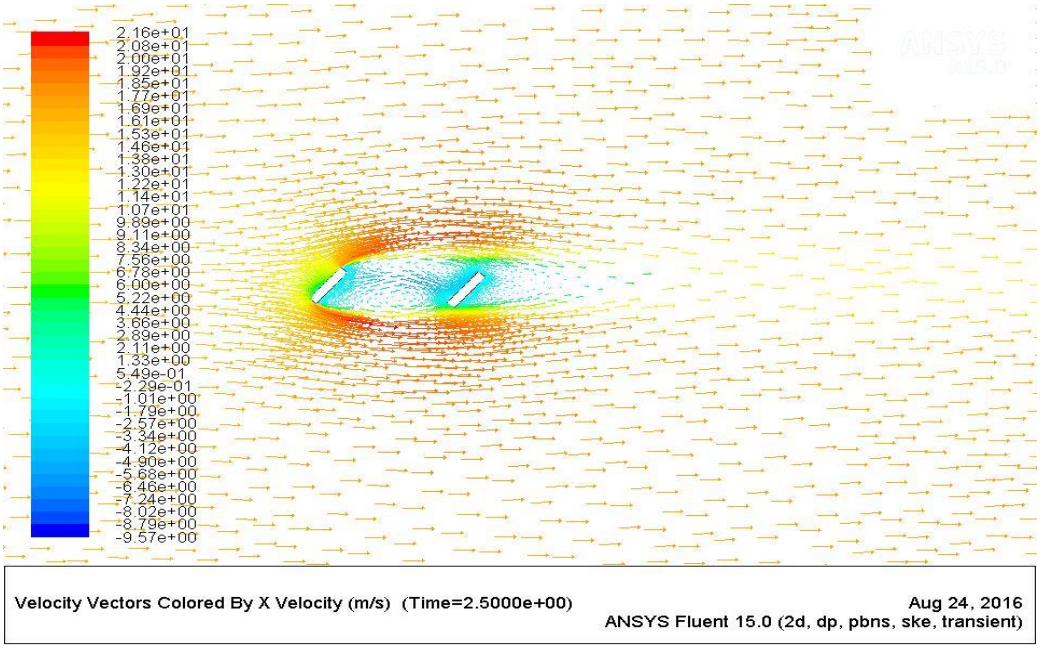

Figure 91. Velocity Vectors Colored by X-Velocity, at gap ratio =2.0 and 60 degree

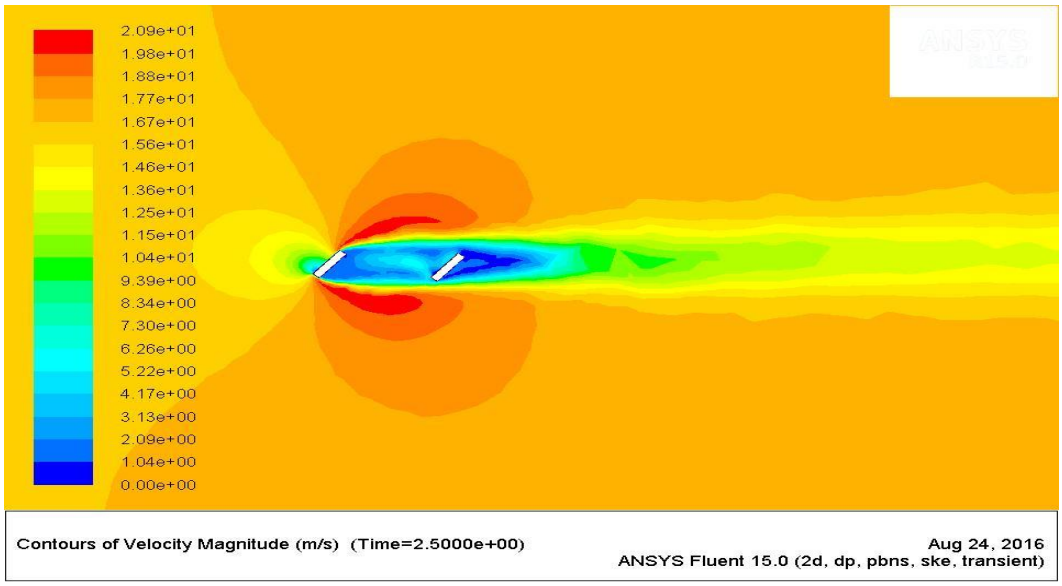

Figure 92. Contours of Velocity Magnitude (m/s), at gap ratio =2.0 and 60 degree

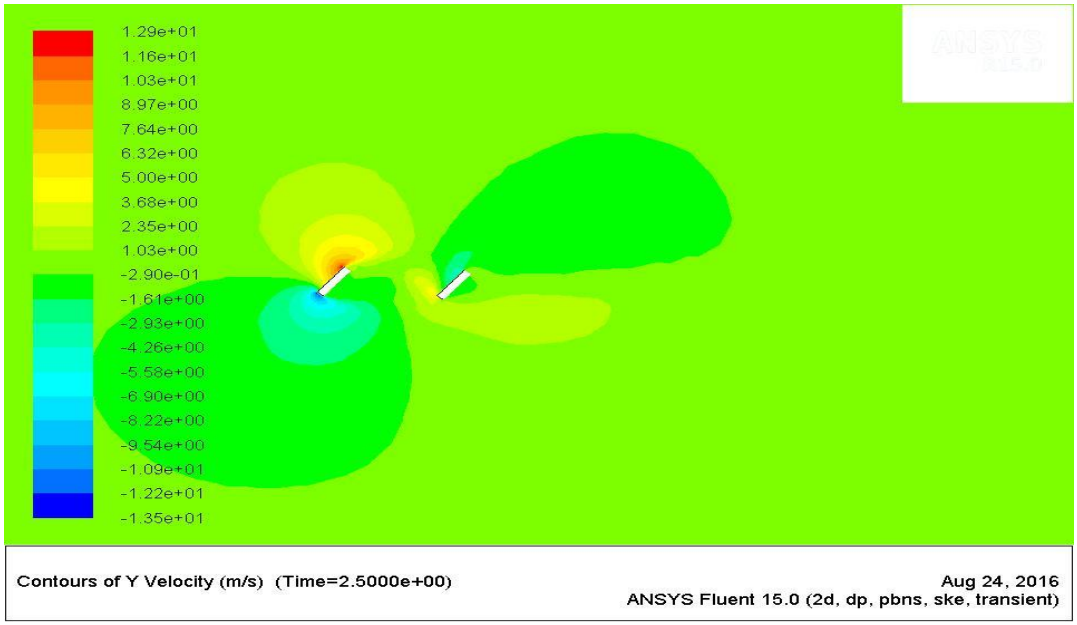

Figure 93. Contours of Y-Velocity (m/s), at gap ratio =2.0 and 60 degree

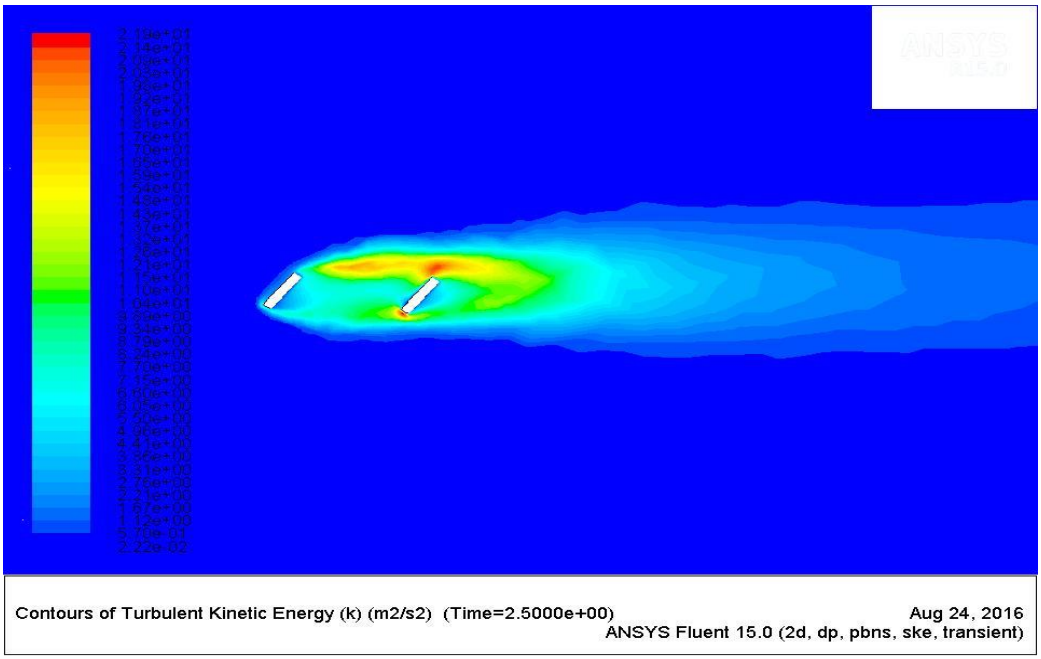

Figure 94. Contours of Turbulent Kinetic Energy (k), at gap ratio =2.0 and 60 degree

As shown in figures 66 – 87 in the declined flat plates by gap ratio 0.5, 1.0, 1.5 and 2.0 the 60 degree pressure is same in all domain except behind the plates as they also demonstrated the same Strouhal number. Vortex appears just between two plates, in upstream angle of attack. The kinetic turbulent energy is also increased for gap ratio 0.5 and 1.0 however by increasing gap ratio a vortex is develop behind of second plate and it is shown in vector velocity. In the gap ratio 2.0 which has an upward and downward angle, turbulent kinetic energy increases.

In below shown inclined plate by 45 degree contours: static pressure, total pressure, x-velocity and vector x-velocity, contour of y-velocity and kinetic energy by order:

Gap ratio 0.5:

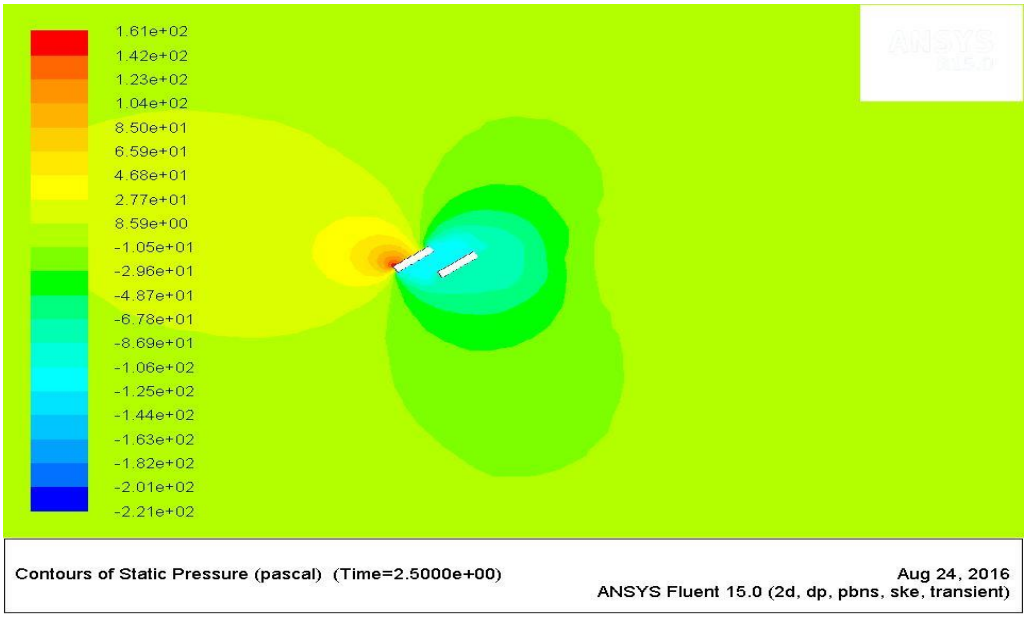

Figure 95. Contours of Static Pressure (Pa), at gap ratio=0.5 and 45 degree

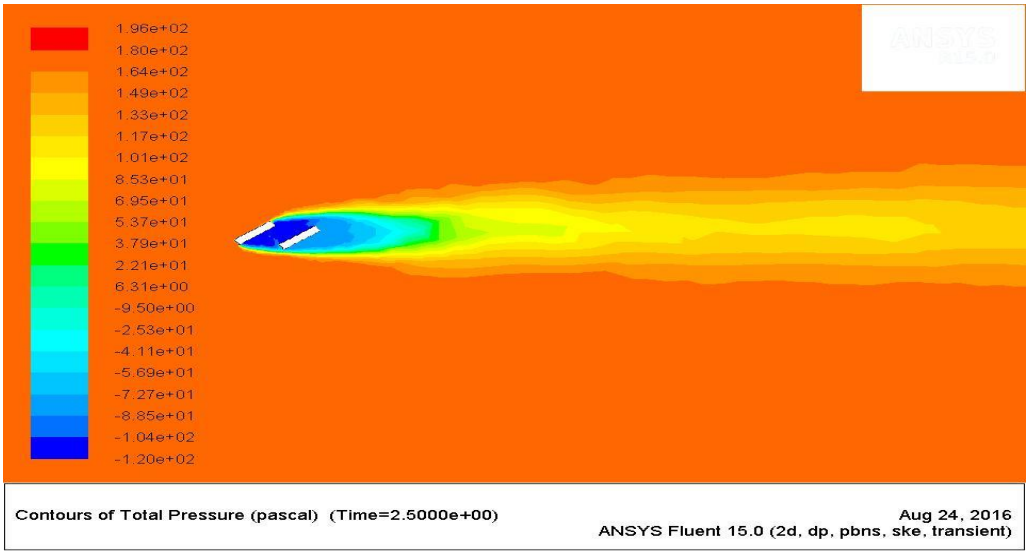

Figure 96. Contours of Total Pressure (Pa), at gap ratio=0.5 and 45 degree

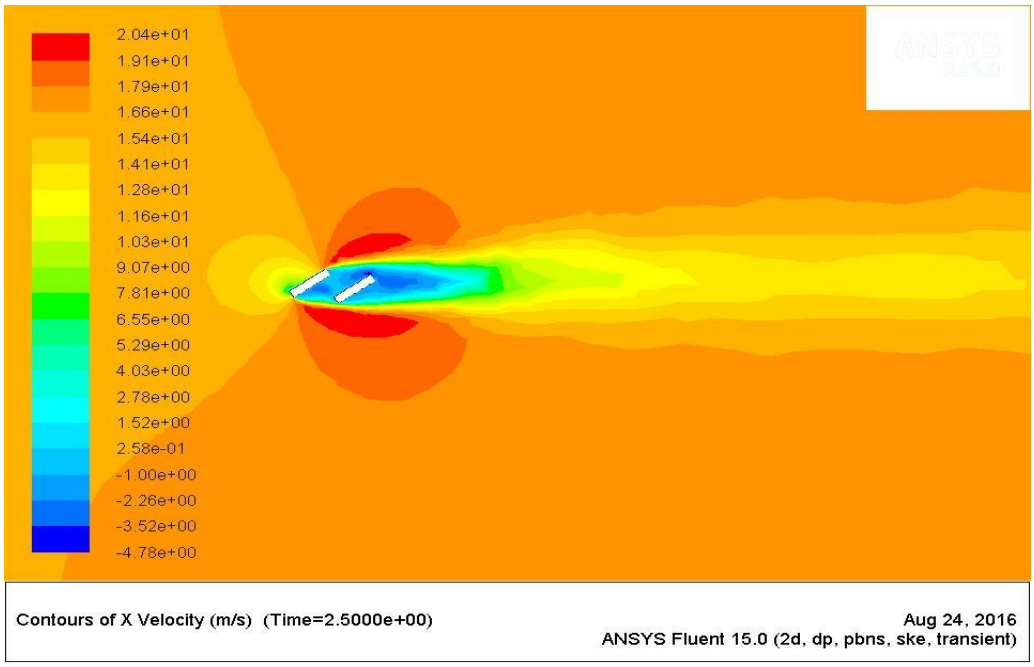

Figure 97. Contours of X-Velocity (m/s), at gap ratio =0.5 and 45 degree

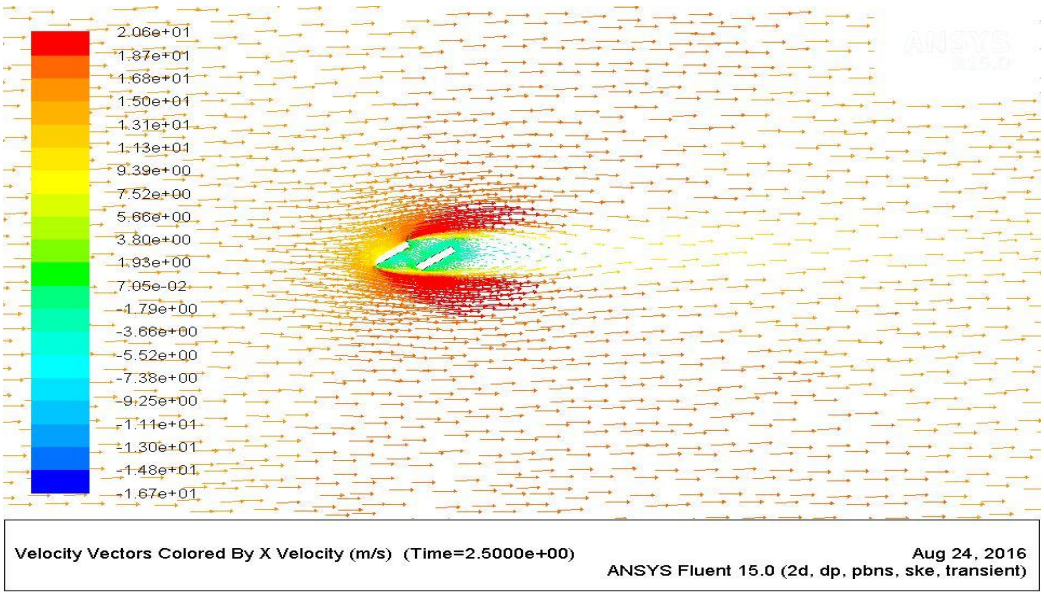

Figure 98. Velocity Vectors Colored by X-Velocity, at gap ratio =0.5 and 45 degree

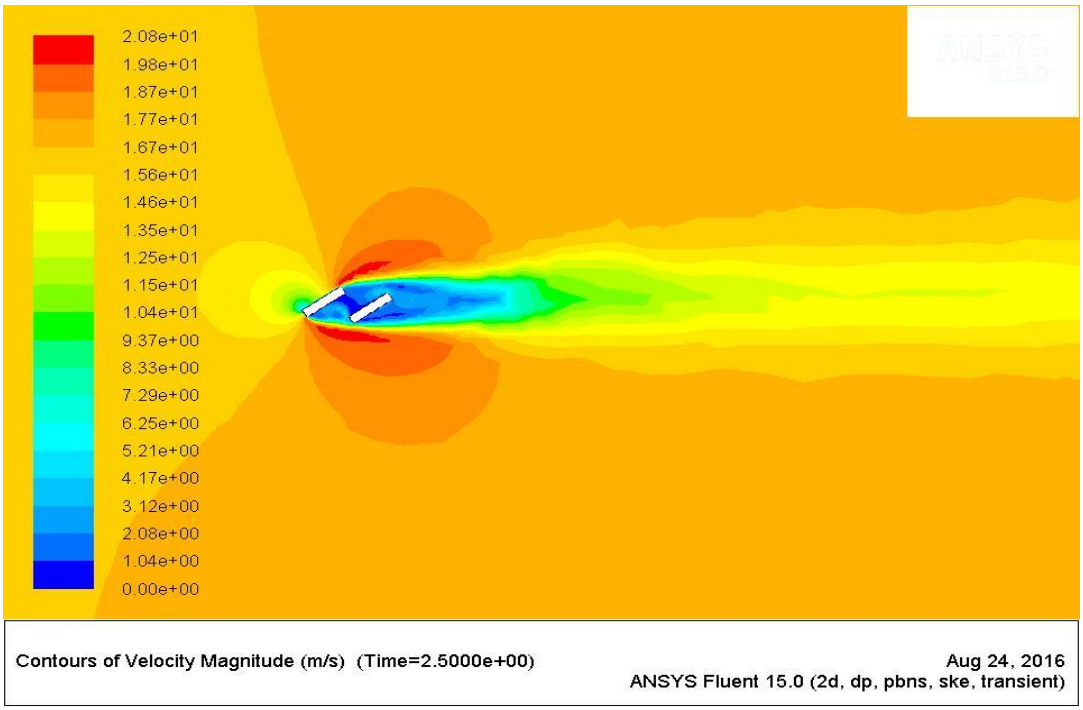

Figure 99. Contours of Velocity Magnitude (m/s), at gap ratio =0.5 and 45 degree

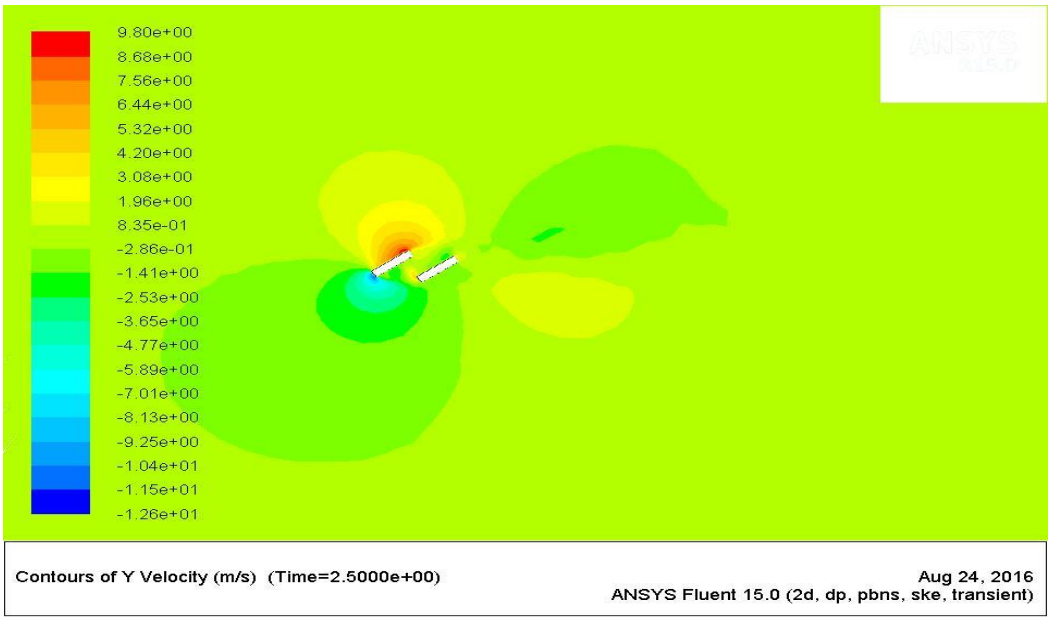

Figure 100. Contours of Y-Velocity (m/s), at gap ratio =0.5 and 45 degree

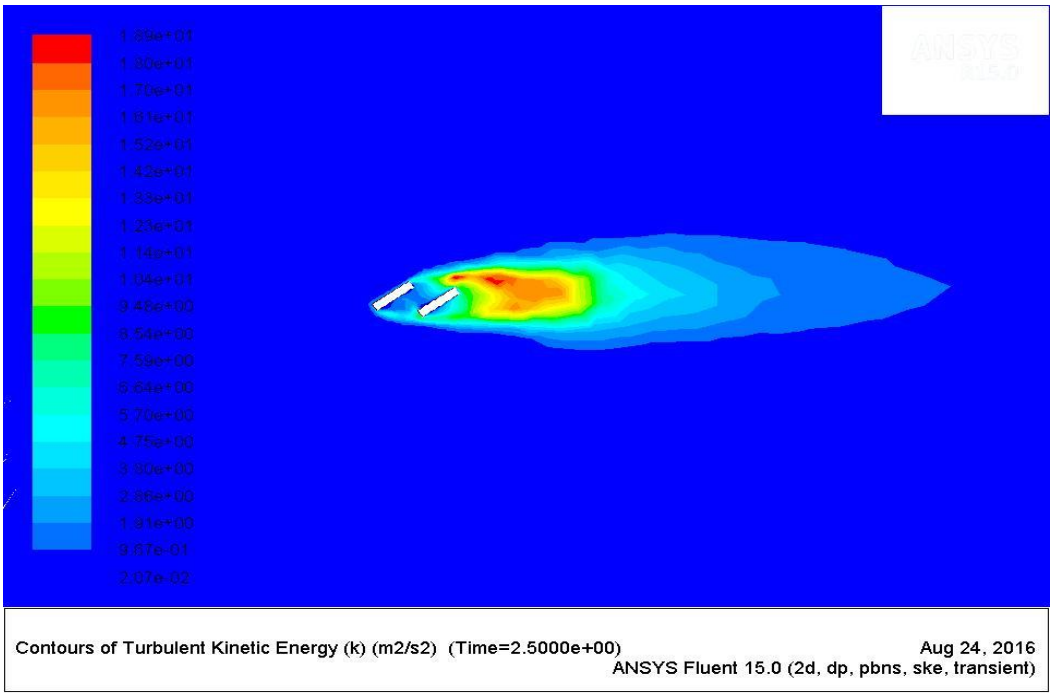

Figure 101. Contours of Turbulent Kinetic Energy (k), at gap ratio =0.5 and 45 degree

Gap ratio 1:

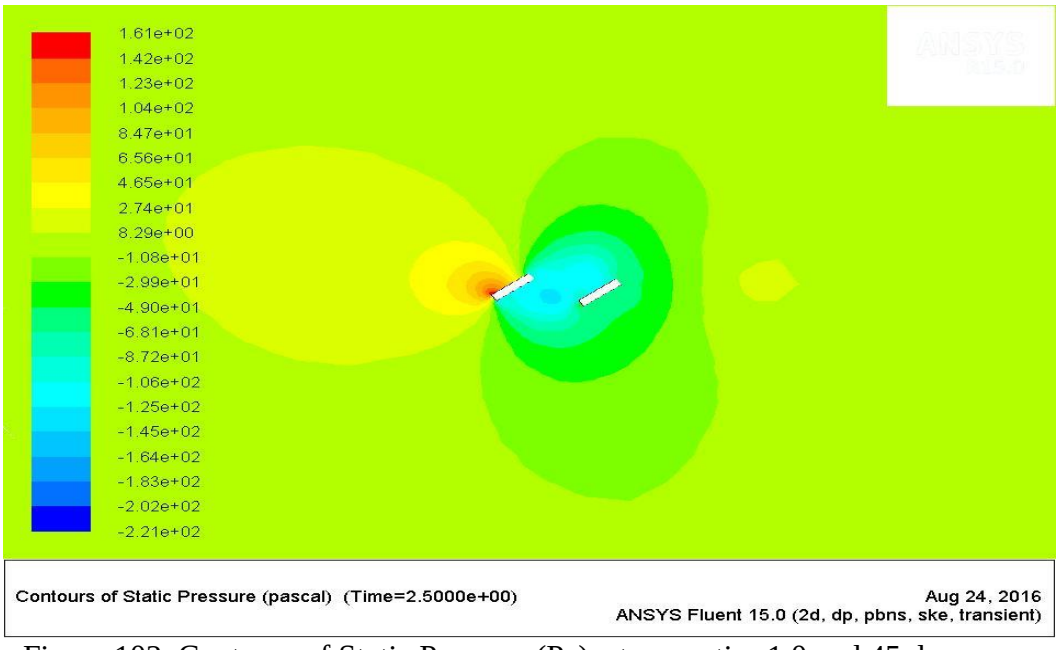

Figure 102. Contours of Static Pressure (Pa), at gap ratio=1.0 and 45 degree

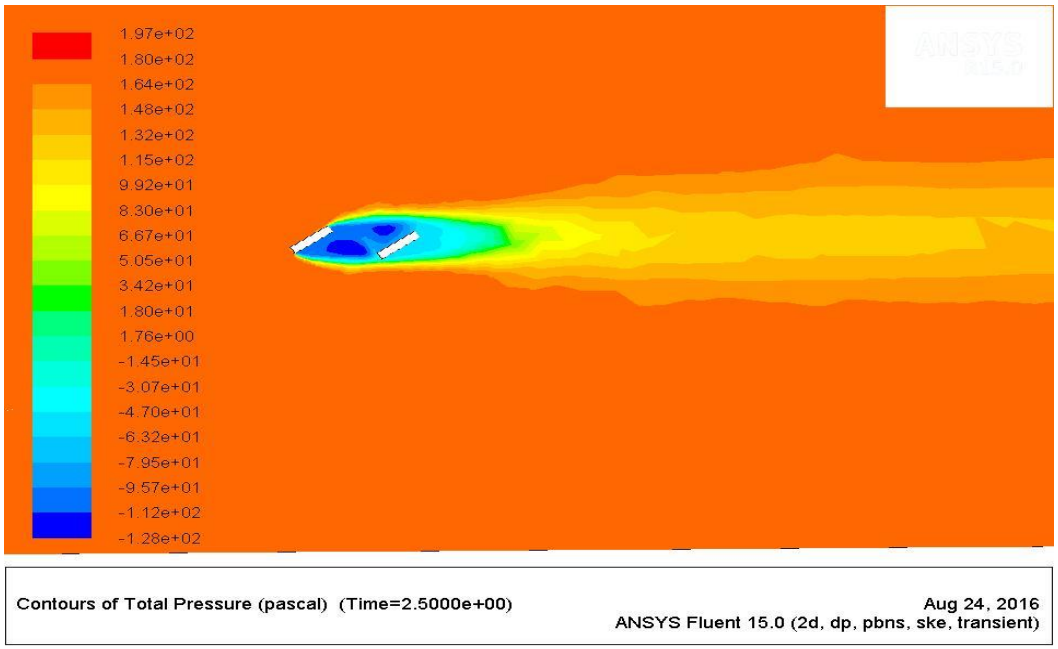

Figure 103. Contours of Total Pressure (Pa), at gap ratio=1.0 and 45 degree

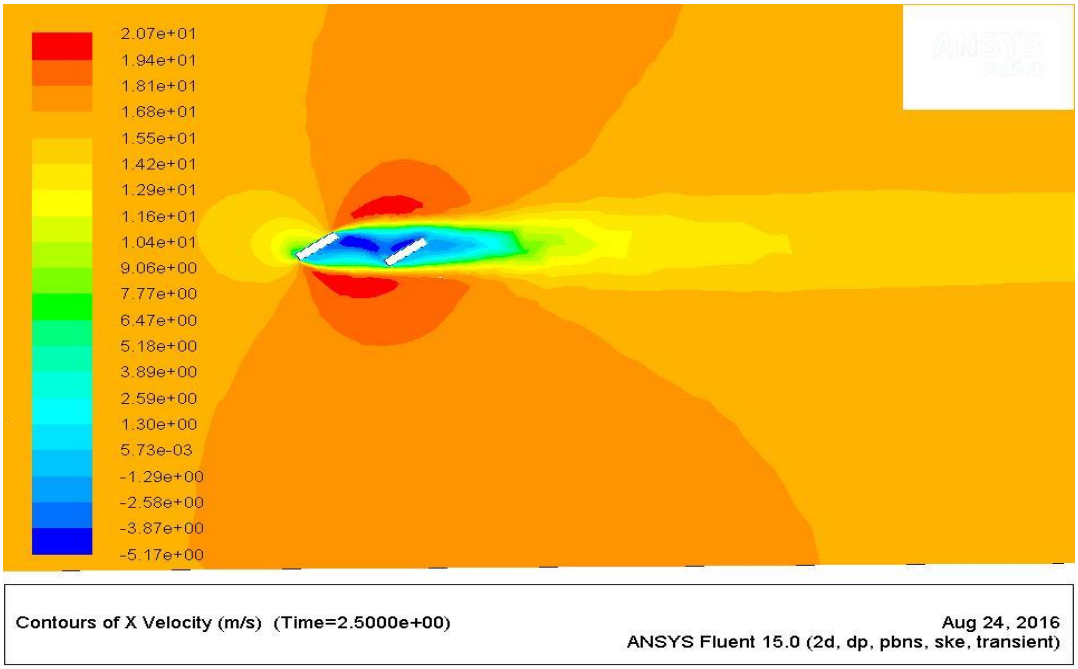

Figure 104. Contours of X-Velocity (m/s), at gap ratio =1.0 and 45 degree

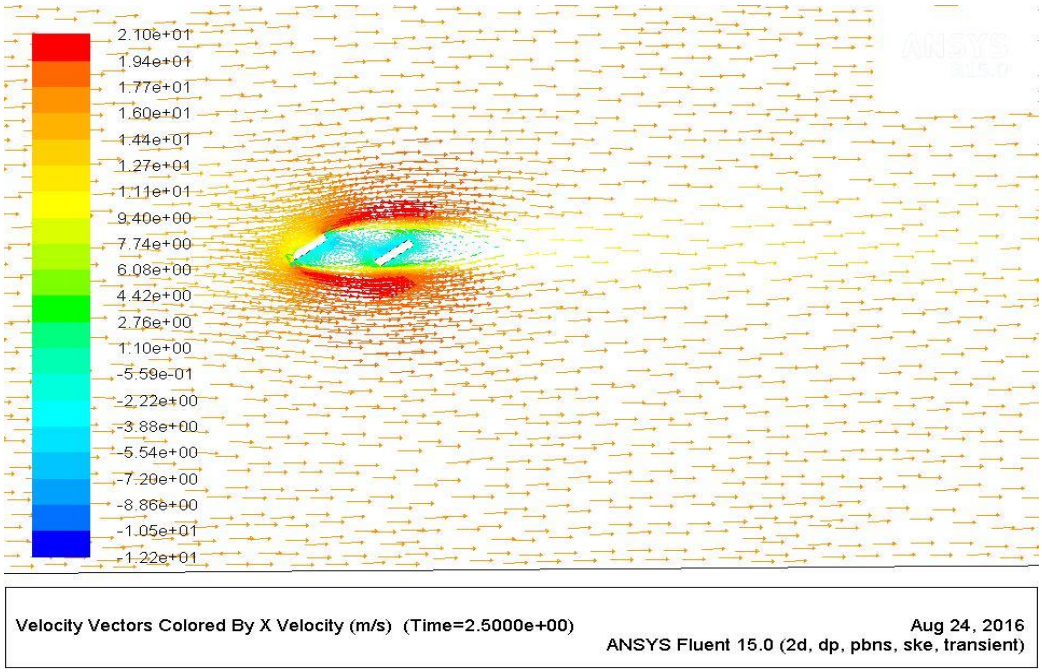

Figure 105. Velocity Vectors Colored by X-Velocity, at gap ratio =1.0 and 45 degree

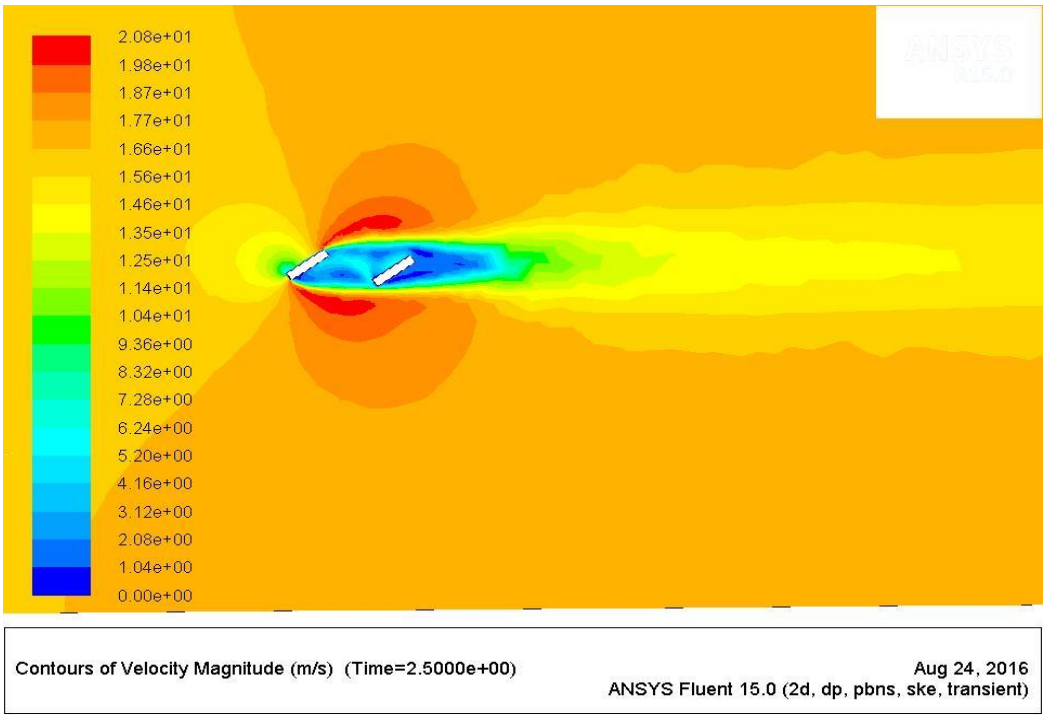

Figure 106. Contours of Velocity Magnitude (m/s), at gap ratio =1.0 and 45 degree

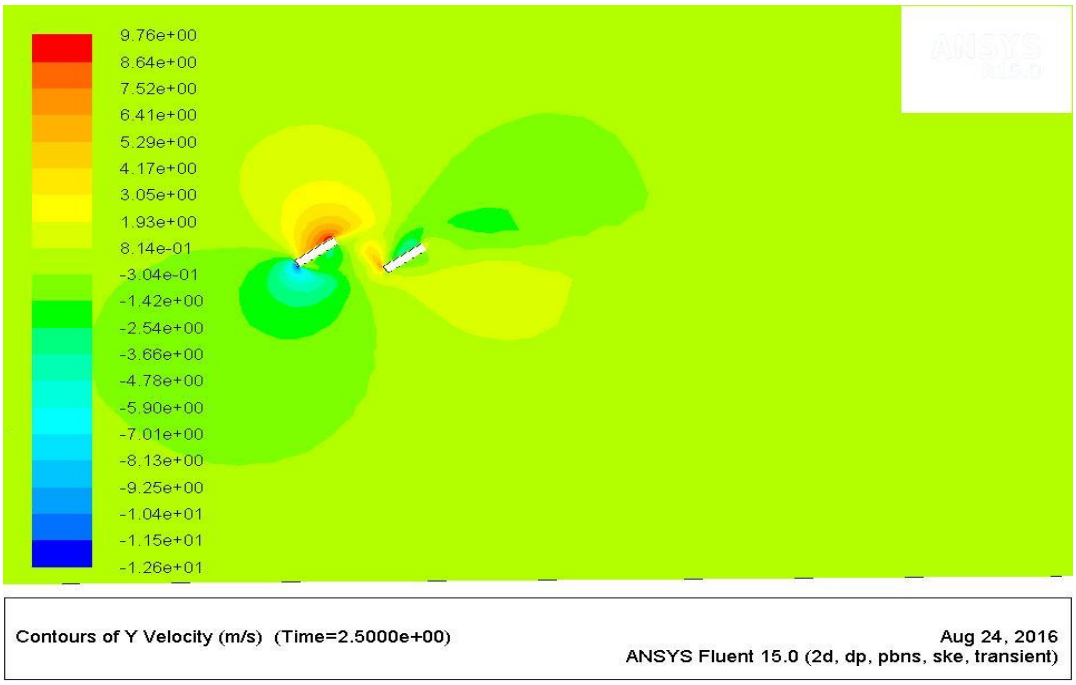

Figure 107. Contours of Y-Velocity (m/s), at gap ratio =1.0 and 45 degree

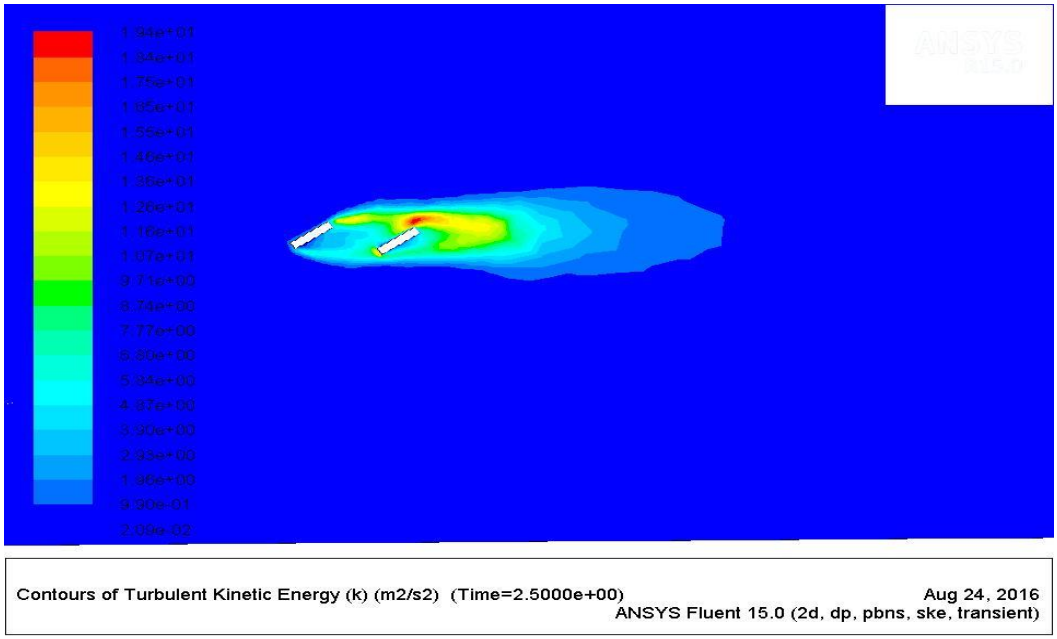

Figure 108. Contours of Turbulent Kinetic Energy (k), at gap ratio =1.0 and 45 degree

Gap ratio 1.5:

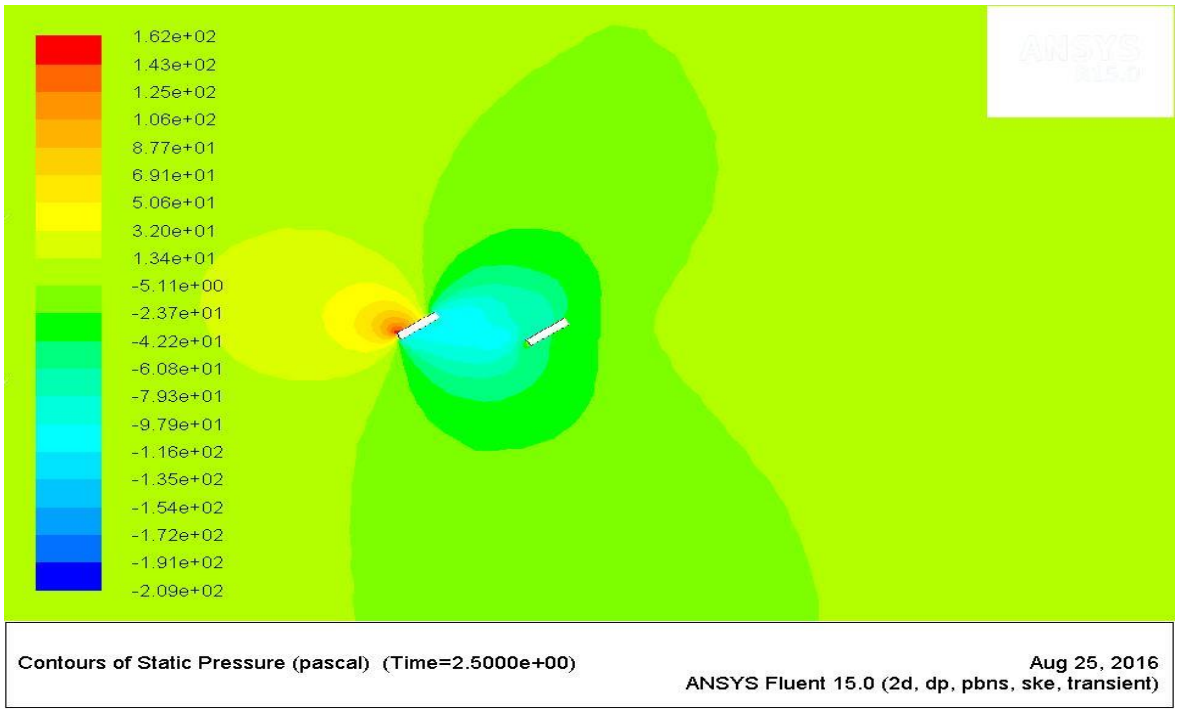

Figure 109. Contours of Static Pressure (Pa), at gap ratio=1.5 and 45 degree

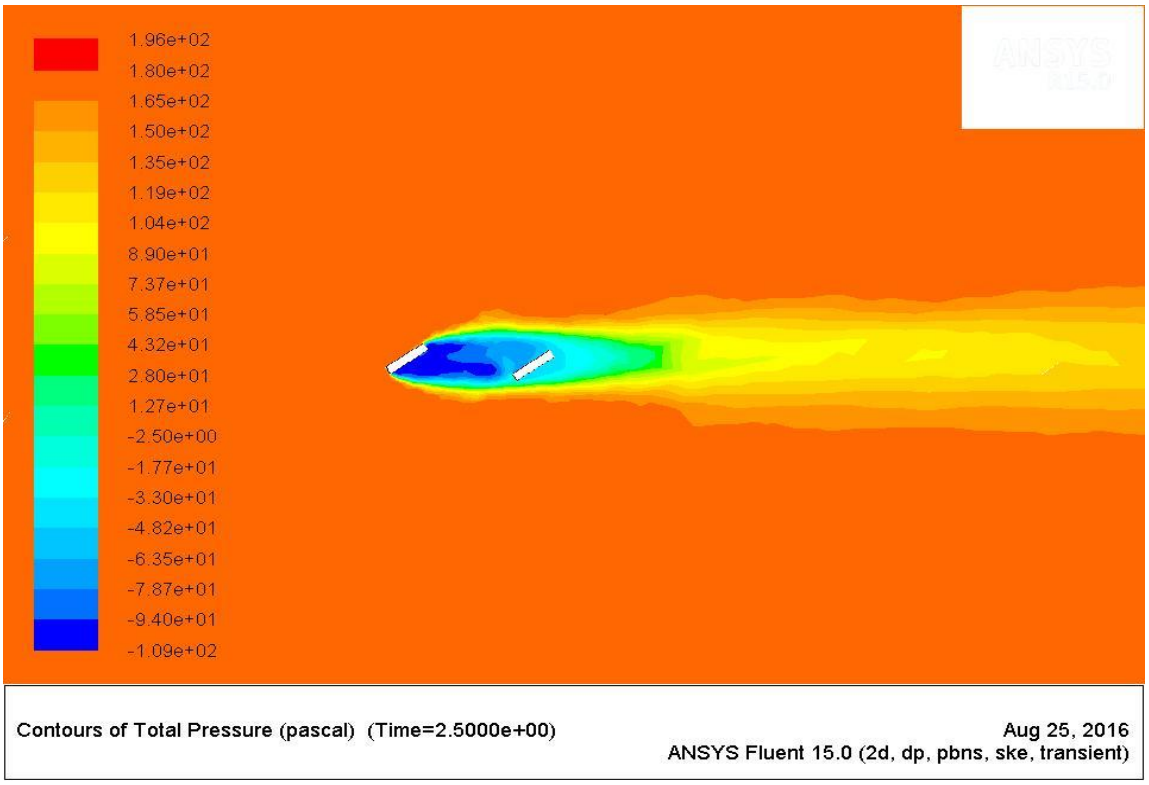

Figure 110. Contours of Total Pressure (Pa), at gap ratio=1.5 and 45 degree

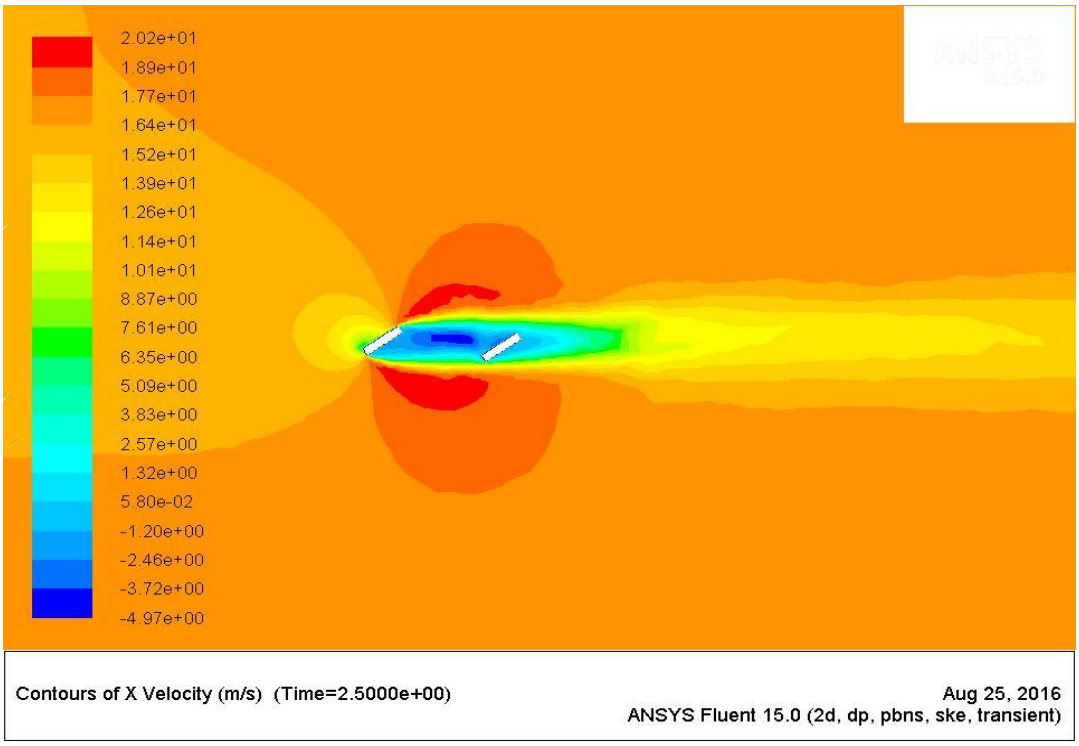

Figure 111. Contours of X-Velocity (m/s), at gap ratio =1.5 and 45 degree

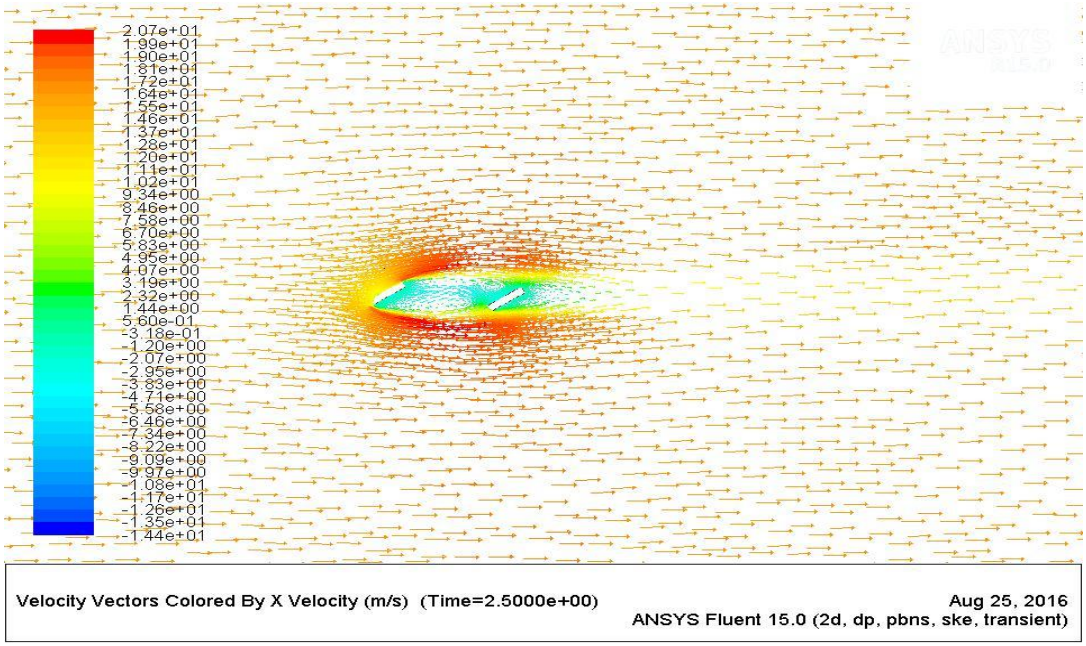

Figure 112. Velocity Vectors Colored by X-Velocity, at gap ratio =1.5 and 45 degree

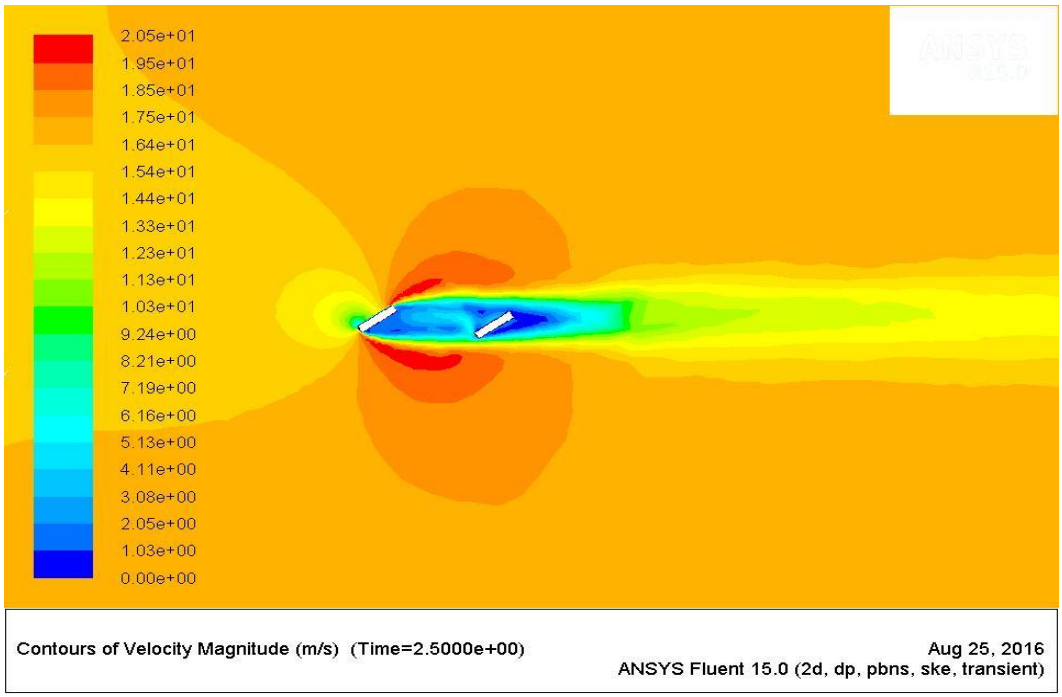

Figure 113. Contours of Velocity Magnitude (m/s), at gap ratio =1.5 and 45 degree

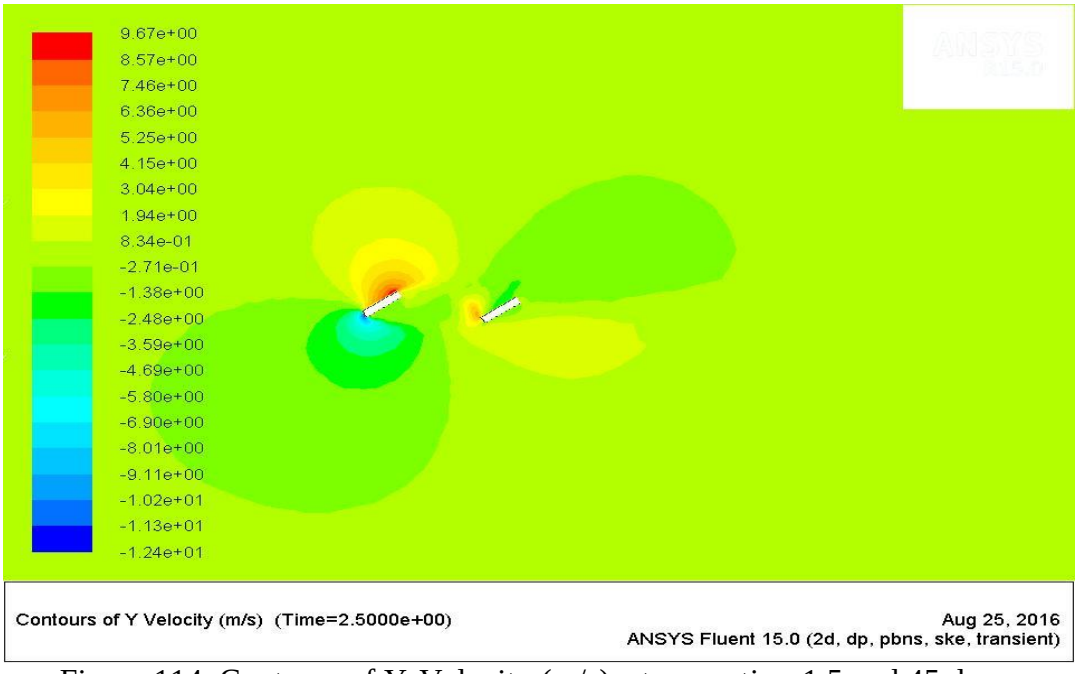

Figure 114. Contours of Y-Velocity (m/s), at gap ratio =1.5 and 45 degree

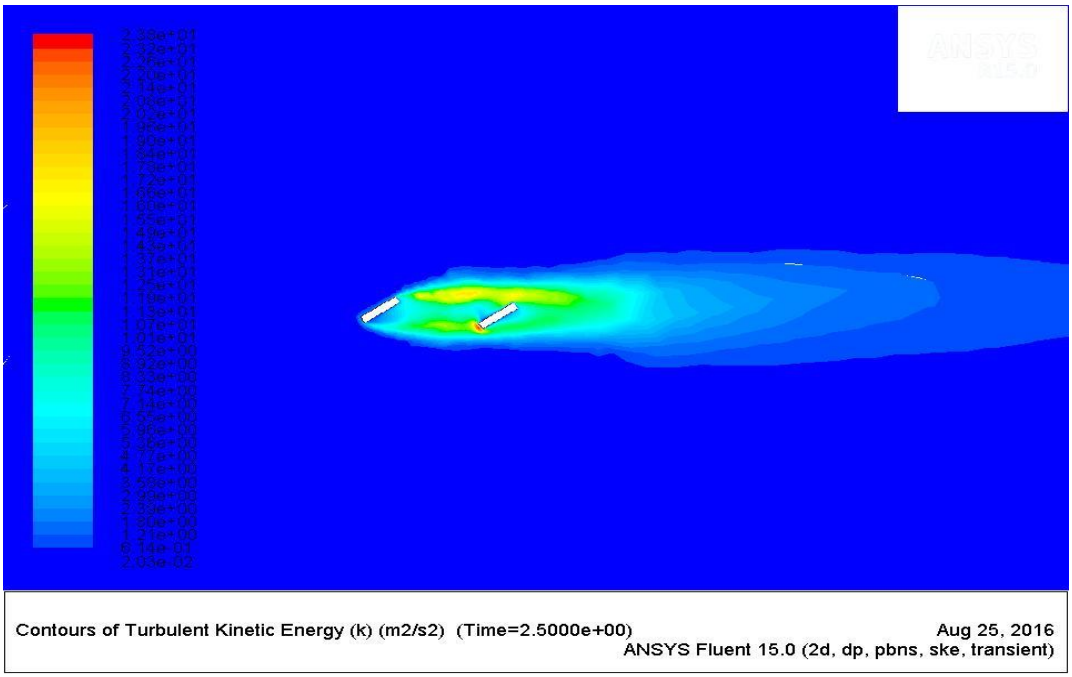

Figure 115. Conours of Turbulent Kinetic Energy (k), at gap ratio =1.5 and 45 degree

Gap ratio 2:

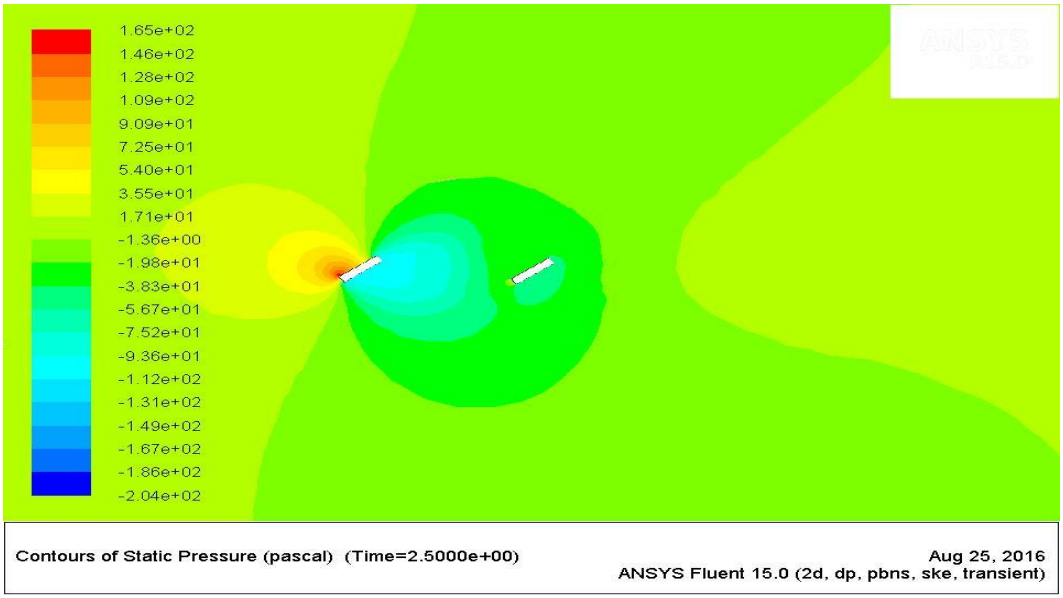

Figure 116. Contours of Static Pressure (Pa), at gap ratio =2.0 and 45 degree

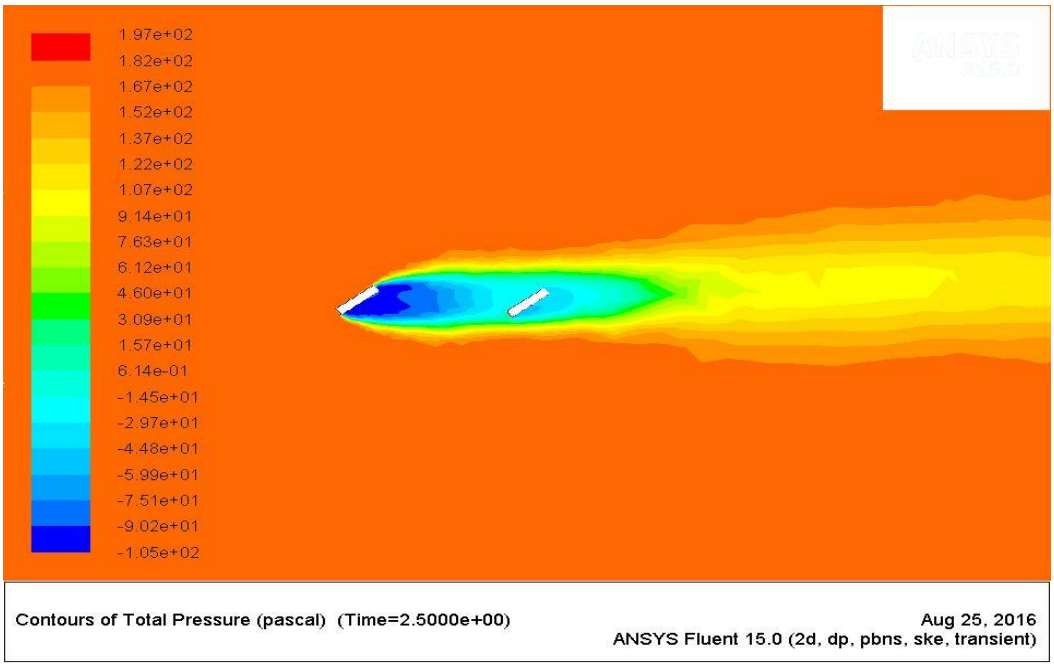

Figure 117. Contours of Total Pressure (Pa), at gap ratio=2.0 and 45 degree

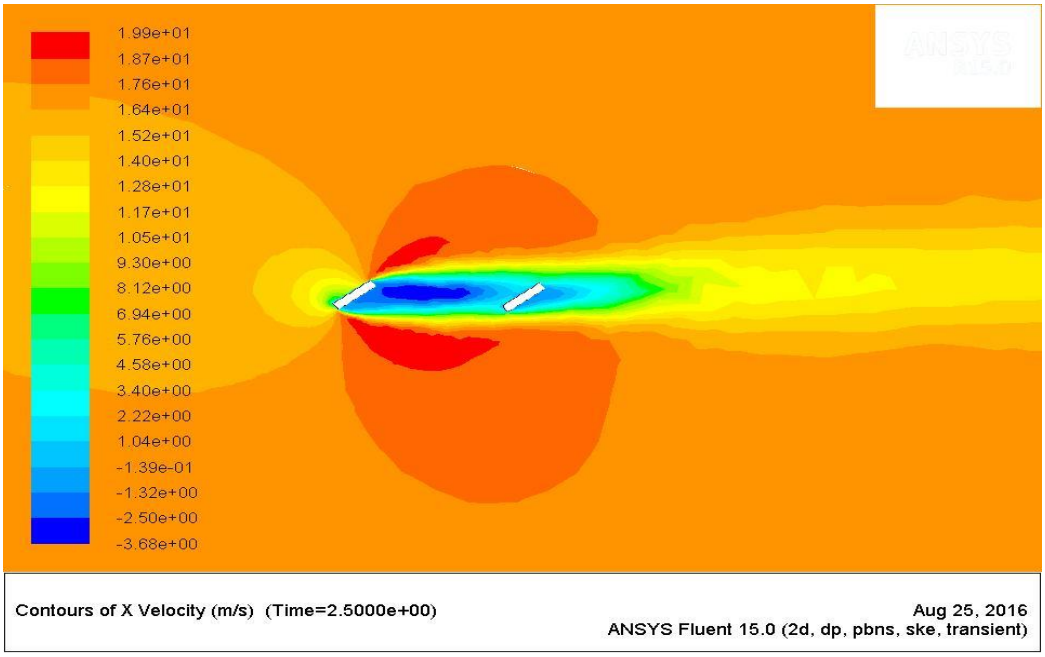

Figure 118. Contours of X-Velocity (m/s), at gap ratio =2.0 and 45 degree

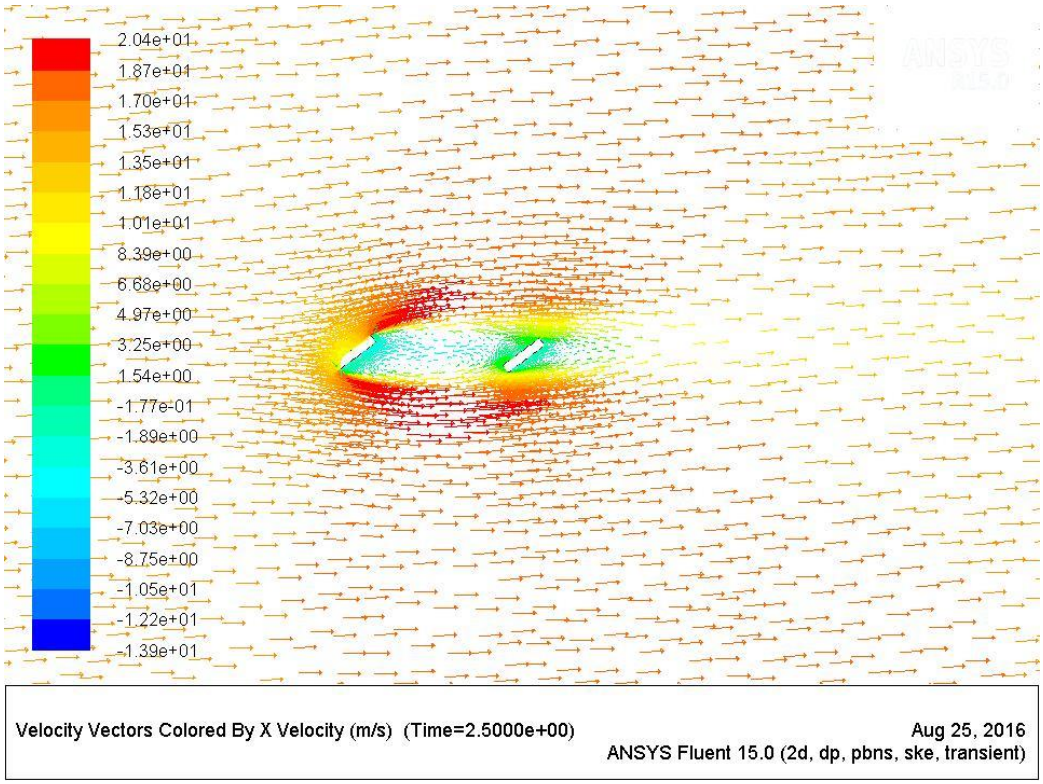

Figure 119. Velocity Vectors Colored by X-Velocity, at gap ratio =2.0 and 45 degree

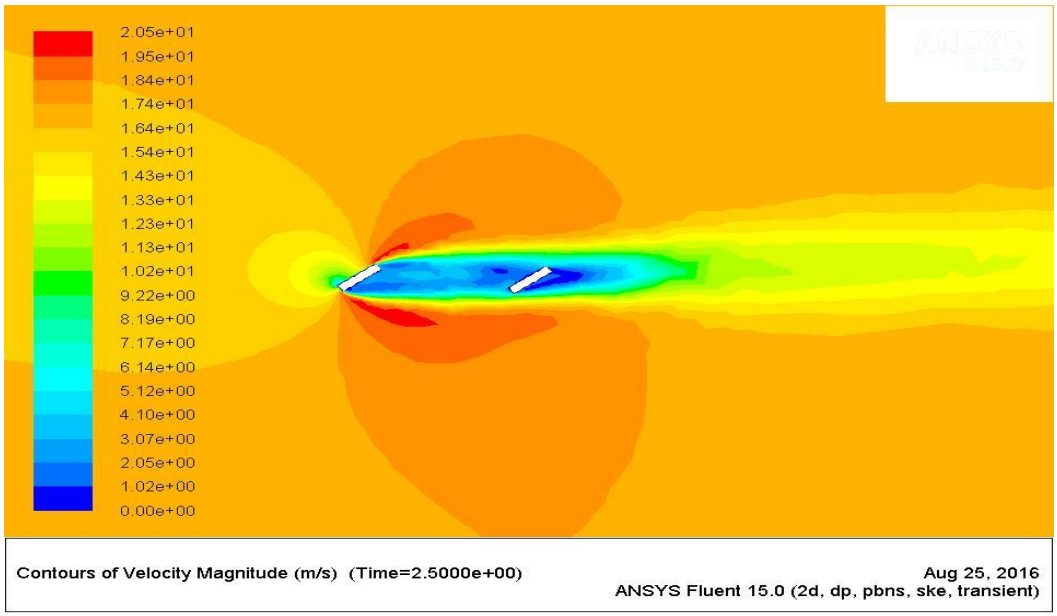

Figure 120. Contours of Velocity Magnitude (m/s), at gap ratio =2.0 and 45 degree

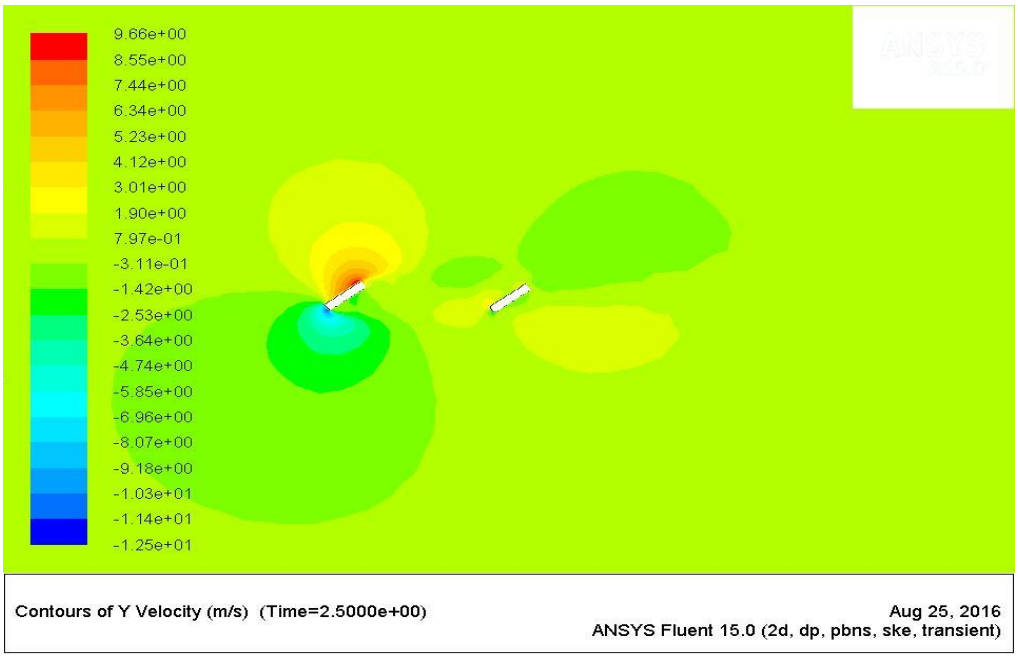

Figure 121. Contours of Y-Velocity (m/s), at gap ratio =2.0 and 45 degree

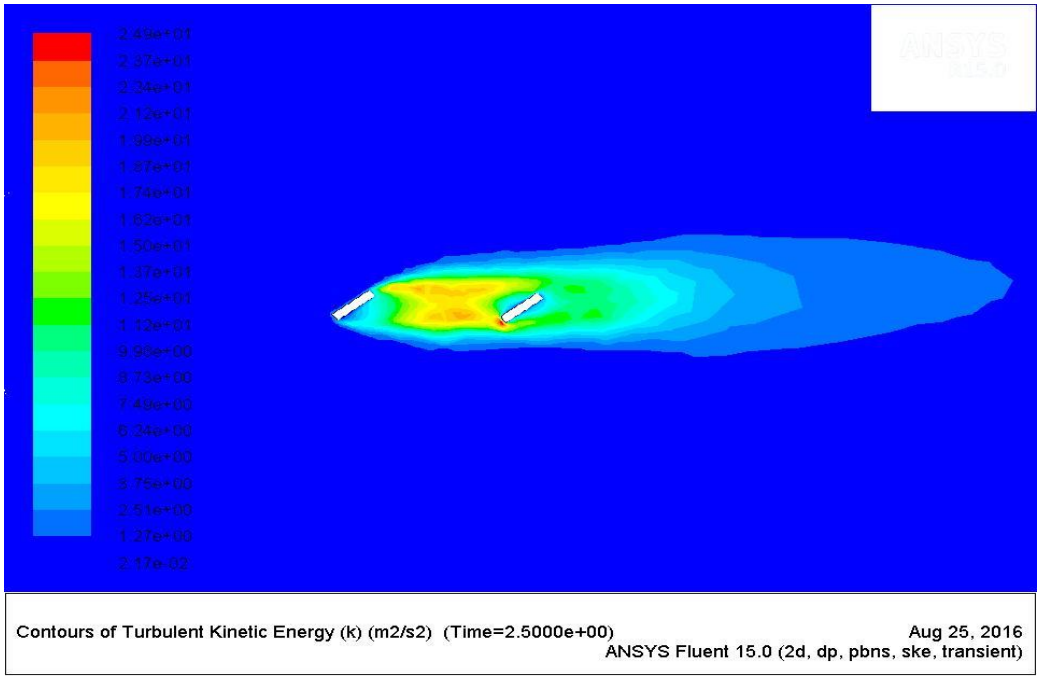

Figure 122. Contours of Turbulent Kinetic Energy (k), at gap ratio =2.0 and 45 degree

4.3 Interpretation of Data

Distinctive flow behaviors are observed in various bluff bodies. Distinction in littler crevice proportions are insignificant. In order to better comprehend this, a strong body having the general length equivalent to the general length of gap proportion 0.5 was concentrated separately and the x-speed shapes and the size of vorticity of both cases were thought about and discovered similar converging properties.

As the crevice proportion expands the flow behavior between the two bodies increases. There is no interaction of the two bodies when the distance is large

Chapter 5

CONCLUSION

5.1 CONCLUSIONS

In other to simulate complicated flows in various engineering field, computational fluid dynamics are generally used these days, their abilities created the nearness of numerous workshops that are attempting to take care of the issues connected with this new innovation. They check the legitimacy and pertinence of various strategies for CFD in various zones. This research aims to assess the ability for the computational fluid dynamics to forecast the flows conduct in structures with insulations as this was done by the utilization of the current wind burrow examination results, thusly the similar problems was broke down by the computational fluid dynamics technique, subsequent information was analyzed with the trial information. Also, nearby assertion between two arrangements of information demonstrated computational fluid dynamics strategy with respect to the confinement and the cost of wind passage model investigations of stream conduct and could be created and connected to the more muddled issues.

For the normal flat plates, increasing the gap ratio, vortex shedding would appear behind the second plate. This means that in between two plates vortex is more developed. Kinetic turbulent energy has reverse relation with gap ratio by increasing gap ratio turbulent kinetic energy decreases.

Inclined flat plates cases which are at an angle of attack of 75 degree usually have their Strouhal number decreased as the gap between the plate increases. However, at angle of attack 45 degree the Strouhal number increases in a gap ratio 1.0 and then for further gap between the plates Strouhal number declines.

5.2 Future Study

Accordingly, the flow comprises of triple decomposition methods and 3D properties provides a viable solution when the speed's properties is also interpreted. Therefore the study of the three dimensions can be recommended.

REFERENCES

[1] Fujii, K. (2005). Progress & future prospects of CFD in aerospace - Wind tunnel and beyond. *Progress in Aerospace Sciences*, 41 (6), 455-470.

[2] Billah, K. and Scanlan, R. (1991). Resonance, Tacoma Narrows Bridge Failure, and Undergraduate Physics Textbooks. *American Journal of Physics*

[3] Fujii, K. (2009, September 23). Realization of prof. kuwahara‟smessages - after almost 30 years‟ effort in CFD - [Web log message]. Retrieved from http://accc.riken.jp/assets/nobeyama/1-2Fujii.pdf

[4] Cengel, A. and CIMBALA, M. (2006). *Fluid mechanics fundamentals and applications*. (p. 570). New York: McGraw-Hill.

[5] Wu, J. and Hu, Y. (1995). A numerical study of wake interference behind two side-by-side and tandem circular cylinders. Journal of the Chinese Society of Mechanical Engineers, 16 (2), 109-122.

[6] Bearman, P.W. (1965). Investigation of the flow behind a two-dimensional model with a blunt trailing edge and fitted with splitter plates. *Journal of Fluid Mechanics*, 21, 241-255.

[7] Bearman, P.W. and Trueman, D.M. (1972). Investigation of flow around rectangular cylinders. *AERONAUT QUART*, 23, 229-237.

[8] Auteri F., Belan M., Gibertini G. aand Grassi D. (2008). Normal flat plates in tandem: An experimental investigation. *Journal of Wind Engineering and Industrial Aerodynamics*, 96 (6-7), 872-879.

[10] Yen S.C., San K.C. and Chuang T.H. (2008). Interactions of tandem square cylinders at low Reynolds numbers. *Experimental Thermal and Fluid Science*, 32 (4), 927-938.

[11] Xu, G. and Zhou, Y. (2004). Strouhal numbers in the wake of two inline cylinders. *Experiments in Fluids*, 37, 248-256.

[12] Wei C.Y., Chang J.R. (2002). Wake and base-bleed flow downstream of bluff bodies with different geometry. *Experimental Thermal and Fluid Science*, 26 (1), 39-52.

[13] Mazharoglu C. & Hacisevki H. (1999). Coherent and incoherent flow structures behind a normal flat plate. *Experimental Thermal and Fluid Science*, 19 (3), 160-167.

[14] Hacisevki, H. & Mazharoglu, C. Triple decomposition technique applied for near wake flow measurement. 272-275.

[15] Kiya, M., Matsumara, M. (1988). Incoherent turbulence structure in the near wake of a normal plate. *Journal of Fluid Mechanics*, 190, 343-356.

[16] Auteri F., Belan M., Gibertini G. & Grassi D. (2008). Normal flat plates in tandem: An experimental investigation. *Journal of Wind Engineering and Industrial Aerodynamics*, 96 (6-7), 872-879.

[17] Bosch, G. & Rodi, W. (1996). Simulation of vortex shedding past a square cylinder near a wall. *International Journal of Heat and Fluid Flow*, 17(3), 267-275.

[19] Ishigai, S. & Nishimura, X., Cho, X. (1972). Experimental study on structure of gas flow in tube banks with axis normal to the flow. *Bull. JSME*, 15, 949-956.

[20] Zdravkovich, M. M. (1987). The effects of interference between circular cylinders in cross flow. *Journal of Fluids and Structures*, 239-261.

[21] Bearman, P. W. & Wadcock, A. J. (1973). The interference between a pair of circular cylinders normal to a stream. *Journal of Fluid Mechanics*, 61, 499-511.

[25] Joshi, D. S., Vanka, S. P. & Tafti, D. K. (1994). Large eddy simulation of the wake of a normal flat plate. *Boundary Layer and Free Shear Flows ASME*, 184, 231-242.

[26] N Meroney, R., Leitl, B. M., Rafailidis, S. and Schatzmann, M. (1999). Wind-tunnel and numerical modeling of flow and dispersion about several

building shapes. *Journal of Wind Engineering and Industrial Aerodynamics*, 81(1-3), 333-345.

[28] Hacisevki, H. (2001). Vortex shedding in tandem arrangement. 23-29, 70-90.

[30] Holmes, J. D. (2001). *Wind loading of structures*. (First ed., pp. 157-158). London: Spon Press.

[33] Sezai, I. (2009). How does a cfd code work? [Web log message]. Retrieved from http://me.emu.edu.tr/sezai/ME555/Chapter%201.pdf

APPENDICES

Appendix A: Wind Tunnel Experiment

An open type subsonic wind tunnel,10 meters long with a working section 0.5m× 0.5m and 1.5m long was used. Contraction ratio of the tunnel is 10:1 and at the entrance a 1.6m× 1.6m triangular sectioned flow straightener sandwiched with two layers of wire mesh was installed and calibrated. The tunnel has a free stream turbulence level of about 0.5-0.8% at the top speed of 30m/s. The velocity measuring system of this wind tunnel is a fully-integrated, thermal anemometer-based system which measures mean and fluctuating velocity components in air [32]. The tunnel speed adjustable through a 12 kW frequency controlled speed. The free stream velocity of air kept constant at 16.4± 0.02 % for this specified experiment. As the vortex shedder, a flat plate made of plexiglass of dimensions 30 mm width; 500 mm height and 6 mm thickness were used. The Reynolds number was 33000 [13].

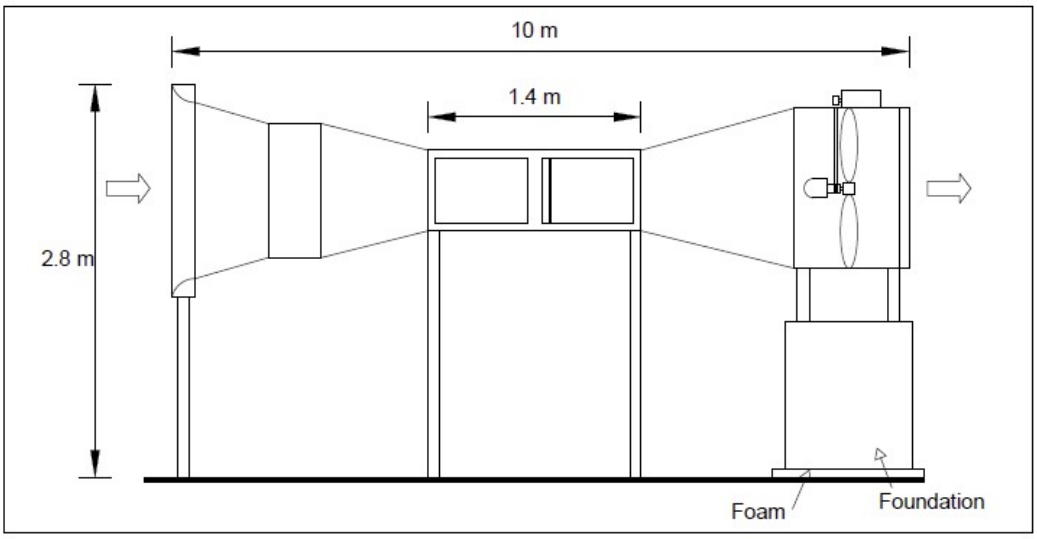

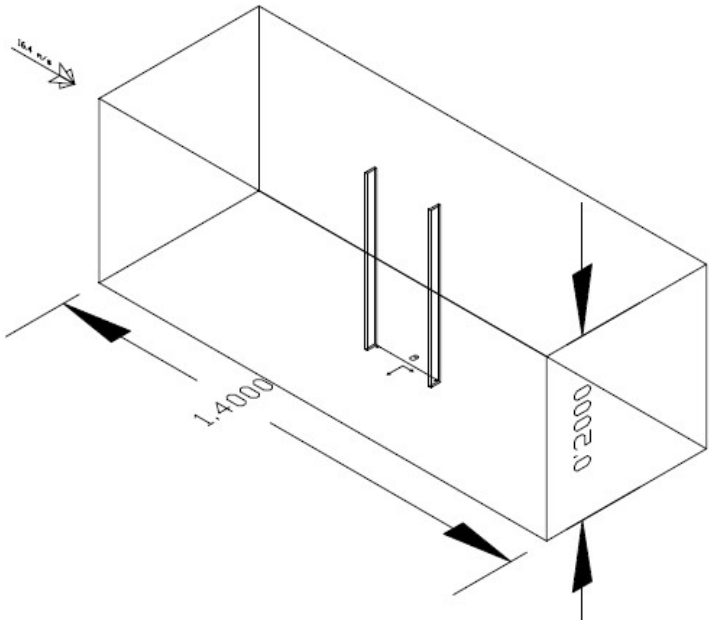

Figure 123. Schematic View of Wind Tunnel and Test Section with Loaded Plates

Appendix B: Turbulence Modeling

B.1 Shear-Stress Transport (SST) $k-\omega$ Model

B.1.1 Transport Equations for the $k-\omega$ Model

The turbulence kinetic energy, k and the specific dissipation rate, ω is obtained from the following transport equations:

$$\frac{\partial}{\partial t}(\rho k)+\frac{\partial}{\partial x_i}(\rho k u_i)=\frac{\partial}{\partial x_j}\left(\Gamma_k \frac{\partial k}{\partial x_j}\right)+\widetilde{G_k}-Y_k+S_k \quad \text{(B-1)}$$

And

$$\frac{\partial}{\partial t}(\rho \omega)+\frac{\partial}{\partial x_i}(\rho \omega u_i)=\frac{\partial}{\partial x_j}\left(\Gamma_\omega \frac{\partial \omega}{\partial xi}\right)+G_\omega-Y\omega+D\omega+S\omega \quad \text{(B-2)}$$

Where,

$\widetilde{G_k}$, is the generation of turbulence kinetic energy due to mean velocity gradients,

G_ω , represents the generation of, ω

Γ_k *and* Γ_ω , represent the effective diffusivity of k and ω

Y_k represent the dissipation of k and ω due to turbulence

S_k *and* S_ω, are user-defined source term.

Appendix C: ANSYS FLUENT Turbulence Models [35]

- Spalart-Allmaras model
- $k-\varepsilon$ models

  Standard $k-\varepsilon$ model

  Renormalization-group (RNG) $k-\varepsilon$ model

  Realizable $k-\varepsilon$ model

- $k-\omega$ models

  Standard $k-\omega$ model

  Shear-stress transport (SST) $k-\omega$ model

- v^2-f model (add-on)

  Transition $k-kl-\omega$ model

  Transition SST model

- Reynolds stress models (RSM)

  Linear pressure-strain RSM model

  Quadratic pressure-strain RSM model

  Low-Re stress-omega RSM model

- Scale-Adaptive Simulation (SAS) model
- Detached eddy simulation (DES) model, which includes one of the following RANS models.

  Spalart-Allmaras RANS model

  Realizable RANS $k-\varepsilon$ model

  SST $k-\omega$ RANS model